STERICALLY DEMANDING LIGANDS AND THEIR EFFECT ON THE STRUCTURE AND REACTIVITY OF MAIN GROUP METAL COMPLEXES

By

Stephen Christopher Chmely

Dissertation

Submitted to the Faculty of the

Graduate School of Vanderbilt University

in partial fulfillment of the requirements

for the degree of

DOCTOR OF PHILOSOPHY

in

Chemistry

August, 2010

Nashville, Tennessee

Approved:

Professor Timothy P. Hanusa

Professor Charles M. Lukehart

Professor David Wright

Professor Eva Harth

Professor Bridget R. Rogers

To Al

ACKNOWLEDGMENTS

There are many people that are very deserving of my gratitude for all of the help that they have provided to me over the many years that my education has required. I would like to thank, first and foremost, James Story and Lynn Peterson: the many hours of music training I received have served as a welcome creative respite from the rigors of analytical thinking. I would also like to thank my chemistry advisors at Western Kentucky University, Les Pesterfield and Kevin Williams, for sparking my interest in inorganic chemistry. Additionally, the training and support that I received from Dr. Williams during my time in his lab helped me to navigate the rigors of graduate school and hit the ground running. For that, I am eternally grateful.

I have spent four years in the lab of Professor Timothy Hanusa, and I owe much of my success to his guidance and support. Before I started at Vanderbilt University, I had neither seen a dry box nor heard of a Schlenk line, but my rotation in his lab solidified my desire to be an organometallic chemist. Dr. Hanusa is always available to answer questions or to offer insights, and his assistance has helped me tremendously.

I would like to thank other faculty members in the Department from whom I took a class or with whom I had a meaningful conversation, including Tara Todd, whose assistance in matters regarding teaching a multitude of classes at Vanderbilt was invaluable, and Chuck Lukehart, who I could always count on to have a suggestion for some synthetic technique to try in the lab. I would also like to extend a special thanks to the other members of my committee, Profs. Wright, Harth, and Rogers, for their helpful suggestions and insights regarding my research.

My fellow students definitely made a positive impact on my experience at Vanderbilt. I would never be able to list all of my fellow students that have made a positive impact on my experience at Vanderbilt, but I am grateful to all of you. I must thank all past and present members of the Hanusa research group, especially Cameron Gren for his support and advice even after graduating, and Jeff Crisp for showing me the ropes and helping me to get started in the group.

The work that I have completed would not have been possible without generous funding. I am thankful to the Chemistry Department for supporting me through teaching assistantships and a teaching fellowship, as well as funding provided to me through the Warren Research Fellowship. Research funds were available to pay for me through the summers from either an ACS-PRF or NSF grant.

I would like to thank my mom, who has offered her support and advice to me for the nearly thirty years that I have been on this earth, and my dad, who I miss very much. I hope that I can be half as good at parenting as you two have been. I'd also like to extend a special thanks to my brothers from another mother, Trey and Chad McClarnon. You guys have been the best friends a guy could ask for, and you kept me sane throughout this process.

Finally, to Allison: thank you for being there for me throughout my undergraduate and graduate career. Without your unending support and friendship, I never would have made it this far. I love you more than you could imagine.

TABLE OF CONTENTS

Appendix

LIST OF TABLES

LIST OF FIGURES

CHAPTER I

COMPLEXES WITH STERICALLY BULKY ALLYL LIGANDS: INSIGHTS INTO STRUCTURE AND BONDING

Introduction

The allyl anion, $[C_3H_5]^-$, is among the smallest π-delocalized ligands found in organometallic chemistry. Its compact size contributes to its conformational flexibility; it binds to metals in both bridged (η^3) and "classic" σ (η^1) modes, and interconversion between them can be rapid. In combination with a wide variety of other ligand types (e.g., halides, phosphines, carbonyls, and cyclopentadienes), allyl anions have been incorporated into complexes from across the periodic table (the s-, p-, d-, and f-block are all represented).[1]

Despite its versatility, the small size of the allyl ligand can be a liability in many contexts, especially in homoleptic complexes, $M(C_3H_5)_n$. With a few important exceptions (e.g., the di(allyl) complexes of Ni, Pd, and Pt, which are valuable in organic synthesis),[2] most $M(C_3H_5)_n$ compounds are poorly studied and infrequently used. A major reason for this is that metal centers in homoleptic allyl complexes are often coordinately unsaturated, and low-energy pathways for decomposition are available. As a result, many of them are thermally unstable and difficult to handle. Wilke cites examples of these in his early review of homoleptic allyl complexes:[3] especially notable are $Fe(C_3H_5)_3$ and $Co(C_3H_5)_3$, which decompose above -40 °C, $V(C_3H_5)_3$, which explodes above -30 °C, and $Zr(C_3H_5)_4$, $Nb(C_3H_5)_4$, and $Ta(C_3H_5)_4$, all of which decompose at

0 °C. Even $Ni(C_3H_5)_2$ decomposes within a day at room temperature under a nitrogen atmosphere.

By occupying larger areas of the metal coordination sphere and physically blocking decomposition routes, sterically bulky ligands have often been used to improve the kinetic stability of organometallic complexes. Cyclopentadienyl chemistry has long benefited from the use of such substituted rings as C_5Me_5 and $C_5H_3(SiMe_3)_2$, which can be used to synthesize compounds of greater diversity and stability than is possible with Cp alone.[4] A similar approach is effective with the allyl ligand. The allyl anion can be substituted with a variety of alkyl, aryl, silyl, and siloxide groups, all of which can have substantial effects on the properties of their associated compounds. For example, methylated allyl ligands are known to provide modest improvements in the thermal stability of complexes,[5] and the bulky nickel allyl complex $Ni(1,1',3,3'\text{-}Ph_4C_3H)_2$ is stable at room temperature.[6] The first widespread studies of the changes in properties that could be conferred on allyl complexes with the use of sterically bulky ligands involved trimethylsilylated ligands. Fraenkel reported the synthesis of lithiated derivatives of $[(SiMe_3)_nC_3H_{5-n}]^-$ anions in the early 1990s,[7] and allyl ligands with one to three trimethylsilyl substituents are known.[8] These and related variants such as dimethyl(*tert*-butyl)silylallyl[9] have remained the most intensively used ligand types in bulky allyl complex chemistry. The trimethylsilyl groups provide good solubility in hydrocarbon solvents, and substantially increase the size and steric demands of the ligands; e.g., at 264 $Å^3$, the *syn, syn*-$[1,3\text{-}(SiMe_3)_2C_3H_3]^-$ anion has almost 5 times the volume of the parent $[C_3H_5]^-$ ion (54 $Å^3$) (Figure 1).[10]

Figure 1. Space-filling models of $[C_3H_5]^-$ (left) and $[1,3\text{-}(SiMe_3)_2C_3H_3]^-$.

How much of an effect such increased bulk has on the properties of the association complexes varies not only with the degree of substitution, but also with the identity of the substituent. The energetic barrier for displacing silyl-based substituents from the plane of a delocalized anion is lower than for hydrocarbyl groups,[11] and such bending effectively reduces the steric impact of the group. Consequently, a single substituent may have minimal effect on the structure of the complex (e.g., $\{Cr(C_3H_5)_2\}_2$ and $\{Cr(1\text{-}(SiMe_3)C_3H_4)_2\}_2$ are related dimers).[12] Conversely, three trimethylsilyl groups on the ligand may not affect structures much more than the presence of two (e.g., $Cr[1,3\text{-}(SiMe_3)_2C_3H_3]_2$ and $Cr[1,1',3\text{-}(SiMe_3)_3C_3H_2]_2$ are comparable monomeric species).[12]

In some cases, substituted allyl ligands provide versions of known compounds that are more robust than the unsubstituted species. For example, unlike the pyrophoric $Ni(C_3H_5)_2$, the trimethylsilylated derivative $Ni[1,3\text{-}(SiMe_3)_2C_3H_3]_2$ only slowly decomposes in air (from hours to days).[13] In addition, the homoleptic thorium complexes $Th[(SiMe_3)_nC_3H_{5-n}]_4$ (n = 1, 2) are stable to 90 °C,[14] in contrast to $Th(C_3H_5)_4$, which decomposes at 0 °C. In other cases, the presence of substituent groups aids in

crystallization, so that solid-state structures may be obtained; calculations suggest that the X-ray crystal structure of the lithium dimer $\{Li[1,1',3\text{-}(SiMe_3)_3C_3H_2]\}_2$ is related to that of the unsubstituted complex, which is known to be a dimer from cryoscopy, but which has not been structurally authenticated.[15]

Of even greater interest is the use of substituted allyl ligands to support entirely new classes of thermally stable, electron-deficient transition metal bis(allyl) compounds $M[1,3\text{-}(SiMe_3)_2C_3H_3]_2$ (M = Cr, 12-e$^-$;[12] Fe, 14-e$^-$;[16] Co, 15-e$^-$[17]); they have no monomeric counterparts with unsubstituted ligands. The neutral monomeric tris(allyl) complexes $Ln[1,3\text{-}(SiMe_3)_2C_3H_3]_3(thf)$ (Ln = Ce, Nd, Tb)[18] and the tetrametallic salt $\{K(thf)_2Sm[1,3\text{-}(SiMe_3)_2C_3H_3]_3\}_2$[19]) are likewise without precedent with unsubstituted allyl ligands.

The following focuses on the second type of complex mentioned above; i.e., those (mostly homoleptic) complexes in which the use of sterically bulky allyl ligands has allowed the isolation of complexes with new structural features that are either unknown or substantially different from counterparts with unsubstituted allyl ligands. A brief review of this area was published several years ago, with an emphasis on transition metal complexes;[20] the following serves to update and expand that review, especially in the area of main group chemistry. Azaallyl compounds, which have some parallels to those discussed here, have been reviewed elsewhere.[21]

General Preparative Routes

The most common starting materials for metal complexes containing bulky allyl ligands have been the alkali metal salts of the allyl anions; these are prepared from the lithium allyls, which in turn are generated from the substituted propene and an alkyllithium reagent (eq 1).[22] Owing to the pervasive use of the $[1,3\text{-}(SiMe_3)_2C_3H_3]^-$ anion, it will be referred to as **A′** in the rest of this document.

$$\mathrm{RLi} + (\mathrm{SiMe_3})_m\mathrm{C_3H_{6-}}_m \xrightarrow[\text{hexane}]{\text{TMEDA}} \mathrm{Li[(SiMe_3)}_m\mathrm{C_3H_{5-}}_m\mathrm{]} + \mathrm{RH}\uparrow$$

$$\xrightarrow{\text{(Na,K)[O-}t\text{Bu]}} \text{(Na,K)[(SiMe3)}m\text{C3H5-}m\text{]}\downarrow + \text{Li[O-}t\text{Bu]} \qquad (1)$$

The limited acidity of propene and its substituted derivatives means that direct reaction to form a salt will only occur with the most active metals (Rb, Cs) (eq 2).

$$\mathrm{Cs} + \mathrm{HA'} \xrightarrow{\text{thf}} \mathrm{Cs[A']} + \tfrac{1}{2}\mathrm{H_2}\uparrow \qquad (2)$$

Both mono- and 1,3-dilithiated allylsilanes can be prepared from 1-((allyldimethylsilyl)methyl)piperidine by treatment with either one or two equivalents of *t*BuLi (eq 3). The lithium salts have been structurally characterized.[23]

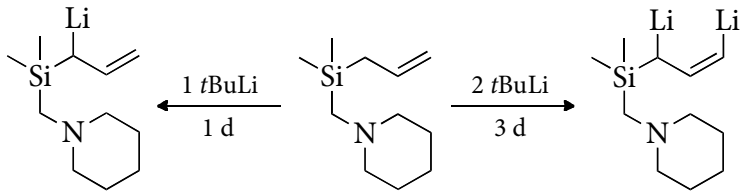

(3)

A silyl-bridged bis(allyl)ligand synthesized from the bis(allyl)silane $Me_2Si(CH_2CHCHSiMe_3)_2$ can be converted into its dilithium or dipotassium salt (i.e., $K_2[3\text{-}(C_3H_3SiMe_3\text{-}1)_2SiMe_2]$) (eq 4); it has been used in the synthesis of *ansa*-bis(allyl) complexes.[24]

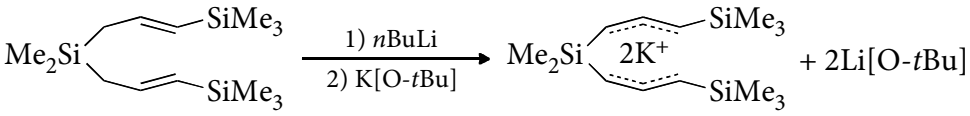

(4)

A cyclic allyl variant with sterically bulky groups, the [1,3-bis(trimethylsilyl)-2-cyclohexen-1-yl] anion, has been described. It retains the two trimethylsilyl groups of the $[A']^-$ anion while providing extra shielding with the cyclohexyl group;[25] such protection might be important in mono(π-allyl) metal complexes. The hydrocarbon is synthesized in 3 steps from 3-bromocyclohexene (eq 5).

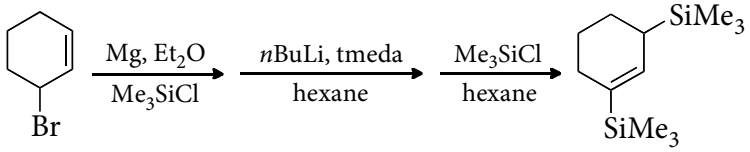

(5)

A related silyl-bridged bis(cyclohexene) ligand has been used to form *ansa*-bis(allyl) complexes.[25]

The terminal substituent in a coordinated allyl ligand can be found in a *syn* or *anti* position; the former conformation places the substituent on the same side of the ligand as the central hydrogen atom; in the *anti* form, the opposite arrangement occurs. To date, π-bound monosubstituted allyl ligands are known only with *syn* orientations, and unless constrained by an *ansa*-bridge, 1,3-disubstituted allyl ligands have *syn*, *syn* configurations in complexes of highly electropositive metals (s- and f-block). Both *syn*, *syn* and *syn*, *anti* arrangements occur in allyl complexes of the d-block transition elements.

Halide metathesis reactions (eq 6) are commonly used as a route to bulky allyl metal complexes. The use of potassium salts of the allyl anion facilities separation of the alkali halide by-product by filtration of the reaction mixture. Lithium salts, in contrast, are readily solvated by ethers (thf, Et_2O), and can remain mixed with, or even incorporated into, the allyl complexes.

$$MX_n + nK[(SiMe_3)_mC_3H_{5-m}] \xrightarrow{\text{thf}} M[(SiMe_3)_mC_3H_{5-m}]_n + nKX\downarrow \qquad (6)$$

Although synthesis with metathetical methods is typically straightforward, a peculiar difficulty with the use of bulky allyl ligands is that the products of halide exchange reactions may not reflect the stoichiometry of the reagents. This seems to occur most often with larger metals, especially among the f-elements, although even variations in the metal cation of the allyl starting material can affect the products isolated. With lanthanide iodides and lithium allyl starting materials, for instance, anionic lanthanates are produced regardless of the lanthanide used. If the potassium derivative of the allyl is used as a

starting material, however, neutral species are formed. The outcomes of some reactions appear to be metal radii dependent. An example of the lack of strict stoichiometric control is provided by the reaction of two equivalents of K[A′] and $NdI_3(thf)_{3.5}$, which produces a mixture of the expected bis(allyl) complex $Nd[A']_2I(thf)_2$ along with the mono(allyl) compound $Nd[A']I_2(thf)_{1.25}$.[19]

An unusual twist on this chemistry is that the trimethylsilyl groups in bulky allyl ligands can themselves be sites of reactivity, and traces of water in reagents can initiate unusual transformations.[26] This underscores the need for a high degree of rigor in the purification of reagents and stringent precautions against adventitious admission of air or moisture into reaction systems.

Structures of Compounds from Groups 1-2

The alkali metals. Fraenkel and coworkers described the synthesis of lithiated derivatives of the trimethylsilylated propenes, and reported various structural and spectroscopic properties for them.[7,27] The tmeda adduct of Li[A′] is a monomer in the solid state, with slightly asymmetrical π-bonding (e.g., the C-C distances in the allyl ligand differ by 0.041 Å);[7a] in solution, however, the molecule appears symmetrical. Lappert has described the structure of the related complex Li[1,3-$(SiMe_2tBu)_2C_3H_3$](tmeda); it is more symmetrical than Li[A′] (e.g., ΔC–C = 0.007 Å), despite the greater bulk of the silyl substituents.[25]

Fraenkel found that the unique trimethylsilyl group at C3 in the tris(trimethylsilylated) complex Li[1,1′,3-$(SiMe_3)_3C_3H_2$] was *exo* in solution, and that the

barrier to rotation of the allyl groups in thf was 16.8 kcal mol^{-1}.[8] Interestingly, despite the bulk of the ligands, Li[1,1′,3-$(SiMe_3)_3C_3H_2$] adopts a dimeric structure in the crystal (Figure 2). The two Li atoms are bridged by the allyl ligands in a μ_2-η^1,η^2 manner, with a σ-bonded distance of 2.232(7) Å (Li1–C6′, Li1′–C6). The lithium is centered over the midpoint of the C4–C5 bond, with an average Li–(C4,C5) distance that is indistinguishably different from the σ-bonded length (2.236 Å). The bridging allyls (C4–C6) are only partially delocalized, with a 0.085 Å difference between the single and double bonds.

Unsubstituted allyllithium is known to be dimeric in thf solution,[28] and calculations at the DFT level indicate that even the substituted complex {Li[C_3-1,1′,3-$(SiH_3)_2H_3$](thf)$_2$}$_2$ would be stable as a dimer.[15] Support for this conclusion is found in a related lithium complex formed from the tetrahydrofurfuryl-substituted derivative of the A′ ligand (Figure 2).[29] The dimeric complex has Li1–O1 and Li2–O2 bond lengths that are indistinguishable at 1.87 Å, and the C–C allyl bonds are slightly more delocalized (Δ = 0.052 Å) than in {Li[1,1′,3-$(SiMe_3)_3C_3H_2$]}$_2$. The lithiums have shifted so that they are closest to the center carbons of the allyl ligands (average of Li1–C2 and Li2–C16 bond lengths is 2.196(7) Å) and the distances from the lithium atoms to the "outer" carbons (C3, C17) are now quite long at an average value of 2.48 Å.

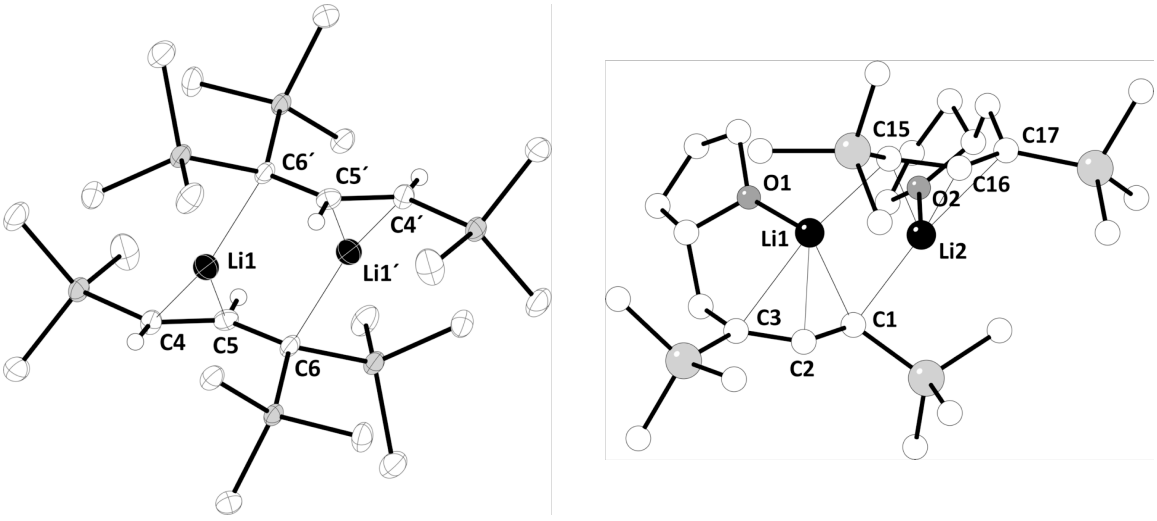

Figure 2. The structures of $\{Li[1,1',3\text{-}(SiMe_3)_3C_3H_2]\}_2$ (left) and bis(μ_2-η^3,η^1-4-(tetrahydrofuran-2-yl)-1,3-bis(trimethylsilyl)but-2-en-1-yl)-dilithium (right).

The unsolvated 1,3-bis[dimethyl(phenyl)silyl]allyllithium, $Li[1,3\text{-}(SiMe_2Ph)_2C_3H_3]$, forms helical polymeric chains in the solid state (Figure 3).[30] The π-bonded allyl ligands are at an angle of 60–62° from the major chain axes, and the Li–C distances range from 2.16 Å to 2.35 Å. The average distance of 2.26 Å is considerably shorter than the corresponding separation in the polymeric $\{Li[1,3\text{-}Ph_2C_3H_3]\bullet OEt_2\}_\infty$ (2.42 Å),[31] which reflects the presence of the coordinated ethers in the latter complex.

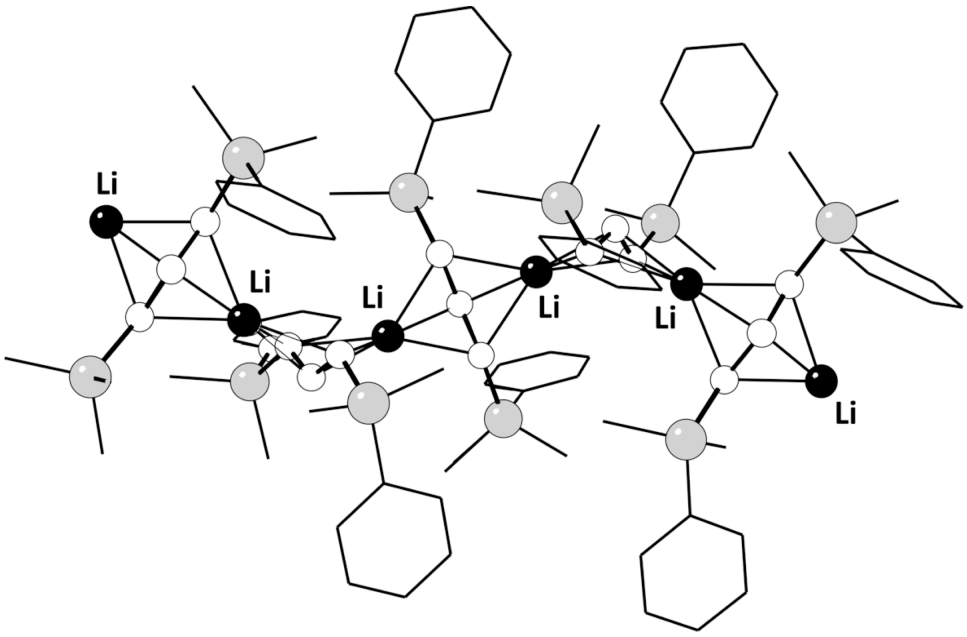

Figure 3. The structure of $\{Li[1,3\text{-}(SiMe_2Ph)_2C_3H_3]\}_\infty$.

Treatment of (1*E*,1′*E*,1″*E*)-3,3′,3″-(methylsilanetriyl)tris(prop-1-ene-3,1-diyl)tris(trimethylsilane) ($MeSiA^{\dagger}_3$) with 3 equivalents of *n*-butyllithium and tmeda produces $Li_3[MeSiA^{\dagger}_3](tmeda)_3$ in 32% isolated yield.[32] The molecular structure of the latter contains a trianionic *ansa*-tris(allyl) ligand with a central tetrahedral Si bound to three allyl moieties and a single methyl group (Figure 4). Each allyl group is in turn bound to a $[Li(tmeda)]^+$ cation. The allyl C–C distances vary over a narrow range of 1.383(7)–1.416(4) Å, which is indicative of a substantial delocalization of the π-electrons in each allyl moiety. As is the case for other solvated lithium allyls, the ^{1}H NMR spectrum of $Li_3[MeSiA^{\dagger}_3](tmeda)_3$ suggests that it is fluxional in solution.

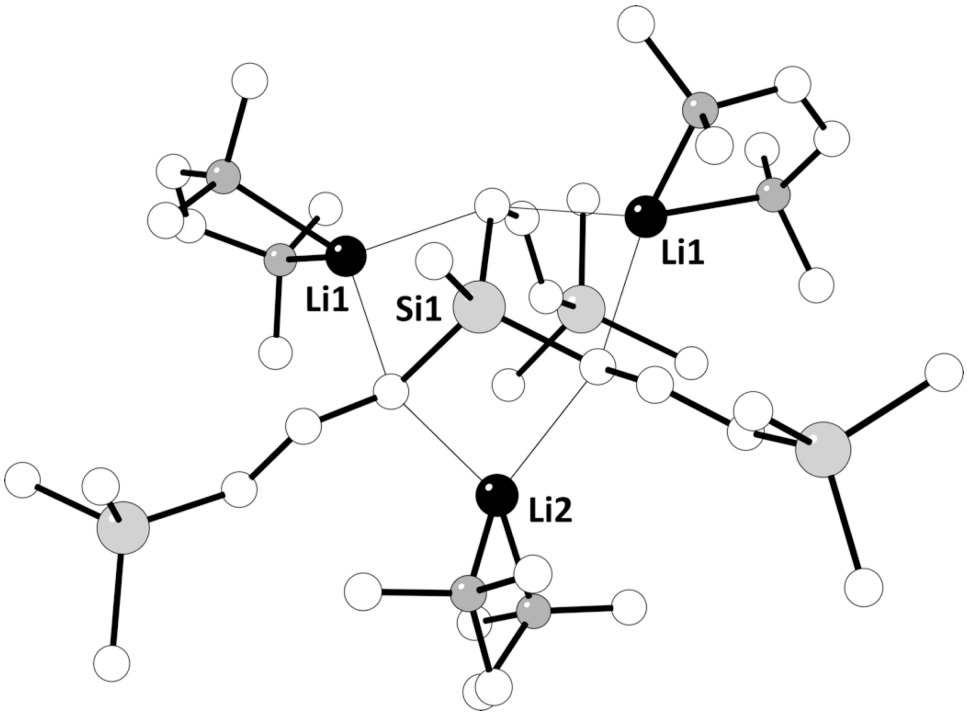

Figure 4. The structure of $Li_3[MeSiA^{\dagger}_3](tmeda)_3$.

Bis(1,3-trimethylsilyl)cyclohexene reacts with *n*-butyllithium and tmeda in hexane at room temperature to yield the lithium derivative (Figure 5).[25] Curiously, although the lithium is well centered over the allyl bond (the difference between Li–C2 and Li–C6 is 0.03 Å), the Li–C1 distance at 2.140(6) Å is much shorter than the average of the Li–C2/Li–C6 distances (2.412(7) Å); it has been suggested that the lithium–allyl bonding might be considered to be of an η^1-type.

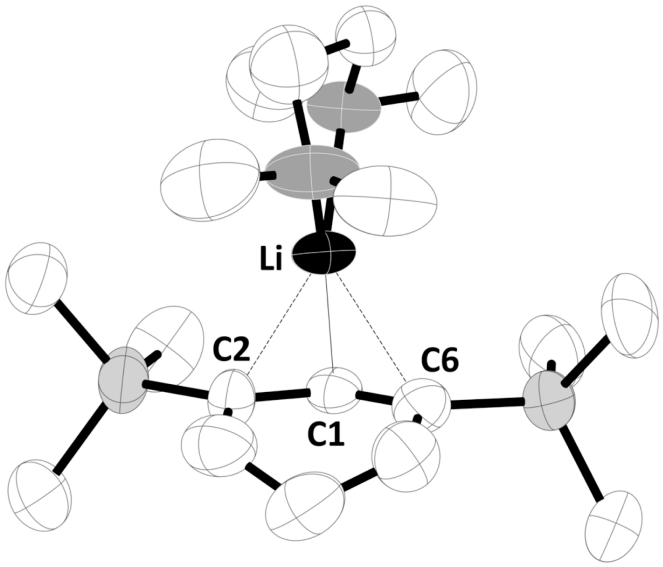

Figure 5. The structure of the lithium derivative of bis(1,3-trimethylsilyl)cyclohexene.

Dilithiation of 1-((allyldimethylsilyl)methyl)piperidine forms the S_6-symmetric complex hexakis(μ_5-η^3,η^3-1-((*N*-(piperidine)–dimethylsilyl)allene)dodecalithium (Figure 6).[23] In addition to the lithium atoms interacting in a π-type fashion with the allyl ligands (Li–C = 2.16–2.37 Å), a hydrogen at the terminal C3 carbon has been replaced with a lithium atom (Li–C = 2.11 Å). Another close Li···C contact is found at 2.25 Å. DFT calculations on model systems indicate that a substantial amount of the negative potential of the allyl dianion resides near C3, which accounts for its association with multiple lithium centers.

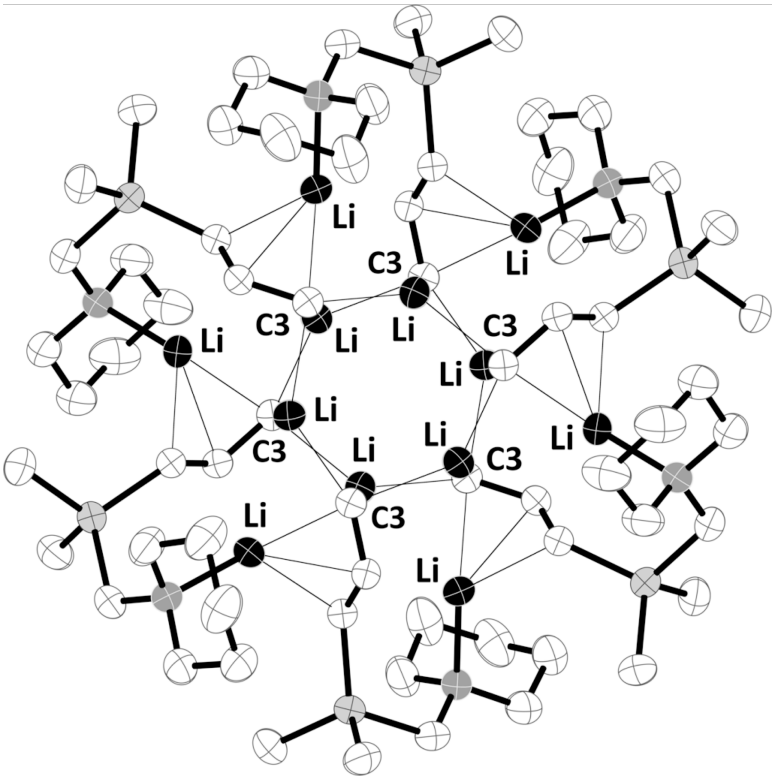

Figure 6. Structure of the dilithium derivative of 1-((allyldimethylsilyl)methyl)piperidine.

With potassium and the heavier alkali metals, allyl complexes are uniformly found as coordination polymers. The potassium salt of the A′ anion, for example, has been crystallized as DME and thf solvates, $\{K[A'](dme)\}_\infty$[33] and $\{K[(A')(thf)_{3/2}]\}_\infty$,[34] and also as the base-free complex, $\{K[A']\}_\infty$.[15] The tetrahydrofurfuryl-substituted derivative of the A′ anion has been crystallized as its potassium salt,[29] and the dimethylsilyl *ansa*-bis(silylcyclohexenyl)dipotassium complex $\{K_2[(\eta^3\text{-}C_6H_4SiMe_3\text{-}6)_2SiMe_2](thf)_3\}_\infty$ has been isolated as a thf solvate.[25] All five compounds are coordination polymers with potassium ions linked by bridging π-allyl ligands. The $\{K[A']\}_\infty$ polymer takes the form of helical chains running parallel to the *a* axis (Figure 7). The range of K–C distances in $\{K[A']\}_\infty$ (2.87–3.15 Å; Δ = 0.28 Å) is broad enough that the average K–C distance of 3.01

Å is not especially significant, although it is comparable to those for potassium cyclopentadienides (e.g., 2.93 Å to 3.10 Å in $\{K[C_5(SiMe_3)_3H_2]\}_\infty$[35]), indicating the similarly ionic bonding in the complexes.

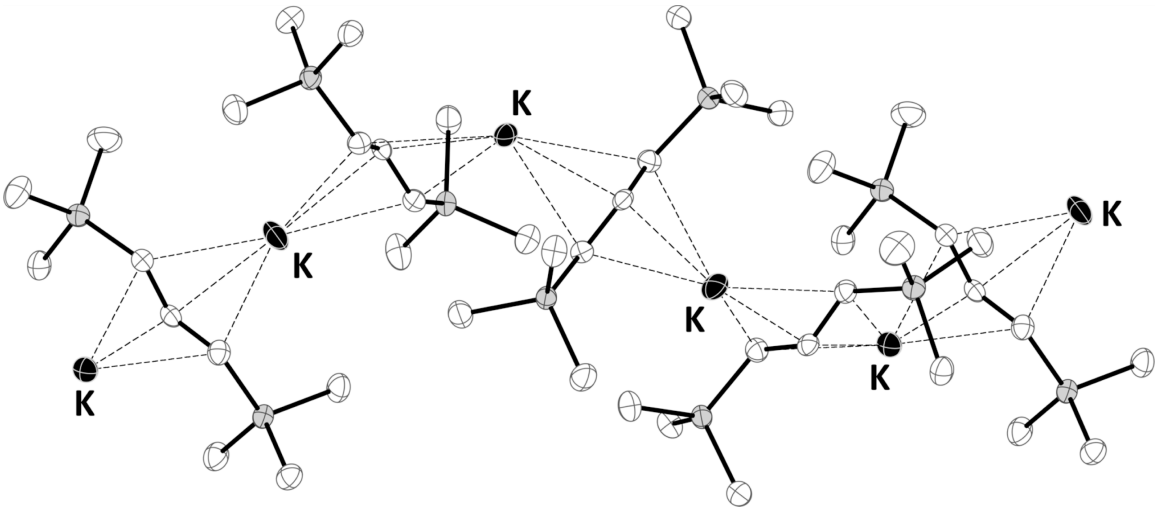

Figure 7. The structure of $\{K[A']\}_\infty$.

The cesium compound $\{Cs[A'](thf)\}_\infty$ forms a strictly linear chain of metal atoms.[34] The immediate environment around the cesium in $\{Cs[A'](thf)\}_\infty$ consists of a thf ligand and two π-bound allyl ligands; there are close intermolecular contacts to methyl groups at 3.67 and 3.95 Å that serve to raise the formal coordination number from 5 to about 7.

The alkaline-earth metals. The alkaline-earth metals display a large range of bonding modes in their allyl complexes. Allyl complexes of beryllium (discussed in detail later) display σ-bound structures when solvated by diethyl ether, although calculations suggest that a π-bound structure could be achieved in the absence of solvent.

Allyls in magnesium complexes are consistently found to be σ-bonded in the solid state, and η^3-coordination of the allyl ligand to magnesium has been suggested as being disfavored.[29] Nevertheless, the balance between covalent and ionic bonding in allylmagnesium complexes (and corresponding σ- and *π*-coordination) may be subtler than indicated by the available solid-state data. For example, infrared and ^{13}C NMR spectra indicate that allyl- and methallyl-d_2-Mg bromides are involved in exchange processes in solution, presumably involving unsymmetrical σ-bonded allylic structures,[36] but the deuterated version of $Mg(C_3H_5)_2$ does not have distinct double bond stretching bands in the IR spectrum, suggesting that delocalized *π*-type bonding exists in the ligands.[36] Such examples raise the question of just what determines the balance between σ- and *π*-bonding in allyl magnesium complexes. Structural and computational studies with bulky allyl complexes have provided some insights into this issue that will be discussed in detail in a later chapter of this document.

Like magnesium, the larger metal calcium also forms a colorless complex of the type $M[A']_2(thf)_2$, but the ligands are *π*-bound. This is suggested by temperature-invariant ^1H NMR data and confirmed by the solid-state structure. The molecule possesses ligands with delocalized bonding, with the difference between the C–C bonds being less than 0.02 Å (Figure 8).[37]

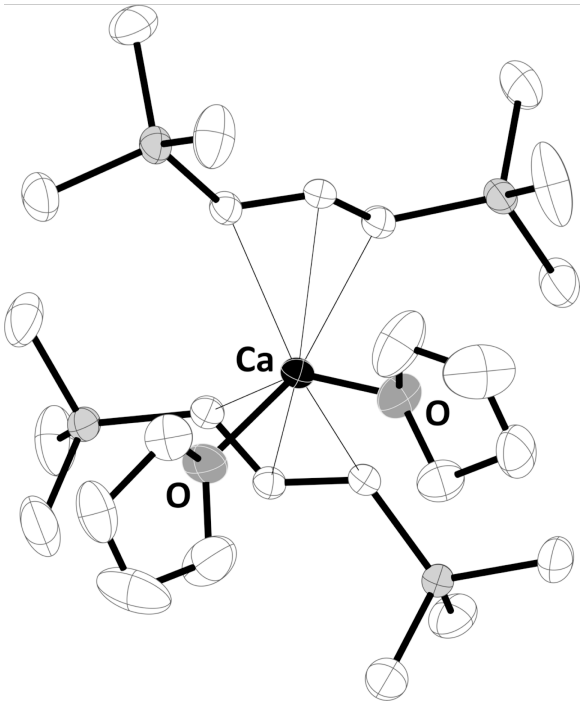

Figure 8. The structure of $Ca[A']_2(thf)_2$.

The allyl ligands are bound in a symmetrical trihapto manner to the metal, with an average Ca–C distance of 2.654(5) Å, respectively. The allyl–M distance is closely similar to that for cyclopentadienyl rings in formally 6-coordinated M^{2+} centers (e.g., 2.64(2) Å in $Ca(C_5Me_5)_2$).[38] It is notable that the allyl groups maintain the same metal–ligand separation as do cyclopentadienyl rings, because in transition metal $(C_3R_nH_{5-n})MCp$ complexes, the allyl ligand binds more closely to the metal than does the Cp ring.[39]

Reactions and Applications

Owing to the relative newness of the area, extensive studies of the reactions of complexes with bulky allyl ligands have yet to be made. In addition to some of the unusual preparative reactions already noted, various multistep but non-catalytic reactions

have been reported. For example, the tris(allyl) complex Y[1-($SiMe_2$-*t*Bu)C_3H_4]$_3$(thf)$_{1.5}$ provides enough access to *tert*-butylnitrile that it can insert four times into the metal-allyl bonds, yielding a *sec*-amido species (Figure 9).[40] The coordination geometry around yttrium includes an oxygen atom from coordinated thf, four nitrogen atoms from the amido ligands, and an N...H contact (2.49 Å) from an amido hydrogen.

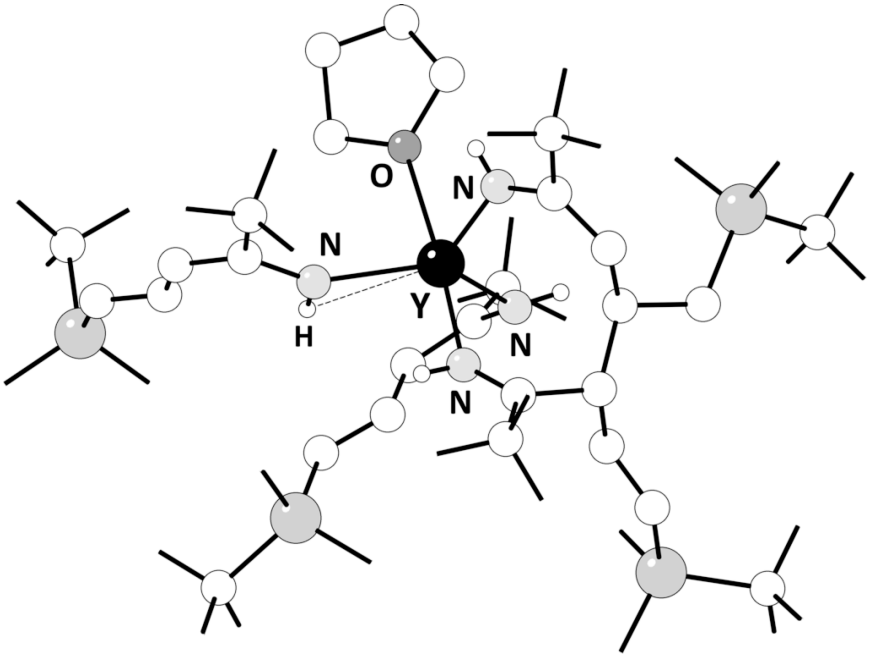

Figure 9. The structure of the nitrile insertion product from Y[1-($SiMe_2$-*t*Bu)C_3H_4]$_3$(thf)$_{1.5}$.

Multistep insertions are likely involved in the reaction between NiA′$_2$ and PMe_3, which yields tetramethyltetraphosphane, $(MeP)_4$. The product was identified with ^1H, ^{13}C, and ^{31}P NMR spectra and its formation studied with DFT methods.[13] Such studies suggest that the direct reaction NiA′$_2$ + PMe_3 → (η^3-A′)$_2$Ni(PMe_3) would not be favorable ($\Delta G°$ = +24.1 kcal mol^{-1}). For steric reasons, slippage of an allyl ligand from η^3

to η^1 would be required for phosphane binding. Subsequent additions of PMe_3 might then occur as the phosphine begins to demethylate, and P–P bond formation ensues.

A variety of f-element complexes with bulky allyl ligands function as polymerization catalysts; this may become a major area of application for these compounds. For example, La[A′]$_2$Cl(thf), Y[A′]$_2$Cl (which may actually be Y[A′]$_3$[41]) and Nd[A′]I$_2$(thf)$_{1.25}$ have been examined with several activators, including methylaluminoxane (MAO), as catalysts for the polymerization of 1,3-butadiene.[40] When activated with MAO, [1,3-(Si(*t*-Bu)Me$_2$)$_2$C$_3$H$_3$]$_2$(Ti,Zr)(μ-Cl)$_2$Li(tmeda) and [1,3-(Si(*t*-Bu)Me$_2$)$_2$C$_3$H$_3$]$_2$(Ti,Zr)Cl$_2$ are polymerization catalysts for ethylene (forming high density polyethylene) and propylene (forming an elastomeric polypropylene with the Ti complexes and a stereoregular polymer with the Zr species).[9]

The cyclic {K(thf)$_2$Sm[A′]$_3$}$_2$ is an effective single-component catalyst for the polymerization of methyl methacrylate (MMA) and ε-caprolactone; Nd[A′]$_2$I(thf)$_2$ polymerizes ε-caprolactone with 85–95% conversion within a minute at 50 °C.[19] [Ln{(η^3-C$_3$H$_3$SiMe$_3$)$_2$SiMe$_2$}$_2${μ-K(thf)$_x$}(thf)$_y$]$_\infty$ (Ln = La, Y, Sc, Nd) and [Li(OEt$_2$)$_4$][Sm{(η^3-C$_3$H$_3$SiMe$_3$)$_2$SiMe$_2$}$_2$] polymerize MMA without activation, and the yttrium compound displays turnover numbers at 0 °C of over 86,000 h^{-1}.[24b]

Polymerization of MMA is also effected by the complexes Eu[A′]$_2$(thf)$_2$, Yb[A′]$_2$(thf)$_2$, Ce[A′]$_3$(thf), Nd[A′]$_3$(thf), Sm[A′]$_2$(thf)$_2$ and [Li(thf)$_4$][Ce{A′}$_3$I], all of which produce atactic polymethylmethacrylate (PMMA).[33] Among the neutral lanthanide allyl complexes, the polymerization activity appears to vary with the radius of the lanthanide metals and with the number of coordinated allyls; i.e., with the access of MMA

to the metal centers. The divalent complexes $Sm[A']_2(thf)_2$ and $Eu[A']_2(thf)_2$, for example, which contain the larger metals samarium and europium ($Sm^{2+} \approx Eu^{2+}$ 1.17 Å for CN number 6),[42] have TOF values over ten times higher than $Yb[A']_2(thf)_2$ (Yb^{2+} = 1.02 Å for CN number 6). Conversely, the complexes containing trivalent cerium ($Ce[A']_3(thf)$) and neodymium ($Nd[A']_3(thf)$) have lower activity than any of the divalent species, probably reflecting the steric congestion around the smaller radii (Ce^{3+} 1.07 Å; Nd^{3+} 1.03 Å for CN 7).

An analysis of lanthanide allyl complexes that have been reported to polymerize MMA reveals that the potassium lanthanate complexes $K[Ln\{A'\}_4]$ are more efficient catalysts than the neutral complexes, and exhibit TOF values that are 10–100 times greater.[33] Interestingly, the potassium complex K[A′] displayed the highest TOF for MMA polymerization of all tested compounds (104,000 h^{-1}). Given its level of activity, it is possible that the increased effectiveness of the salt complexes stemmed from the presence of the alkali cations, a hypothesis supported by the higher TOF values that accompanied increased amounts of K[A′] in catalyst mixtures. Cation effects are recognized as important variables in anionic polymerization,[43] and the presence of alkali metal ions should be considered in studies of allyl lanthanide salt complexes in such polymerizations.

The homoleptic complexes MA'_2 (M = Cr, Fe, Co, Ni) have been tested as catalysts for the polymerization of norbornene.[44] Even when activated with methylaluminoxane (MAO), the Fe and Co compounds are only weakly active, but the Cr and Ni complexes are both active and generate high molecular weight poly(norbornene)s. This is rare

behavior for any type of chromium catalyst. Ethylene was polymerized by CrA'_2 alone, and its activity was depressed by the presence of MAO. In contrast, a $CrA'_2/B(C_6F_5)_3$ mixture was active for ethylene polymerization but not for norbornene; NMR evidence suggests that the $B(C_6F_5)_3$ generates the $[CrA'_2]^+$ cation, which is presumably the active polymerization agent. Ethylene/norborne copolymerization was possible in the $CrA'_2/B(C_6F_5)_3$ system, although the activity was low, and only limited norbornene insertion (11%) was observed.

Conclusions

It has been scarcely a decade since the chemistry of metal complexes containing sterically enhanced allyl ligands expanded beyond the organolithium compounds with which many of the ligands were originally associated. The increase in thermal and kinetic stability associated with the bulky ligands has allowed the synthesis of new types of compounds (e.g., CrA'_2), stabilized versions of known complexes (e.g, NiA'_2), the first structural authentication of mixed bonding modes in a single allyl complex (i.e., in $[MnA'_3]^-$) and has added cation-π bonding to the σ/π duality of allyl bonding (e.g., in $\{Mg[A']_2\}_2$).

There are certainly many challenges that lie ahead in the field of bulky allyl complexes. Synthetically, almost none of the second and third row transition metals are represented, even though in some cases the unsubstituted versions have been known for a long time ($Pd(C_3H_5)_2$, $Pt(C_3H_5)_2$). A broader range of bulky substituents, including hydrocarbyl groups such as *i*Pr and *t*Bu, needs to be explored, as they will provide

electronic features different from the trialkylsilyl groups that have served as the workhorses of the chemistry. Some of the polymerization reactions observed to date are promising, especially with the biologically compatible s-block metals, but considerable progress in improving stereocontrol will be needed to increase their attractiveness as practical initiators.

On the whole, however, the substituent chemistry already known demonstrates how much the chemistry of the "little" allyl ligand can "grow up" when augmented with bulky groups. Advancements in the coming years can be expected to be interesting indeed.

CHAPTER II

BONDING MOTIFS IN BULKY ALLYL COMPLEXES OF BERYLLIUM AND MAGNESIUM: THE ROLE OF SOLVENT

Introduction

A characteristic feature of the allyl anion is its ability to adopt σ- or π-coordination modes in metal complexes.[1] Whether "classically" σ-bound (η^1), or in a more symmetrical, bridged π-bound (η^3) form, the preference for a specific allyl arrangement has a strongly metal-driven component. Complexes of the alkali metals[19,25,33-34,45] and f-block elements, for example, almost always possess π-bonded allyls,[18,33,46] but the post-transition p-block metals typically display σ-bound allyl ligands.[47] In this regard, the alkaline-earth elements represent something of a watershed. Bonding in heavy alkaline earth organometallic compounds is largely ionic, reflecting the low electronegativity of calcium, strontium, and barium;[48] not surprisingly, the allyl complex $[Ca\{C_3(SiMe_3)_2H_3\}\bullet(thf)_2]$ has π-bound ligands.[49]

In contrast, allyls in magnesium complexes are consistently found to be σ-bonded in the solid state, however, and η^3-coordination of the allyl ligand to magnesium has been suggested as being intrinsically disfavored.[29] That there should be a crossover between the structure and reactivity of organomagnesium compounds and analogues with the heavier Group 2 metals is not unexpected.[50] Nevertheless, the balance between covalent and ionic bonding in allylmagnesium complexes (and corresponding σ- and π-coordination) may

be subtler than indicated by the available solid-state data. For example, an early calculation on [(C_3H_5)MgH] (gas-phase) suggested that the lowest energy conformation of the allyl ligand was intermediate between the classical σ-bonded and bridged π-bonded forms;[51] a similar calculation on [(C_3H_5)MgF], however, favored a more classically σ-bound form.[36] IR and ^{13}C NMR spectra indicate that allyl- and methallyl-*d*2-Mg bromides appear to be involved in an exchange process in solution, presumably via unsymmetrical σ-bonded allylic structures.[36] Yet unlike the Grignard reagents, the methylene resonances of [$Mg(C_3H_5)_2$] in THF are not significantly broadened at reduced temperature, and the deuterated compound does not have distinct double bond stretching bands in the IR spectrum, suggesting that delocalized π-type bonding is present.[36]

Despite its being a member of the highly electropositive s-block elements, little is known about the bonding of allyl ligands to beryllium, the lightest of the Group 2 metals. In fact, the large charge/radius ratio of beryllium insures that its compounds display considerable covalency.[52] A wide variety of ligand types has been incorporated into beryllium complexes, including alkyls,[53] alkynyls,[54] aryls,[55] amides,[56] thiolates,[56] arsenides,[57] carbenes,[58] trimethylsilyls,[59] tris(pyrazolyl)hydroborates[60] and various types of substituted cyclopentadienyl ligands;[4c,61] compounds of the latter, such as beryllocene,[62] often display unusual structures. Di(allyl)beryllium and several adducts were reported by Wiegand and Thiele,[63] who prepared the parent compound from the reaction of diethylberyllium and tri(allyl)boron. The unsolvated product is virtually insoluble in hydrocarbon solvents, melts above 200 °C, and is presumably polymeric, although its

structure has not been determined. It dissolves in THF, from which a disolvate ($[Be(C_3H_5)_2(thf)_2]$), structure also unknown, can be isolated.

Sterically enhanced allyl ligands[20,64] and those with pendant groups[29,65] have been used to suppress oligomerization and enhance solubility in a wide range of metal complexes, and we were lead to investigate their use with beryllium and magnesium. Examples like those above raise the question of where the balance between σ- and π-bonding in allyl beryllium and magnesium complexes lies, and in particular, do solvent coordination and steric effects alter the preferred arrangements? We have addressed this issue through the preparation of allyl complexes containing sterically bulky allyl ligands and with density functional theory (DFT) calculations on selected beryllium and magnesium allyl species.

Experimental

General Considerations. The syntheses and manipulations described below were conducted with rigorous exclusion of air and moisture using high-vacuum, Schlenk, or glovebox techniques. **CAUTION! BERYLLIUM SALTS ARE EXTREMELY TOXIC AND SHOULD BE HANDLED WITH APPROPRIATE CARE.** Proton (^1H) NMR and carbon ($^{13}C\{^1H\}$) NMR spectra were recorded on a Bruker DPX-300 at 300 MHz or a Bruker DPX-400 at 400 MHz and 100 MHz and were referenced to residual proton and ^{13}C resonances of C_6D_6. Variable temperature ^1H NMR spectra were recorded on a Bruker DRX-500 at 500 MHz and were referenced to residual proton resonances of toluene-d_8. Beryllium (^9Be) NMR spectra were recorded on a Bruker DPX-400 at 56.2 MHz and were referenced to an external standard of $Be(H_2O)_4^{2+}$ (as the sulfate salt).

Solution FTIR spectra were acquired on a Thermo Mattson Satellite FTIR using a sealed cell with KBr windows and a 1.0 mm path length. Elemental analysis was performed by Desert Analytics (Tucson, AZ).

Materials. Hexane and diethyl ether were distilled under nitrogen from potassium benzophenone ketyl. Anhydrous tetrahydrofuran (THF) was purchased from Aldrich and used as received. Anhydrous metal salts were purchased from Strem Chemicals and used as received. Benzene-d_6 and toluene-d_8 were vacuum-distilled from Na/K (22/78) alloy and stored over Type 4A molecular sieves prior to use. K[1,3-$(SiMe_3)_2C_3H_3$][33] and $[MgA'_2(thf)_2]$[66] were prepared following the published procedures.

Synthesis of $[Be(C_3(SiMe_3)_2H_3)_2(Et_2O)]$ $[BeA'_2(Et_2O)]$ (1). A solution of KA′ (0.4487 g, 2.0 mmol) in Et_2O was added to a stirred solution of $BeCl_2$ (0.0799 g, 1.0 mmol) in Et_2O at room temperature. After 2 h of stirring, all volatiles were removed under vacuum and the remaining residue was extracted over a medium porosity frit with hexane. The filtrate was collected and all volatiles were removed under high vacuum over 18 h to afford a viscous colorless oil. Large, colorless, air-sensitive blocks suitable for X-ray diffraction of $BeA'_2(Et_2O)$ were obtained from a concentrated hexane solution of the above at -10 °C (0.346 g, 77% crude yield). Elemental analysis calcd for $C_{22}H_{52}BeOSi_4$ (%): 1.99 Be; found 1.56 Be. ^{1}H NMR (400 MHz, C_6D_6, 298 K): δ (ppm) = 0.23 (s, 36H, $Si(C\underline{H}_3)_3$); 3.33 (d, 4H, C1,C3-allyl-H, ^4J = 15 Hz); 6.53 (t, 2H, C2-allyl-H, ^3J = 15 Hz); 0.79 (t, 6H, $(C\underline{H}_3CH_2)_2O$, ^3J = 7.1 Hz); 3.40 (q, 4H, $(CH_3C\underline{H}_2)_2O$, ^3J = 7.0 Hz). $^{13}C\{^1H\}$ NMR (100 MHz, C_6D_6, 298 K): δ (ppm) = 0.44 (s, $Si(\underline{C}H_3)_3$); 13.9 (s, $(CH_3\underline{C}H_2)_2O$); 31.9

(s, C1,C3-allyl-C); 68.5 (s, ($\underline{C}H_3CH_2)_2O$); 153.8 (s, C2-allyl). ^{9}Be NMR (56.2 MHz, C_6D_6, 298 K): δ (ppm) = 18.2.

Observation of Schlenk Equilibrium in Solution. A solution of KA′ (0.2244 g, 1 mmol) in Et_2O was added to a stirred solution of $BeCl_2$ (0.0799 g, 1 mmol) in Et_2O at room temperature. This reaction was allowed to proceed for 1 h, after which time 1 mL of the reaction mixture was passed through a 0.22 μm syringe filter into an NMR tube. ^{9}Be NMR (56.2 MHz, Et_2O, 298 K): δ (ppm) = 4.7 (s, $BeCl_2(Et_2O)_2$); 7.6 (s, A′$BeCl(Et_2O)_2$); 18.4 (Be$A'_2(Et_2O)_2$). The relative peak heights correspond to a ratio of 1:2:1, respectively.

Synthesis of [Mg{$C_3(SiMe_3)_2H_3$}$_2$$Et_2O$] [Mg$A'_2Et_2O$] (2) and {Mg[1,3-$(SiMe_3)_2C_3H_3$]$_2$}$_2$ [MgA'_2]$_2$ (3). A suspension of $MgBr_2$ (0.205 g, 1.11 mmol) in Et_2O was cooled to -40 °C. To this, a cold (-40 °C) solution of KA′ (0.500 g, 2.23 mmol) in Et_2O was added dropwise. The resulting suspension was stirred at room temperature for 1 h and filtered over a medium porosity frit. All volatiles were removed from the resulting yellow filtrate to yield **2** as a light yellow solid. ^{1}H NMR data were consistent with a mono-Et_2O solvate.

Drying the solvate overnight under vacuum followed by recrystallization from a minimum amount of hexanes (~ 5 mL) afforded a crop of light yellow plates of **3** (0.381 g, 88%); mp 92-98 °C. Anal. Calc. $C_{18}H_{42}MgSi_4$: C, 54.71; H, 10.71; Mg, 6.15. Found: C, 51.39; H, 10.76; Mg, 5.82. The low carbon value is attributed to the high air sensitivity of the complex. ^{1}H NMR (tol-d_8, 298 K): δ 6.83 (br s, $w_{½}$ = 37.2 Hz, 2 H), 3.43 (br s, $w_{½}$ = 33.2 Hz, 4 H), 0.22 (s, 36 H). Broadening is due to the complex nature of the species in solution. Variable temperature NMR spectra are supplied below. ^{13}C{^{1}H} NMR (C_6D_6,

298 K): δ 73.5 (br), 70.9 (br), 70.5 (br), 66.9 (s), 33.6 (s), 31.6 (s), 29.1 (s), 28.2 (s), 25.3 (s), 24.7 (s), 22.7 (s), 14.0 (s), 13.8 (s), 1.66 (s, $SiMe_3$), 0.80 (s, $SiMe_3$), -1.14 (s, $SiMe_3$), -2.32 (s, $SiMe_3$).

Computational Details. All calculations were performed with the Gaussian 03W suite of programs.[67] For the [Be(C_3H_5)X] species, Truhlar's BB1K functional was used;[68] this is a one-parameter hybrid based on the BB95 functional that is expressly designed for thermochemical kinetics. For basis sets, Dunning's augmented triple zeta aug-cc-pVTZ was used for C, H, and Br. The importance of including core valence correlation in reproducing binding energies in alkali and alkaline-earth metal complexes[69] lead to the use of the cc-pCVTZ basis set on Be (13s,7p,3d,1f)/[6s,5p,3d,1f] and on Mg (17s,12p,4d,2f)/[7s,6p,4d,2f]. All molecules were optimized with ultrafine grids and the GDIIS algorithm[70] (keywords: "Opt=(GDIIS) Integral=(Grid=Ultrafine)"). The nature of the stationary points (minima or transition structures) was determined with analytical frequency calculations.

For the [Be(1,3-(SiH_3)$_2$$C_3H_3$)$_2$] species, the B3PW91 functional, which incorporates Becke's three-parameter exchange functional[71] with the 1991 gradient-corrected correlation functional of Perdew and Wang,[72] was used. This hybrid functional has previously been shown to provide realistic geometries for organometallic species.[41,73] For basis sets, Dunning's augmented double zeta aug-cc-pVDZ was used on all atoms. Atomic coordinates for all optimized structures are given in Appendix C.

General Procedures for X-ray Crystallography. Crystals were located and placed onto the tip of a 0.1 mm diameter glass capillary tube or fiber and mounted on a Bruker

SMART CCD Platform diffractometer for a data collection at 100.0(1) or 200(2) K. A preliminary set of cell constants and an orientation matrix were calculated from reflections harvested from three orthogonal wedges of reciprocal space. The full data collection was carried out using Mo-Kα radiation (graphite monochromator) with a frame time of 60 seconds and a detector distance of 3.98 cm. A randomly oriented region of reciprocal space was surveyed: four major sections of frames were collected with 0.50° steps in ω at four different ϕ settings and a detector position of -38° in 2θ. The intensity data were corrected for absorption. Final cell constants were calculated from the xyz centroids of 7742 strong reflections from the actual data collection after integration.

The structures were solved using SHELXS-97[74] and refined using SHELXL-97.[74] The structure of **1** refined as a pseudo-merohedral twin (approximating C-centered monoclinic), with a refined mass ratio of 61:39. Application of the twin law, [1 0 0 / -1 -1 0 / -1 0 -1], reduced the R_1 residual from 24.3 % to 4.61 %. The final full matrix least squares refinement converged to R_1 = 0.0461 (F^2, $I > 2s(I)$) and wR_2 = 0.0960 (F^2, all data). Relevant crystal and data collection parameters and atomic coordinates for each compound are given in Appendix B.

Results and Discussion

Beryllium allyls. The colorless complex **1** was synthesized via the salt metathesis reaction of $BeCl_2$ and KA′ in Et_2O (eq 7). The product is highly air- and moisture-sensitive, and is extremely soluble in a wide range of solvents, from ethers to alkanes.

$$BeCl_2 + 2\ K[A'] \xrightarrow[-2\ KCl]{Et_2O,\ 0\ °C} [BeA'_2(Et_2O)] \quad (7)$$

Table 1. Selected bond distances and angles for $[BeA'_2(Et_2O)]$.

atoms	distance (Å)	atoms	angle (°)
Be–C1	1.752(5)	C1–Be–C4	137.65(16)
C1–C2	1.479(4)	O–Be–C1	109.38(14)
C2–C3	1.343(4)	O–Be–C4	112.91(14)
Be–C4	1.756(4)		
C4–C5	1.484(3)		
C5–C6	1.336(4)		
Be–O	1.661(4)		

Single crystals of **1** were grown from hexane, and the complex was found to be monomeric in the solid state (Figure 10). Selected bond distances are highlighted in Table 1. The compound crystallizes in the triclinic space group $P\bar{1}$, and each Be center is surrounded by two σ-coordinated allyl moieties and the oxygen of a diethyl ether molecule in a distorted, but nearly perfectly flat, trigonal planar environment (sum of angles around metal = 359.9°). It represents the first crystal structure of an allyl beryllium complex.

The Be–C distances of ca. 1.75 Å are similar to those observed in the three-coordinate *m*-terphenyl complexes Ar*BeX$(OEt)_2$ (Ar* = -C_6H_3-2,6-$(mesityl)_2$) of 1.740(6) Å (X = Cl) and 1.749(7) Å (X = Br), and in $BePh_2(OBu_2)$ (1.734(2) Å).[58b] The C1–C2/C2–C3 and C4–C5/C5–C6 distances differ by 0.14 Å, and are strongly localized into single and double bonds. The Be–O distance of 1.661(4) Å is within the normal range for Be–O bonds (1.60–1.69 Å), and is comparable to that in $BeMes_2(OEt_2)$ (1.638(5) Å)[55a] and $BePh_2(OBu_2)$ (1.647(2) Å).[58b]

Complexes of the type BeR_2 are good Lewis acids and form stable etherates, and obtaining solvent-free complexes can be challenging.[1] Unlike the related magnesium complex **3** (vide infra), **1** does not desolvate under vacuum. An attempt to use the

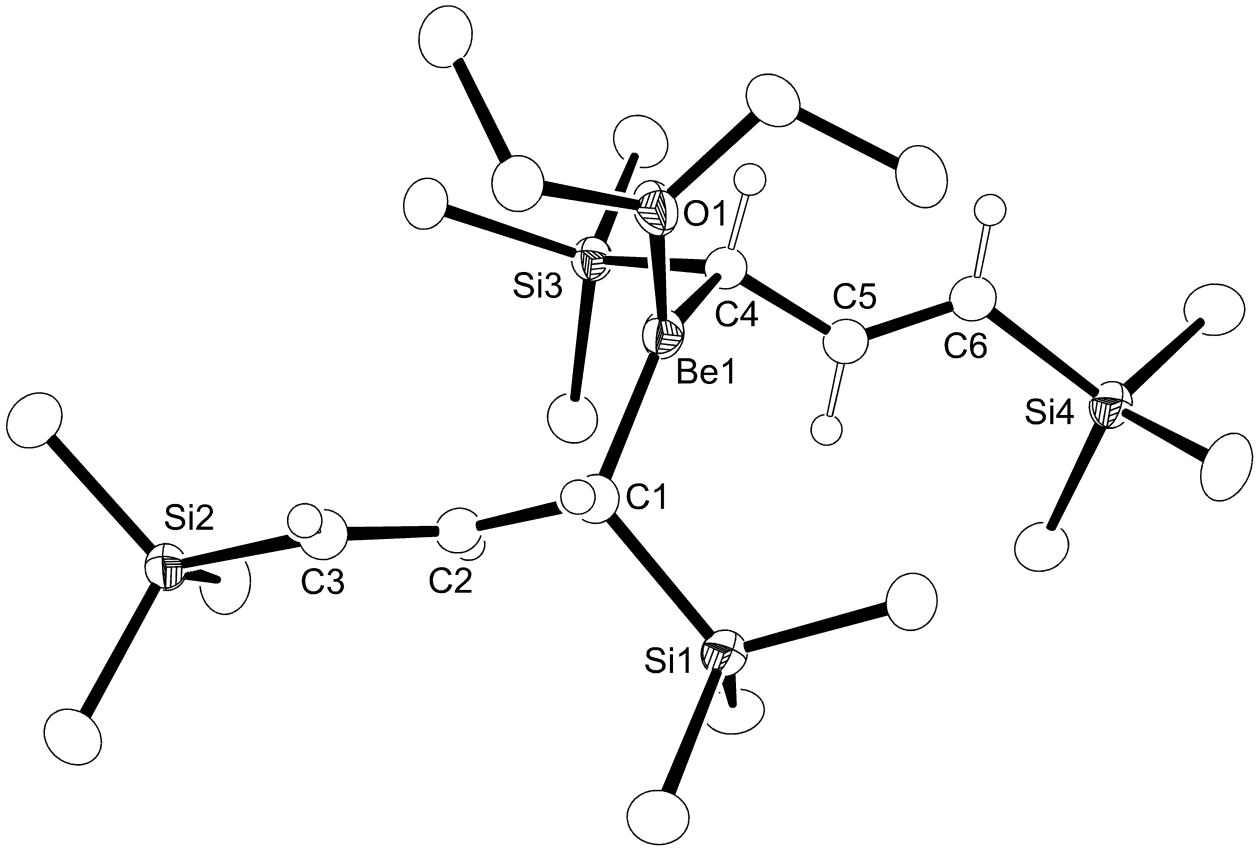

Figure 10. ORTEP of $BeA'_2(Et_2O)$ (**1**) with the numbering scheme used in the text. Non-allylic hydrogens have been omitted for clarity and thermal ellipsoids are shown at the 50% probability level.

azeotropic "toluene reflux" method[38] to remove the coordinated ether (8 h total time) was also unsuccessful, although the complex showed no signs of decomposition during the process. An effort was made to form an adduct with 2,2′-bipyridine by treating a suspension in ether of the colorless $[BeCl_2(bipy)]$[75] with KA′; the mixture immediately turned deep red, similar to the result from the reaction of bipy with $[Be(C_3H_5)_2(thf)_2]$.[63] Attempted removal of the solvent generated an insoluble brown solid and a deep green oil, the latter possibly containing $[Be(bipy)_2]$.[75]

As is the case for the σ-bonded complex $[GaA'_3]$,[47a] the ^1H NMR spectrum of **1** at room temperature presents a simple "π-like" pattern of an apparent singlet (the H from $SiMe_3$), doublet, and triplet (Figure 11). The compound is clearly fluxional in solution, however, and on cooling, the doublet from the terminal protons shifts downfield and eventually broadens into a singlet (by -50 °C); by -70 °C it almost disappears into the baseline, whereas the triplet from the central proton simply broadens and the $SiMe_3$ resonance shifts but remains unsplit, suggesting that the exchange process involving σ/π fluxionality is of low energy.

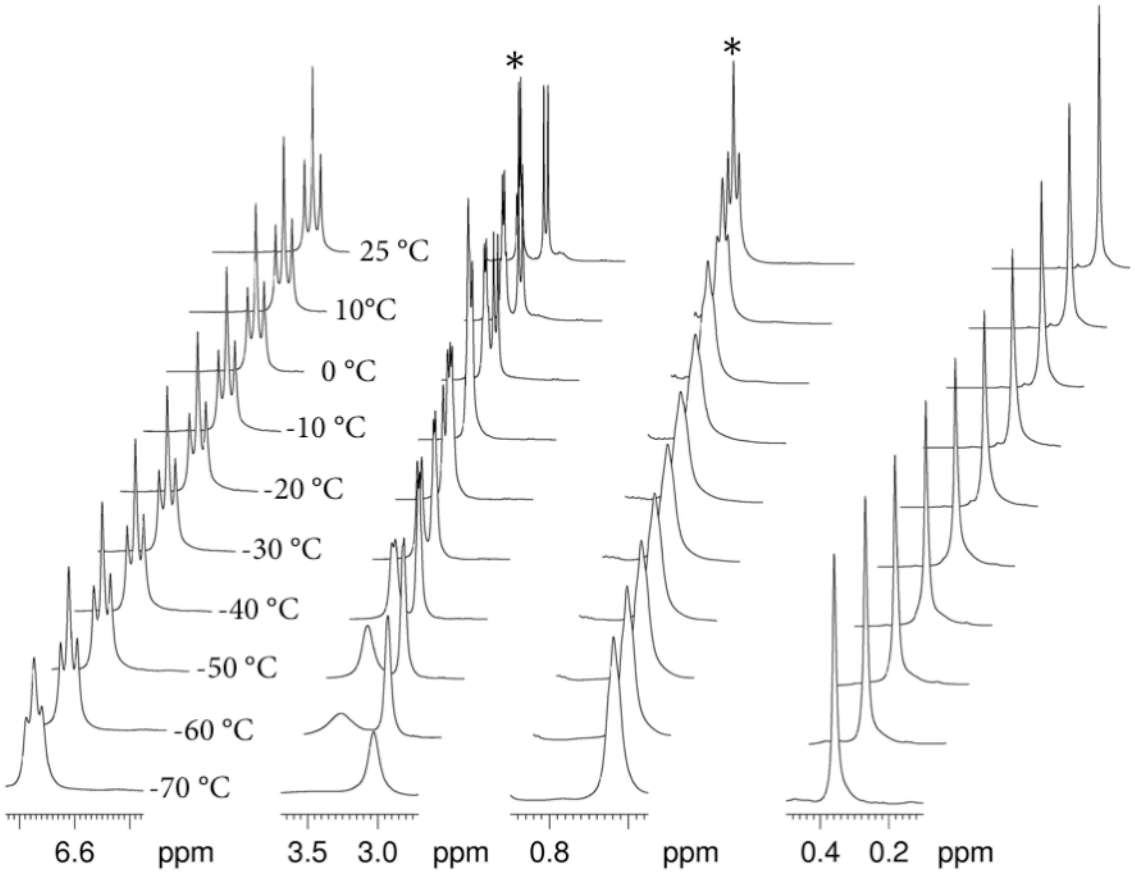

Figure 11. Variable temperature ^{1}H NMR spectra of [BeA′$_2$(Et$_2$O)]. An asterisk (*) marks the resonances of the diethyl ether ligand. The vertical heights of the regions are not to scale.

Evidence for the persistence of a σ-bonded structure in solution is provided by IR and beryllium NMR measurements. A broad absorption at 1568 cm^{-1} is observed in an Et_2O solution for **1**; this is close to the double bond stretching frequencies observed in ether for diallyl magnesium and allyl magnesium bromide (1577 and 1588 cm^{-1}, respectively); both compounds are known to have σ-bonded allyl ligands.[36] John and coworkers have tabulated ^{9}Be NMR chemical shift values that are diagnostic for coordination numbers in solution.[76] Specifically, organoberyllium complexes that contain multihapto ligands, like beryllocene (δ = -18.5 ppm in toluene), resonate substantially upfield of 0 ppm (> -15 ppm), whereas those with lower formal coordination numbers, like the diethyl etherate of dimethylberyllium (δ = 20.8 ppm in Et_2O), resonate well downfield of 0 ppm. This pattern is similar to that observed with ^{25}Mg NMR.[77] Complex **1** has a ^{9}Be chemical shift of δ 18.2 ppm, which is consistent with a 3-coordinate geometry in solution on the ^{9}Be NMR timescale. DFT investigations were used to predict the ^{9}Be chemical shift value of **1**, and with the method described by John (B3LYP/6-311+G(2d,p)//B3LYP/6-31G(d)),[76] it was calculated to be δ 20.4 ppm, in good agreement with the observed value.

Grignard-type organomagnesium complexes (RMgX, where R = alkyl or aryl and X = halide) are known to undergo rapid scrambling in solution. There is evidence for this so-called Schlenk-type equilibrium in the ^{9}Be NMR spectrum of the reaction between equimolar amounts of KA′ and $BeCl_2$ (eq 8).

$$KA' + BeCl_2 \xrightarrow[-1\ KCl]{Et_2O,\ 0\ ^\circ C} [BeA'Cl(Et_2O)] \rightleftharpoons [BeA'_2(Et_2O)] + [BeCl_2(Et_2O)] \quad (8)$$

After the reaction was allowed to proceed for 1 h, three peaks were observed in the ^{9}Be NMR spectrum of the filtered reaction mixture; their shifts and assignments are listed in Table 2. The resonance at δ 18.4 ppm almost matches that for **1** alone, and the peak assigned to $[BeCl_2(Et_2O)_2]$ is close to the value reported for the isolated complex measured in Et_2O (δ 3.1 ppm).[78] It also has the narrowest width of the three resonances, a feature associated with 4-coordinate beryllium structures of high symmetry.[76] This is the first time Schlenk equilibrium in organoberyllium compounds has been directly observed with ^{9}Be NMR spectroscopy.[79] The relative peak heights indicate that a statistical distribution of species exists, unlike the case with RBeX compounds containing less bulky R groups (e.g., Me, Ph), where the equilibrium lies toward the RBeX side.[53b]

Table 2. NMR parameters for the products from the equimolar reaction of KA′ and $BeCl_2$ in Et_2O.

Compound	δ (ppm)[a]	relative area	$w_{1/2}$ (Hz)
$[BeCl_2(Et_2O)_2]$	4.7	1	14.2
$[A'BeCl(Et_2O)_2]$	7.6	2	27.4
$[BeA'_2(Et_2O)]$	18.4	1	91.9

[a] shifts in ppm from 1.0 M $Be^{2+}(aq)$ (as the sulfate salt)

Magnesium allyls. The colorless complex $[MgA'_2(thf)_2]$ was synthesized previously[66] by the salt metathesis reaction of 1 equiv of $MgBr_2$ and 2 equiv KA′ in THF. The molecule is fluxional in solution; at –45 °C, the ^{1}H NMR spectrum indicates that the compound possesses σ-bonded A′ ligands, as evidenced, for example, by the appearance of inequivalent $SiMe_3$ groups. At room temperature and above, the spectrum presents an increasingly simplified "π-like" pattern with an apparent triplet, an apparent doublet, and

a singlet (for the $SiMe_3$ groups). Similar solution behavior is observed in the [GaA'_3] complex,[47a] and reflects the presence of equilibrating allylic isomers.

In the solid state, molecules of [$MgA'_2(thf)_2$] are nearly C_2-symmetric; each Mg center is surrounded by two σ-coordinated allyl moieties and two THF solvent molecules in distorted tetrahedral environment. The Mg–C distances of ca. 2.20 Å are typical for terminal Mg-allyl groups in neutral complexes, such as those in the dinuclear compound [$(\sigma\text{-}C_3H_5)Mg(tmeda)(\mu_2\text{-}Cl)]_2$ (2.179 Å)[80] and the coordination polymers [$Ln(\eta^3\text{-}C_3H_5)_3(\mu\text{-dioxane})Mg(\eta^1\text{-}C_3H_5)_2(\mu\text{-dioxane})_{1.5}]_\infty$ (Ln = La, Y; Ln–C = 2.188–2.197 Å).[81]

In an attempt to confirm experimentally the prediction that π-bonding would be preferred in magnesium allyl complexes in the absence of coordinated bases (vide infra), the more easily desolvated compound [$MgA'_2(Et_2O)$] (**2**) was synthesized in a manner similar to that of [$MgA'_2(thf)_2$], with a salt metathesis reaction of $MgBr_2$ and KA′ in diethyl ether. Under vacuum, the coordinated ether is lost, which leads to the formation of the dimeric $[MgA'_2]_2$ (**3**).

Crystals of **3** were grown from a concentrated hexane solution. Selected bond distances and angles of the structure (Figure 12) are highlighted in Table 3.

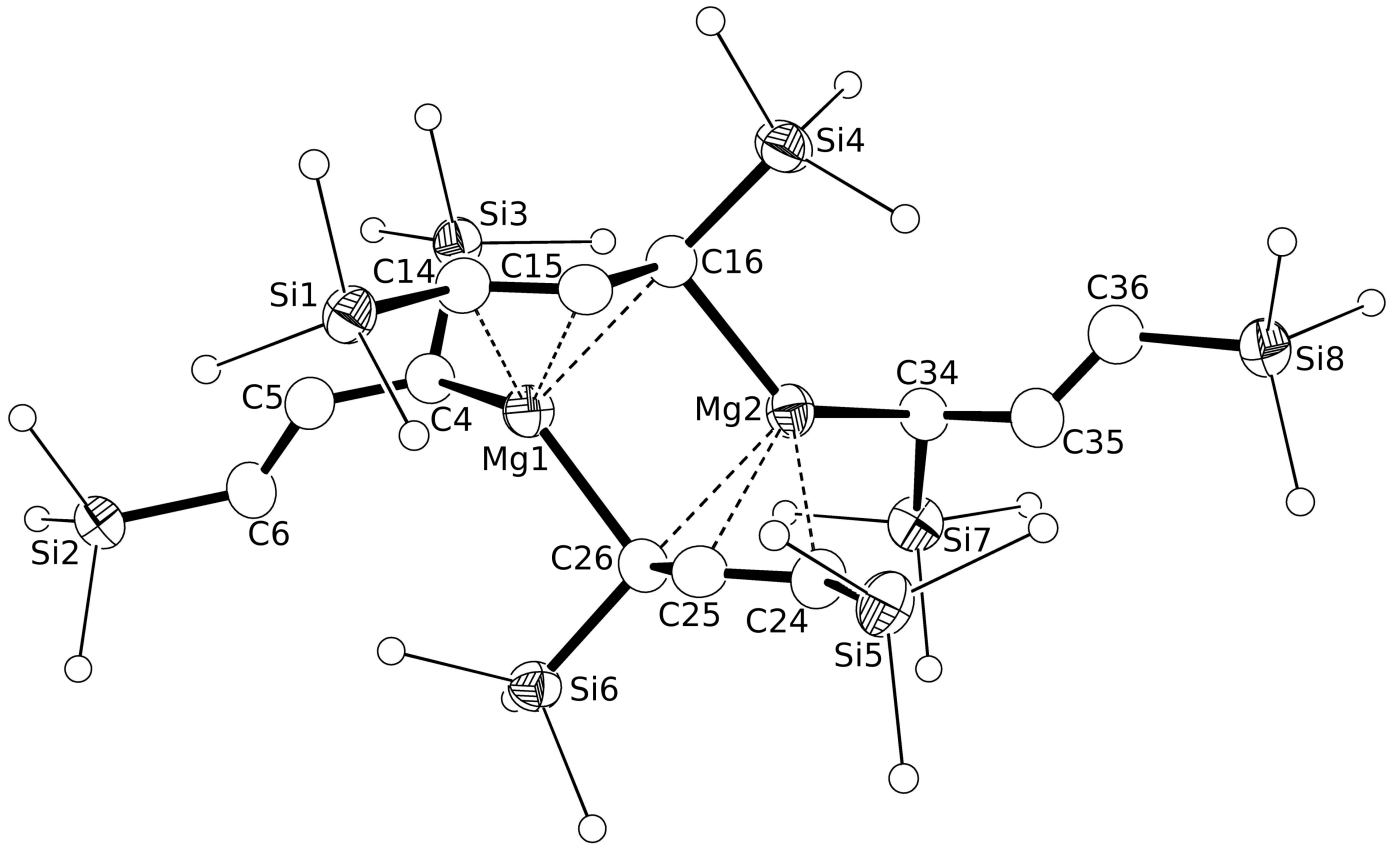

Figure 12. ORTEP of the non-hydrogen atoms of $[MgA'_2]_2$ (**3**) with the numbering scheme used in the text. For clarity, methyl groups are rendered as spheres of arbitrary size. Thermal ellipsoids are shown at the 50% probability level.

Table 3. Selected bond distances and angles for $[MgA'_2]_2$.

atoms	distance (Å)	atoms	angle (°)
Mg1–C4	2.139(2)	C4–Mg1–C26	126.76(9)
Mg1–C26	2.234(3)	C16–Mg2–C34	128.42(10)
Mg2–C16	2.232(2)	C4–C5–C6	128.6(2)
Mg2–C34	2.138(2)	C14–C15–C16	128.6(2)
C4–C5	1.476(3)	C24–C25–C26	129.4(2)
C5–C6	1.335(3)	C34–C35–C36	129.4(3)
C34–C35	1.484(3)		
C35–C36	1.328(4)		
C24–C25	1.353(3)		
C25–C26	1.468(3)		
C14–C15	1.355(3)		
C15–C16	1.471(3)		

The base-free complex is a dinuclear species in the solid state in which the two Mg atoms are coordinated in an irregular fashion. A σ-bound, terminal allyl is present on each magnesium, and two allyl ligands bridge between the metals. The $Mg–C'_{terminal}$ distances are identical within error, and are 0.06 Å shorter than the corresponding distance in the solvated **1**; the ligands have strongly localized single and double bonds (Δ_{CC} = 0.15 Å). The bridging allyls (C14–C16; C24–C26) are also of a localized type, with an average difference between the single and double bonds of 0.12 Å. Both metals contact the bridging allyls through one relatively short distance of ca. 2.23 Å (Mg1–C26, Mg2–C16).

The magnesium atoms are clearly not σ-bonded to the other carbon atoms in the bridging allyl ligands. The distance of Mg2 to C24–C26 is surprisingly uniform at 2.435(2)–2.464(3) Å, despite the difference in π-electron density on the ligands implied by the unequal C–C bond lengths. The Mg1 to C14–C16 distances are more varied, ranging from 2.438(2)–2.514(2) Å, and also span unequal C–C bond lengths. These Mg–C contacts are substantially longer than the ca. 2.25–2.35 Å distances calculated for

symmetrical π-type bonding interactions in $[Mg(C_3R_2H_3)_2]$ (vide infra), and are not well described by either an electrostatic M^{n+}–$[\pi\text{-}C_3H_5]^-$ or multicenter covalent bonding model; these models cannot reliably be distinguished by structural criteria alone.[51]

A cation-π description would fit the bonding of the magnesium centers to the C14–C16 and C24–C26 carbons. Allyl ligands can display cation-π interactions with alkali metals,[47b,82] but **3** appears to be the first structurally authenticated compound that exhibits cation-π interactions between Mg^{2+} and an allyl ligand. Mg–(π-donor) interactions have been studied by a variety of computational approaches; for $[M(C_2H_4)]^{2+}$, Sastry calculated a Mg–C distance of 2.41 Å and an interaction energy of 69 kcal mol^{-1};[83] for $[M(C_6H_6)]^{2+}$, a Mg–C distance of 2.40 Å and a binding energy of ca. 109 kcal mol^{-1} were determined. Others have found similar results for $[Mg(C_6H_6)]^{2+}$.[84] The bond distances (perhaps lengthened because of steric effects) and the expected strength of the cation-π interactions (sufficient to hold the dimer together in hydrocarbon solvents) are appropriate for **3**.

Similar to complex **2**,[66] the pale yellow ether solvate $[MgA'_2(Et_2O)_2]$ presents a "π-like" symmetry pattern of an apparent triplet, an apparent doublet, and a singlet in its ^1H NMR spectrum at room temperature. After removing coordinated solvent molecules under vacuum, however, the spectrum of the resulting pale yellow, base-free **3** becomes considerably more complex. Accordingly, variable temperature ^1H NMR spectra (Figure 13) were recorded from 210–350 K for the solvent-free **3**.

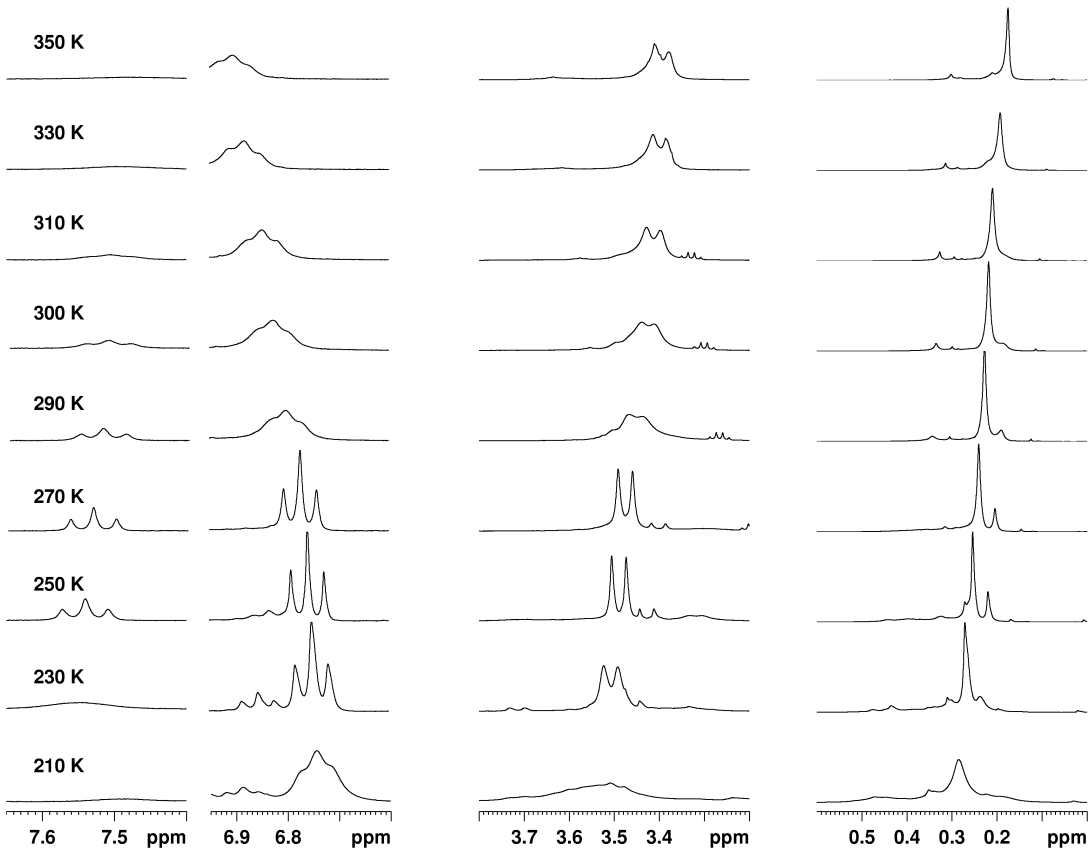

Figure 13. Variable Temperature ^{1}H NMR spectrum of $[MgA'_2]_2$. Plotted peaks are not to vertical scale.

At room temperature (300 K), the spectrum contains two broad peaks and a sharp singlet, suggestive of a less resolved version of the "π-like" spectra observed for **2**. The effect of temperature on the spectrum of **3** is different, however. Raising the temperature leaves the resonance associated with C2 as a broad singlet, for example; but that associated with the C1/C3 carbons splits into two broad singlets ($w_{½}$ = 19 Hz) whose separation increases with temperature. Conversely, at low temperature (230 K), the C2 resonance splits into two inequivalent triplets (J_{HH} = 16 Hz) and a broad singlet. The C1/C3 resonance sharpens to an inequivalent pair of nearly baseline-resolved doublets by 250 K with a J_{HH} = 16 Hz. Although not easily interpreted, the spectra suggest that the conformational changes in **3** are more complex than would be expected for a purely monomeric complex.

Computational investigations. Wu examined allyl metal bromides for a wide range of main-group metals at the MP2//HF level of theory, and determined that the minimum energy structure of [(C_3H_5)BeBr] contains a σ-bound allyl ligand.[85] In contrast, John and coworkers examined π-bonding for the allyl ligand in the compound [$(\eta^3$-$C_3H_5)$BeAs(*t*-Bu)$_2$], which was used as a model for the ring-slipped [$(\eta^3$-$C_5H_5)$BeAs(*t*-Bu)$_2$], and found that a π-bonded allyl on beryllium was reasonable.

This question was investigated for [(C_3H_5)BeH] at the BB1K/aug-cc-pVTZ level of theory,[68] and found that *both* σ- and π-bonded modes were minima (N_{imag} = 0) on the potential energy surface, with the π-bonded species 3.3 kcal mol^{-1} ($\Delta G°$) below the energy of the σ- bonded form (Figure 14). Little change in the C–C framework of the allyl ligand itself occurs in the move to the transition state; the major change is a rotation of

the BeH unit over the center of the allyl. The activation barrier to the transition geometry (N_{imag} = 1) is only 0.84 kcal mol^{-1} above the σ-bonded form, suggesting that $\eta^1 \rightleftarrows \eta^3$ equilibrium in solution should be facile. The same pattern is found for [(C_3H_5)BeBr] with DFT methods, but the higher electronegativity of bromine favors the σ-bonded form to a greater extent, so that the π-bonded form is only 1.2 kcal mol^{-1} ($\Delta G°$) more stable. The activation barrier to the transition geometry is 1.7 kcal mol^{-1} above the σ-bonded form.

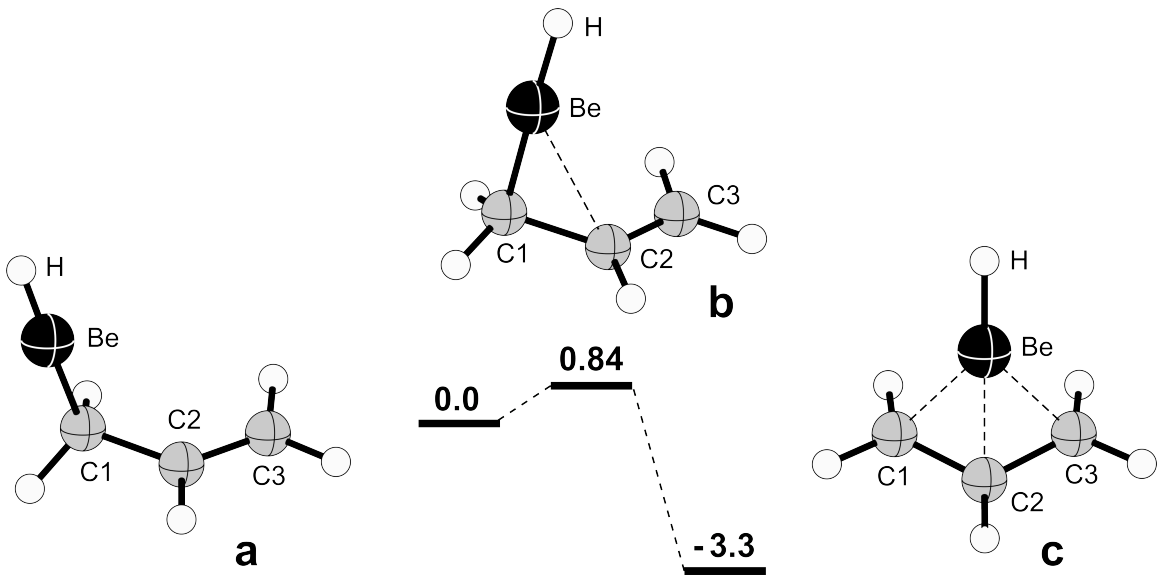

Figure 14. Free-energy profile (kcal mol^{-1}) for the $\eta^1 \rightleftarrows \eta^3$ bonding shift in $[(C_3H_5)BeH]$. Selected bond distances (Å) and angles (°) in (a): Be–C1, 1.681; C1–C2, 1.484; C2–C3, 1.323; Be–C1–C2, 107.5 (b): Be–C1, 1.677; Be…C2, 2.311; C1–C2, 1.482; C2–C3, 1.328; Be–C1–C2, 93.8 (c) (*Cs*) Be–C1, 1.839; Be–C2, 1.821; C1–C2, 1.390; Be–C1–C2, 67.0.

Additional DFT investigations were performed on a set of allyl complexes related to [BeA′$_2$(Et$_2$O)]. Silyl substitution has been shown to be a good compromise between unsubstituted and bis(trimethylsilylated) allyls in terms of computational time and accuracy,[66] and was employed for geometry optimizations with the B3PW91 functional and the aug-cc-pVDZ basis set for all atoms. The optimized geometries of these molecules are shown in Figure 15. Unlike the case with the magnesium counterpart,[66] (vida infra) but like the [(C$_3$H$_5$)BeX] species studied above, both σ- (with C_i symmetry, Figure 15a) and π-bound (with C_2 symmetry, Figure 15b) structures of [Be(1,3-(SiH$_3$)$_2$C$_3$H$_3$)$_2$] are local minima on the potential energy surface; $\Delta G°$ is lower for the π-bound structure by 4.0 kcal mol^{-1}. The σ-bound structure has distinctly localized C–C/C=C bonds, but the C1–C2 and C2–C3 distances of 1.429 and 1.401 Å, respectively, in the C_2 structure indicate that considerable delocalization of the π electrons in the allyl ligand has occurred. The Be–C1 and Be–C2 distances of 1.858 Å and 1.828 Å, respectively, are clearly within bonding distance (cf. the average Be–C distance in the π-bound ring of beryllocene of 1.92 Å[62b]); Be–C3 is slightly longer (1.985 Å). In view of the spread in the Be–C distances, it is probably appropriate to view the bonding as "slipped π".[66]

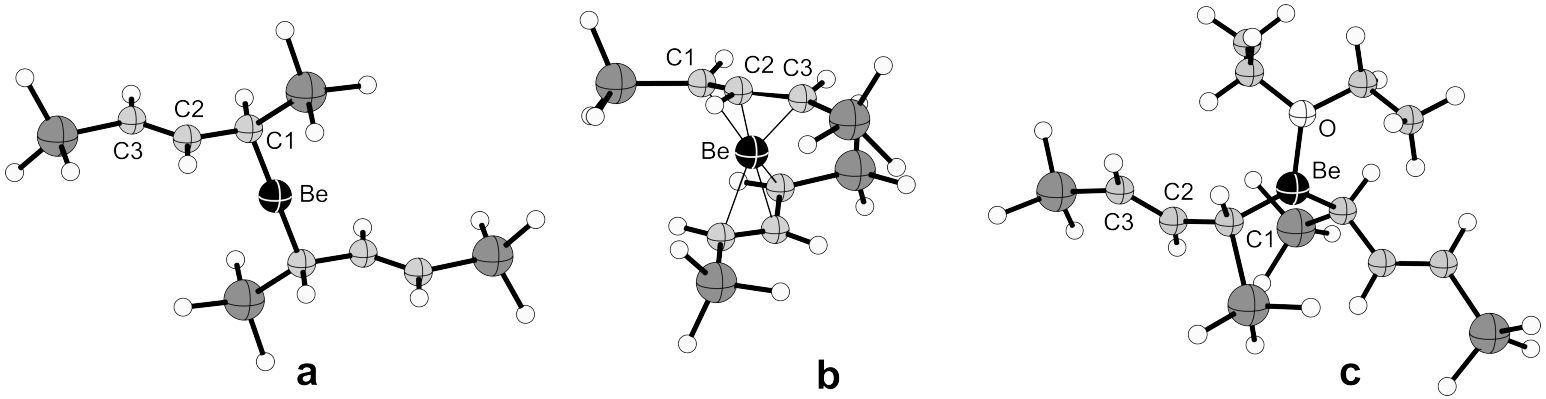

Figure 15. The optimized geometries of [Be(1,3-$(SiH_3)_2C_3H_3)_2$] showing both σ- (a) and π-type (b) bonding of the allyl moieties, and the effect of adding a single molecule of Et_2O (c). Selected bond distances (Å) for (a) (C_i): Be–C1, 1.684; C1–C2, 1.496; C2–C3, 1.349. (b) (C_2) Be–C1, 1.858; Be–C2, 1.828; Be–C3, 1.985; C1–C2, 1.429; C2–C3, 1.401. (c) Be–O, 1.698; Be–C1, 1.757; C1–C2, 1.485; C2–C3, 1.335.

DFT methods were also used to model the effect of solvation on [Be(1,3-$(SiH_3)_2C_3H_3)_2$]. Addition of a single Et_2O to the π-bound structure of [Be(1,3-$(SiH_3)_2C_3H_3)_2$] causes a simultaneous slip of both allyls to σ-bonding (Figure 15c), consistent with the solid state structure of for [BeA′$_2$(Et_2O)]. Although this shift may partially be driven by steric effects, exactly the same effect is found with the calculated structure of the less crowded [Be(σ-$C_3H_5)_2(Me_2O)$], so that electronic influences of the coordinated bases are likely involved as well.

DFT investigations (B3PW91/TZP-quality basis sets) were also carried out on a set of allyl Mg molecules related to **2** and **3**. Starting from a classical σ-bonded geometry, [Mg($C_3H_5)_2$] minimizes to a structure with C_2 symmetry (Figure 16a). The Mg–C1 and Mg–C2 distances of 2.226 Å and 2.231 Å, respectively, are clearly within bonding distance (cf. the average Mg–C distance in magnesocene of 2.30 Å);[86] Mg–C3 is slightly longer (2.326 Å). The C1–C2 and C2–C3 distances of 1.412 and 1.389 Å, respectively, indicate that considerable delocalization of the π electrons in the allyl ligand has occurred. As with the Be complex, in view of the spread in the Mg–C distances, it is probably appropriate to view the bonding as "slipped π". Attempts to maintain a σ-bonded structure during optimization by imposing symmetry restrictions (C_i) lead to a higher energy saddle point geometry (+4.5 kcal mol^{-1}) with two imaginary frequencies (29*i*, 91*i*).

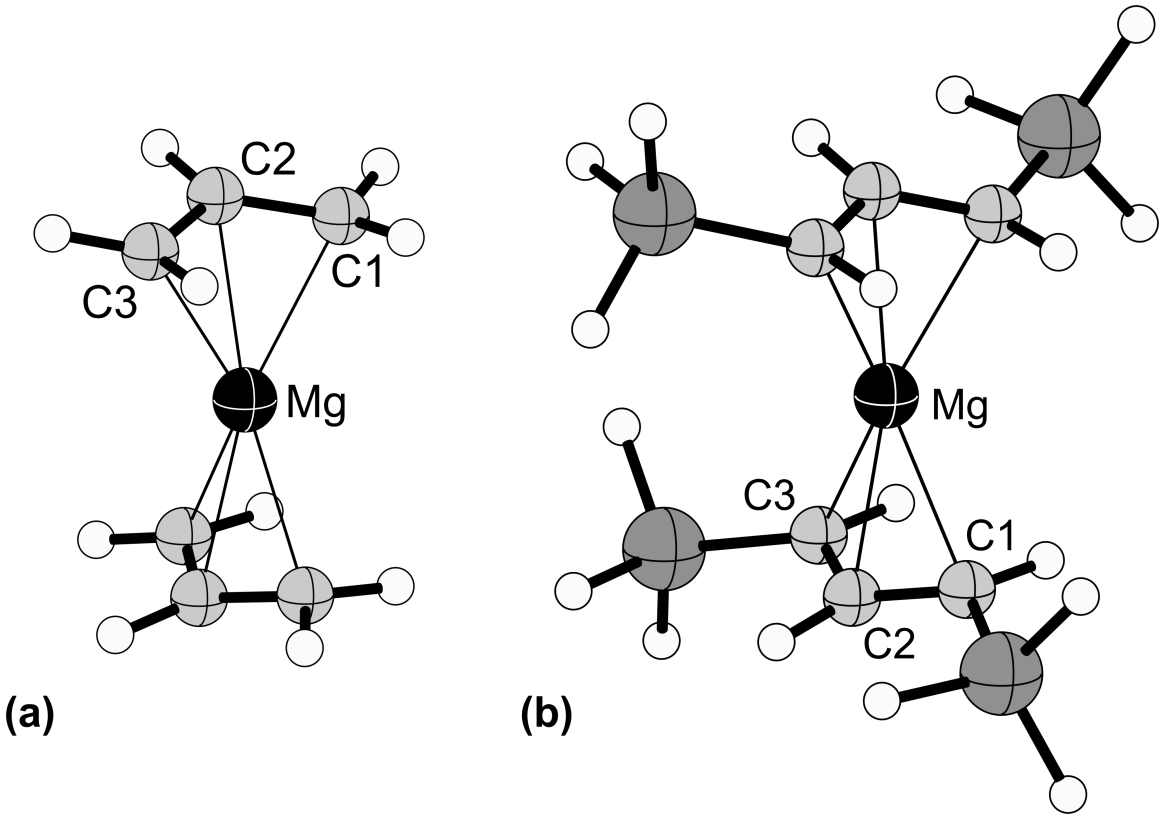

Figure 16. The calculated "slipped-π" structure of unsubstituted $[Mg(C_3H_5)_2]$ (a) and the calculated structure of $[Mg\{C_3(SiH_3)_2H_3\}_2]$ (b). Selected bond distances (Å) and angles (°): Mg–C1, 2.261; Mg–C2, 2.222; Mg–C3, 2.289; C1–C2, 1.410; C2–C3, 1.403; C1–C2–C3, 126.66°; relative twist of ligands, 89.1°.

Substitution of the allyl ligands with silyl moieties slightly refines the π-bound structure (Figure 16b). There is shrinkage of the range of Mg–C distances (Δ = 0.067 Å) compared to those in the unsubstituted allyl complex (Δ = 0.10 Å). Moreover, the C1–C2 and C2–C3 distances differ now by only 0.007 Å, indicating essentially complete delocalization of the π electrons. The near 90° twist of the ligands contrasts with the planar environment around Mg in the related 1-azaallyl complex $[Mg\{N(SiMe_3)C(t\text{Bu})C(H)(SiMe_3\}_2]$.[87] There are also hydrogen atom displacements that are similar to those found in other main-group and transition metal π-allyl structures; for example, the central C2–H bond is tipped toward the magnesium atom, and forms an angle of 10.9° with the C3 plane.[49] At this level of theory, $[Mg(C_3R_2H_3)_2]$ appears to be most stable with symmetrically π-bound allyl ligands.

Calculations indicate that addition of a single THF ligand to $[Mg(\pi\text{-}C_3H_5)_2]$ results in slippage of one allyl ligand to the classical σ-bonding mode (Figure 17a). The Mg–C(σ) distance is now 2.141 Å, and the C1–C2 and C2–C3 distances differ by 0.12 Å; they are substantially localized into single and double bonds. The other allyl has adopted a "slipped-π" geometry, with a Mg–C range of 2.26–2.36 Å, but the C4–C5 and C5–C6 bonds differ only by 0.013 Å, indicating that the π-electrons remain delocalized. The rearrangements here are reminiscent of those in $[Mg(\eta^1\text{-}C_5H_5)(\eta^5\text{-}C_5H_5)(thf)_2]$, in which the change of one η^5-Cp in $[Mg(\pi\text{-}C_5H_5)_2]$ to η^1-Cp on coordination of the THF was ascribed to steric crowding.[88]

Addition of a second THF molecule to $[Mg(\eta^1\text{-}C_3H_5)(\eta^3\text{-}C_3H_5)(thf)_2]$ causes both allyl ligands to assume σ-bonding modes (Figure 17b). The calculated C_2-symmetric

structure has Mg–C bond lengths of 2.176 Å, which are close to those observed in **2**. These results indicate how the presence of solvent molecules can drive the conversion from a delocalized π- to classical σ-bonding. However, unlike in the case for **1**, addition of coordinated bases causes successive slippage of the allyl ligands. This is likely an effect of the smaller radius of Be as compared to Mg.

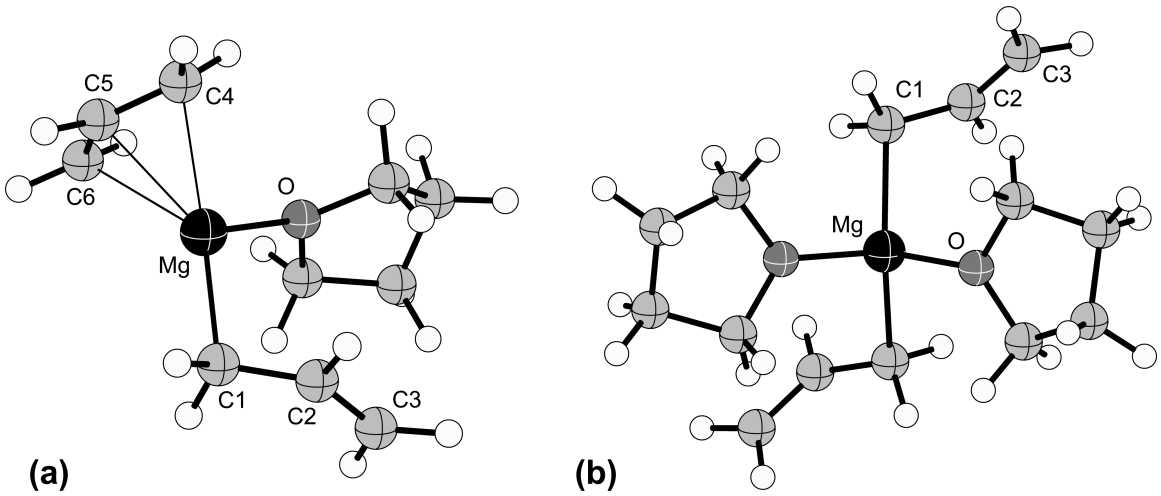

Figure 17. Calculated structure of $[Mg(C_3H_5)_2(thf)$ (a) and calculated structure of $[Mg(C_3H_5)_2(thf)_2]$ (b). Selected bond distances (Å) and angles (°) in (a): Mg–O, 2.070; Mg–C1, 2.141; Mg···C2, 2.95; C1–C2, 1.463; C2–C3, 1.343; C1–C2-C3, 128.67; Mg–C4, 2.298; Mg–C5, 2.264; Mg–C6, 2.363; C4–C5, 1.404; C5–C6, 1.391; C4–C5–C6, 127.68. Selected bond distances (Å) and angles (°) in (b): Mg–O, 2.105; Mg–C1, 2.176; Mg···C2, 3.02; C1–C2, 1.460; C2–C3, 1.344; C1–C2–C3, 128.78.

Conclusion

In summary, the first structural authentication of a σ-bound allyl beryllium complex has been achieved. The molecule is fluxional in solution, and a limiting spectrum was not obtained at -70 °C, indicating that the rearrangements are facile. In addition, the first spectroscopic evidence via ^{9}Be NMR spectroscopy of Schlenk-type equilibrium for an organoberyllium complex has been observed. A series of DFT experiments suggests that a beryllium complex that contains π-bound allyls is not only possible, but energetically favorable in the absence of coordinated bases.

In addition, it appears that true π-type bonding in magnesium allyl compounds, in which the metal symmetrically bridges a delocalized ligand, could be energetically favorable arrangement, but only in the absence of any perturbing forces.[84] Calculations indicate that a shift to classic σ-bonding will occur on coordination of a solvent, which may involve both donor and steric effects. Even when solvent influences are removed, as in **3**, the energetic benefits of cation-π interactions help drive a dimerization process, so that the magnesium centers engage in σ-,σ-,cation-π interactions. True π-bonding might still be observable in a magnesium complex, but only in special cases (e.g., with a set of substituted ligands that could enforce mononuclearity). With these results, it now appears that π-bonded allyls are reasonable for the entire set of Group 2 elements from Be to Ba.[89]

CHAPTER III

SOLUTION INTERACTION OF POTASSIUM AND CALCIUM BIS(TRIMETHYLSILYL)AMIDES; PREPARATION OF $Ca[N(SiMe_3)_2]_2$ FROM DIBENZYLCALCIUM

Introduction

The bis(trimethylsilylamides) of the alkaline-earth metal calcium, strontium, and barium have found expanding use as reagents in synthetic and materials chemistry.[90] Befitting their importance, multiple preparative routes have been developed for these silylamides. The THF-solvated calcium complex $Ca[N(SiMe_3)_2]_2(thf)_2$, for example, was originally obtained from the direct reaction of activated elemental calcium and $HN(SiMe_3)_2$ in refluxing THF,[91] by the reaction of $Ca(bht)_2(thf)_3$ (bht = 2,6-di-*tert*-butyl-4-methylphenoxide) and $Li[N(SiMe_3)_2]$ in hexane,[91] and by the transmetallation of $Hg[N(SiMe_3)_2]_2$ with calcium in THF.[92] Westerhausen prepared the unsolvated complex from the reaction of distilled calcium with $Sn[N(SiMe_3)_2]_2$.[93] Subsequently reported preparations include the reaction of calcium metal and $HN(SiMe_3)_2$ in the presence of ammonia,[94] the redox transmetallation/ligand exchange reaction of calcium and $HN(SiMe_3)_2$ in the presence of $HgPh_2$ or $BiPh_3$ under ultrasonication,[95] and the reaction of $K[N(SiMe_3)_2]$ with CaI_2 in diethyl ether[96] or toluene.[97] The product obtained from the halide metathesis route has been used to synthesize a wide variety of organometallic and inorganic compounds, including metallocenes,[96a,98] heterobimetallic alkoxides,[99] aminotroponate and aminotroponiminate calcium amides,[100] heterobimetallic amides[101]

and *N*-heterocyclic carbene adducts.[102] It has also been used in the study of enolization reactions of ketones.[96b,103]

There have been no specific difficulties mentioned in the literature with the synthesis or subsequent use of $Ca[N(SiMe_3)_2]_2$ (**1**) obtained by halide metathesis. Given the importance of **1** as a reagent, however, and the ease of calciate formation during the formation of other calcium amides (e.g., $K[Ca\{N(Ph)R\}_3]$; R = Me, *i*Pr),[104] investigations into alternative synthetic preparations for it are of utmost importance. This study has shown that **1** prepared from CaI_2 and $K[N(SiMe_3)_2]$ (**2**) can be contaminated with potassium in a manner that can be difficult to detect with NMR spectroscopy. The details of these findings are reported below.

Experimental

General Considerations. All manipulations were performed with the rigorous exclusion of air and moisture using high vacuum, Schlenk, or glovebox techniques. ^1H NMR spectra and ^{13}C NMR spectra were obtained at 22 °C at 300 MHz (Bruker DPX-300) and 101 MHz (Bruker AV-I), respectively, and were referenced to residual solvent resonances. Elemental analyses were performed by Robertson Microlit Laboratories, Madison, NJ or Desert Analytics, Tucson, AZ; metal analysis was conducted with ICP-OES.

Materials. Anhydrous calcium iodide and $K[N(SiMe_3)_2]$ were obtained commercially (Aldrich, 99% and 95%, respectively) and used as received. Benzylpotassium was prepared using a reported procedure.[105] Reaction solvents (THF, toluene, benzene,

hexanes, pentane) were sparged with nitrogen for 30 minutes and dried over type 4A molecular sieves prior to use. C_6D_6 and toluene-d_8 were vacuum-distilled from Na/K (22/78) alloy and stored over type 4A molecular sieves.

Preparation of $Ca(CH_2Ph)_2(thf)$. To a 250 mL round bottom flask equipped with a magnetic stir bar was added benzylpotassium (2.66 g, 20.4 mmol) and THF (50 mL). CaI_2 (3.00 g, 10.2 mmol) was added in small portions and the resulting suspension was stirred overnight. The reaction mixture was then filtered through Celite to remove KI and any unreacted CaI_2. Removal of solvent from the resulting orange filtrate left a dark red viscous oil. Subsequent trituration with benzene (50 mL) for 30 min followed by the addition of pentane (50 mL) resulted in a fine orange precipitate. The orange precipitate was isolated by filtration, washed with pentane (2 x 30 mL) and dried under vacuum to afford 2.07 g (69%) of $Ca(CH_2Ph)_2(thf)$. Anal. Calcd for $C_{18}H_{22}CaO$: Ca, 13.6; K, 0.0. Found: Ca, 13.4; K, 0.68. The complex is insoluble in common hydrocarbon solvents. ^1H NMR (THF-d_8, 22 °C): δ (ppm) = 1.50 (s, 2H, CH_2), 5.74 (t, 2H, $^3J_{HH}$ = 7.2 Hz, *m*-H), 6.32 (d, 2H, $^3J_{HH}$ = 7.2 Hz, *o*-H), 6.48 (t, 1H, $^3J_{HH}$ = 7.4 Hz, *p*-H).

Preparation of $Ca[N(SiMe_3)_2]_2$ (1). To a 20 mL scintillation vial equipped with a magnetic stir bar was added $Ca(CH_2Ph)_2(thf)$ (0.500 g, 1.70 mmol), toluene (5 mL), and hexamethyldisilazane (0.961 mL, 4.61 mmol, 2.7 equiv). The suspension was heated to 60 °C for 4 hours then allowed to cool to room temperature. Filtration through Celite yielded a clear solution, which was dried under reduced pressure, and the resulting residue was recrystallized from hexanes at -40 °C over 16 h. The resulting X-ray quality crystals were isolated from the supernatant, washed with cold hexanes (2 x 5 mL), and

dried under vacuum to afford 601 mg (98%) of **1**. Anal. Calcd for $C_{12}H_{36}CaN_2Si_4$: C, 39.94; H, 10.06; N, 7.76; Ca, 11.11; K, 0.0. Found: C, 39.25; H, 10.40; N, 7.39; Ca and K (average of two determinations each), 10.78 and 0.11, respectively. ^{1}H NMR (C_6D_6, 22 °C): δ (ppm) = 0.31; ^{13}C NMR (C_6D_6, 22 °C) δ (ppm) = 6.91; 6.47.

Preparation of $\{K[Ca(N(SiMe_3)_2)_3]\}_\infty$ (3). CaI_2 (1.00 g, 3.40 mmol) was suspended in toluene (50 mL). To this, a toluene solution of $K[N(SiMe_3)_2]$ (1.36 g, 6.81 mmol) was added dropwise at room temperature. The resulting suspension was heated to reflux for 4 days, after which time X-ray quality crystals of **2** were isolated by filtration of the hot suspension and cooling the filtrate to room temperature. ^{1}H NMR (C_6D_6, 25 °C): δ (ppm) = 0.29.

Computational Details. All calculations were performed with the Gaussian 03W suite of programs.[67] For geometry optimization and energy calculations, the B3PW91 functional, which incorporates Becke's three-parameter exchange functional[71] with the 1991 gradient-corrected correlation functional of Perdew and Wang,[72] was used. For all atoms except K and Ca, the polarized double zeta cc-pVDZ basis sets were used.[106] The cc-pCVTZ basis set was used on Ca ((14s,12p,6d)/[6s,5p,3d]) and the corresponding "Feller Misc. CVTZ" on potassium ((15s,12p,2d)/[6s,5p,2d]) ((*s*,*p*) exponents from Ahlrichs;[107] polarization and core/valence exponents from Feller[69]). The molecules displayed no imaginary frequencies; all geometries were minima on their potential energy surfaces. Atomic coordinates for all optimized structures are given in Appendix C.

General Procedures for X-ray Crystallography. A crystal was located and placed onto the tip of a 0.1 mm diameter glass capillary tube and mounted on a Bruker SMART

CCD Platform diffractometer for a data collection at 123(2) K. A preliminary set of cell constants and an orientation matrix were calculated from reflections harvested from three orthogonal wedges of reciprocal space. The intensity data were corrected for absorption. Final cell constants were calculated from the *xyz* centroids of 7444 strong reflections from the actual data collection after integration.

The structure was solved using SHELXS-97[74] and refined using SHELXL-97.[74] The structure of **2** refined as a full rotational twin with a refined mass ratio of 50:50. The final full matrix least squares refinement converged to $R_1 = 0.0422$ (F^2, $I > 2s(I)$) and $wR_2 = 0.0840$ (F^2, all data). Relevant crystal and data collection parameters and atomic coordinates are given in Appendix B.

Results and Discussion

Preparation of $Ca[N(SiMe_3)_2]_2$ (1) from $Ca(CH_2Ph)_2(thf)$ and $HN(SiMe_3)_2$. Monosolvated dibenzylcalcium can be prepared via the reaction of benzylpotassium and calcium iodide in THF, followed by trituation in benzene and pentane. Unlike the similarly prepared tetrasolvated complex $Ca(CH_2Ph)_2(thf)_4$,[108] the orange monosolvate is insoluble in hydrocarbon solvents, and is probably extensively aggregated. Although THF can be difficult to remove from organocalcium species,[109] the extra metal coordination made possible by aggregation probably assists in the partial desolvation.

Harder has mentioned the reaction of the unsolvated complex (p-tBu-benzyl)$_2$Ca with $HN(SiMe_3)_2$ in refluxing benzene to prepare $Ca[N(SiMe_3)_2]_2$.[108] We have found that desolvation of $Ca(CH_2Ph)_2(thf)$ is not necessary prior to its reaction with an excess of hexamethyldisilazane in toluene at room temperature to yield the corresponding calcium amide and toluene (eq 1).

$$Ca(CH_2Ph)_2(thf) + 2.7\ HN(SiMe_3)_2 \xrightarrow{\text{toluene}} Ca[N(SiMe_3)_2]_2 + 2\ MePh + THF \quad (1)$$

After removing all volatile species, **1** was recrystallized from cold hexane. Its composition was confirmed with elemental analysis and its structure verified with X-ray diffraction.[93] In C_6D_6, the complex displays only a *single* peak in its ^1H NMR spectrum at δ 0.31 ppm at room temperature (22 °C) and two broad singlets in its ^{13}C NMR spectrum at δ 6.91 and 6.47.

If the tetrasolvated complex $Ca(CH_2Ph)_2(thf)_4$[108] is treated with excess $HN(SiMe_3)_2$, the corresponding $Ca[N(SiMe_3)_2]_2(thf)_2$ is isolated in 74% yield. It was identified by comparison with the known NMR spectrum.[92] It can be partially desolvated by drying under vacuum (roughly 0.3 THF per calcium center remains after 8 hours).

Preparation of 1 via halide metathesis. The original procedure for the preparation of **1** via halide metathesis involved the reaction of **2** with CaI_2 in Et_2O; precipitated KI was removed by filtration.[96] The same reaction was subsequently conducted in toluene, generating **1** in 80% yield.[97] It was previously noted[97,101] that the as-prepared material displays *two* peaks in both its ^1H and ^{13}C NMR spectra in benzene-d_6 or toluene-d_8 at room temperature. The two resonances were assigned to the bridging and terminal $N(SiMe_3)_2$ groups in the dimeric $\{Ca[N(SiMe_3)_2]_2\}_2$, and are comparable to those reported by Westerhausen (i.e., two peaks at δ 0.33 and 0.21 ppm in toluene-d_8 at -63 °C).[93] Although the aforementioned states that $Ca[N(SiMe_3)_2]_2$ is fluxional in solution, and that the low temperature spectrum reflects separate resonances from the bridging and terminal resonances of dimeric $\{Ca[N(SiMe_3)_2]_2\}_2$, there is no explicit mention of the value of the shift(s) in the room temperature ^1H NMR spectrum. In the ^{13}C NMR spectrum (toluene-d_8), coalescence of the two peaks observed at room temperature (29 °C) is not achieved until 67 °C.

The discrepancy in the NMR spectra between the analytically clean $Ca[N(SiMe_3)_2]_2$ prepared from dibenzylcalcium and that synthesized through halide metathesis led us to conduct a series of systematic doping experiments that mixed discrete amounts of **2** with **1** (Figure 18). The addition of one-half equivalent of **2** to **1** does not produce a second

peak in the ^{1}H NMR spectrum, but rather causes a shift in the single trimethylsilyl resonance from δ 0.31 to 0.25 (Figure 18, spectrum b). The resonance is unchanged when the K:Ca ratio is raised to 1:1 (Figure 18, spectrum c). Only when the K:Ca ratio is greater than 1:1 does clear evidence of the added potassium appear in the form of a second peak near δ 0.12 (Figure 18, spectrum d), matching the value of δ 0.12 observed for **2** in benzene-d_6 (22 °C) (Figure 18, spectrum e).

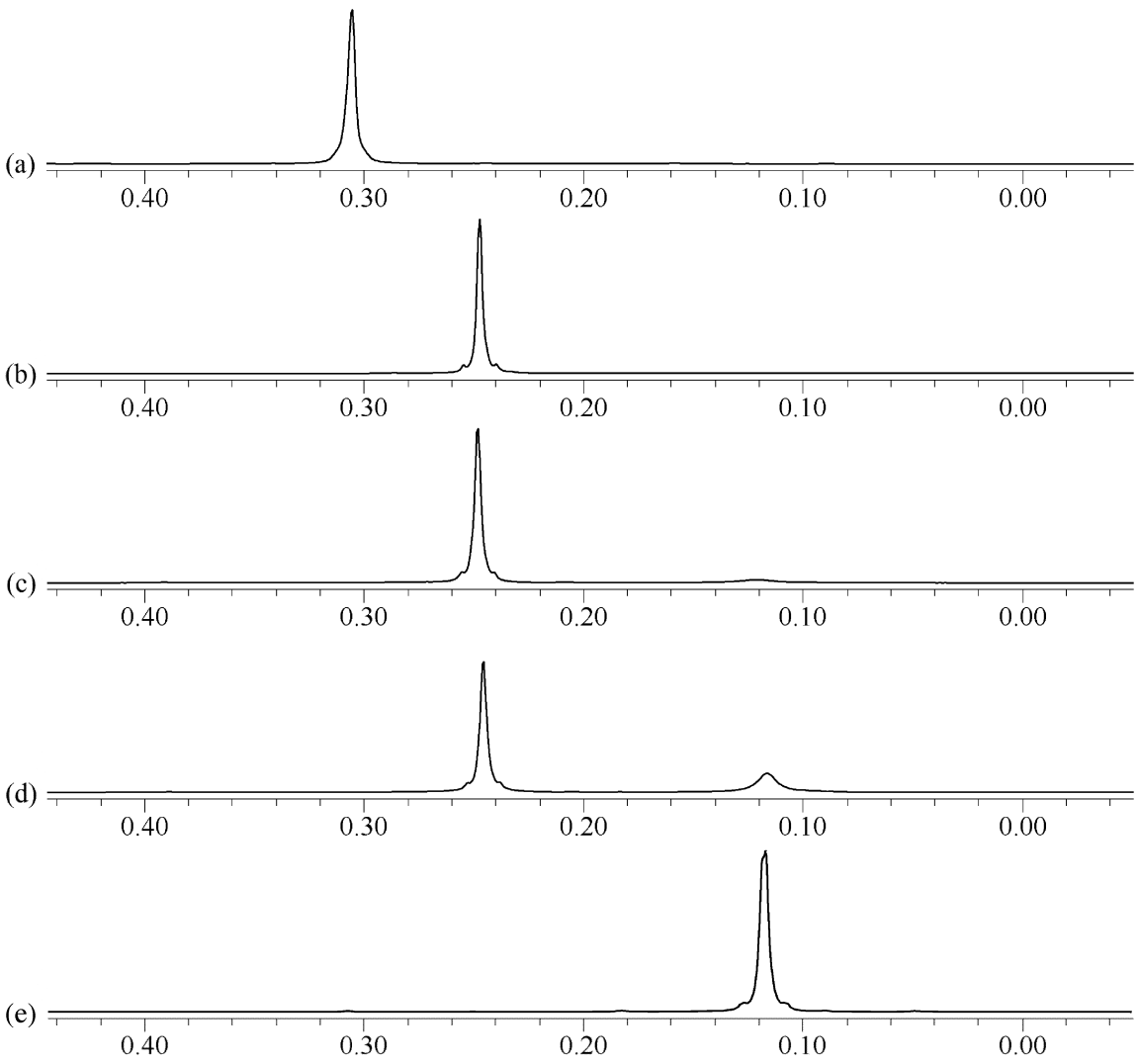

Figure 18. Effect on the ^{1}H NMR spectrum of doping a solution of **1** with **2** in C_6D_6 at 22 °C. (a) **1** prepared from dibenzylcalcium; (b) **1** + 0.5 eq **2**; (c) **1** + 1.0 eq **2**; (d) **1** + 2.0 eq **2**; (e) **2** only.

The spectra suggest that some species of calciate, i.e., $K_xCa_y[N(SiMe_3)_2]_{x+2y}$, forms with even substoichiometric amounts of **2** (vida infra). This is an interesting complement to Westerhausen's observation that calciates of the type $[L_nK_2Ca\{N(Ph)R\}_4]$ (L = neutral coligands) form during the metathesis reaction of K[N(Ph)R] with CaI_2 if any excess of the potassium amide is present, even if not in exact stoichiometric ratios.[104]

Preparation of calciate $\{K[Ca(N(SiMe_3)_2)_3]\}_\infty$ (3). We have specifically reexamined the halide metathetical preparation of **1** in toluene, using 1:2 molar ratios of CaI_2 and **2**. Two peaks near δ 0.25 and 0.12 are observed in the ^1H NMR spectrum of the isolated product, although their ratio varies with the time and temperature of the reaction. Two peaks at δ = 0.25 and 0.12 with a peak ratio of 1.0:16.5, respectively, are found in material prepared at room temperature and with a 1-hour reaction time, reflecting large amounts of unreacted **2**. The peak ratio changes to 1.0:0.3 if the reaction time is increased to 48 hours, and if the time is extended to 4 days at reflux temperature, the δ = 0.12 peak disappears entirely. Conversion to the calciate $K[Ca\{N(SiMe_3)_2\}_3]$ (**3**) must be the thermodynamically favored process, even if sufficient CaI_2 is present to form **1**. The gradual consumption of **2** and its incorporation into a heterometallic species is supported by elemental analysis of material isolated at an intermediate stage of the reaction (ca. 16 hours at room temperature, solids removed by filtration). The material was found to be iodide free (< 0.1%), but contained potassium in a Ca:K ratio of 1.0:1.3.

X-ray quality crystals of **3** were isolated by filtration of the refluxing suspension of **1** and **2** and cooling to room temperature. Compound **3** (Figure 19) crystallizes in the

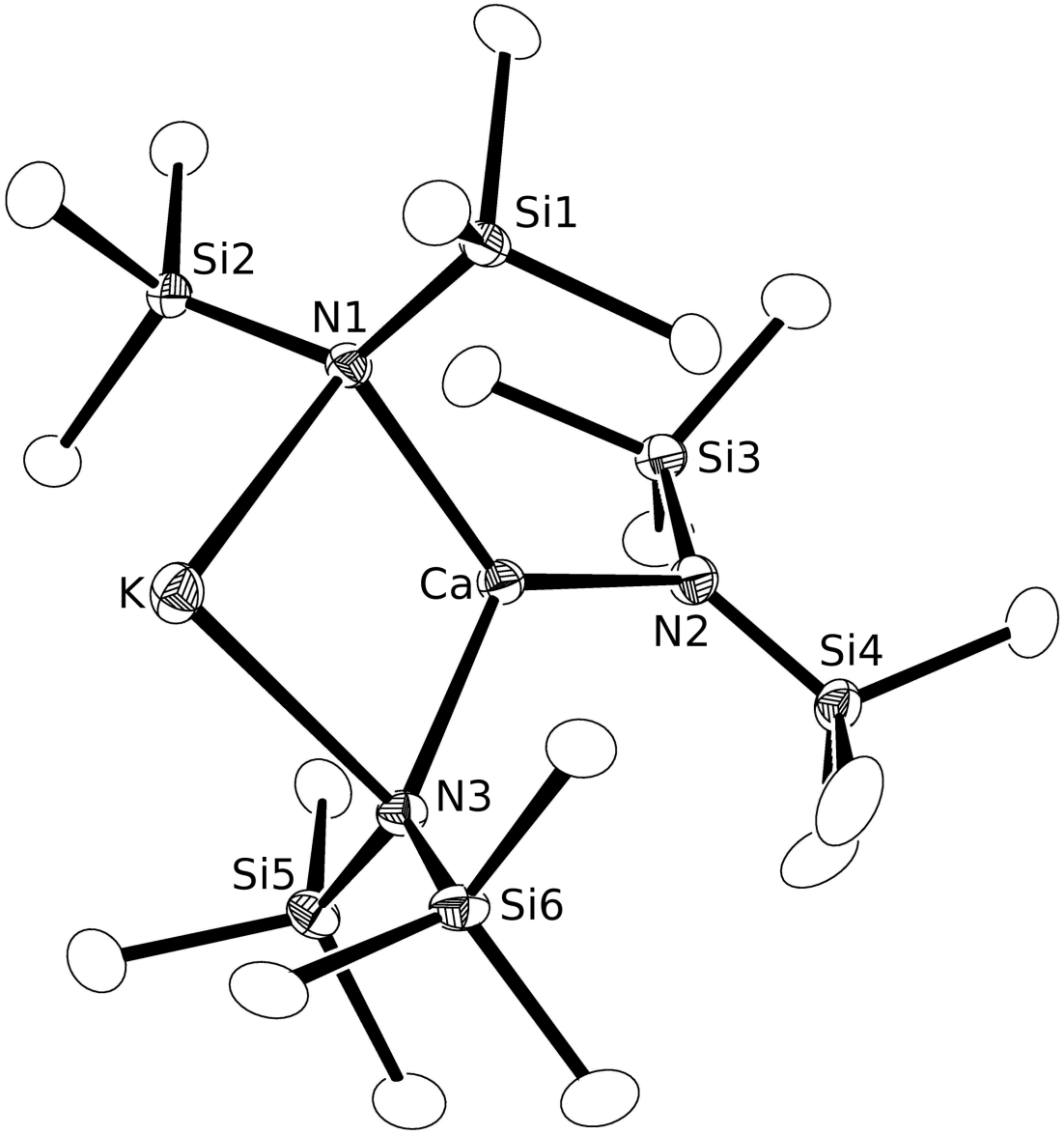

Figure 19. ORTEP of the non-hydrogen atoms of $\{K[Ca(N(SiMe_3)_2)_3]\}_\infty$ (**3**) with the numbering scheme used in the text. Thermal ellipsoids are shown at the 50% probability level.

triclinic $P\bar{1}$ space group and displays a four-membered ring containing a potassium and calcium atom as well as the nitrogen atoms of two hexamethyldisilazide moieties. The bond distances and internal angles of the four-membered ring (Table 4) are very similar to the related compound $\{K(thf)[Ca(N(SiMe_3)_2)_3]\}_\infty$.[96b]

Table 4. Selected bond distances and angles for $\{K[Ca(N(SiMe_3)_2)_3]\}_\infty$.

atoms	distance (Å)	atoms	angle (°)
Ca–N2	2.325(2)	N1–K–N3	79.96(5)
Ca–N3	2.376(2)	N1–Ca–N3	103.60(6)
Ca–N1	2.386(2)	Ca–N1–K	88.82(6)
K–N1	2.882(2)	Ca–N3–K	87.59(6)
K–N3	2.943(2)	Si1–N1–Si2	122.28(1)
N1–Si1	1.714(2)	Si3–N2–Si4	127.42(1)
N1–Si2	1.709(2)	Si5–N3–Si6	122.48(1)
N2–Si3	1.695(2)		
N2–Si4	1.691(2)		
N3–Si5	1.717(2)		
N3–Si6	1.709(2)		
K···C9	3.235(3)		
K···C10	3.185(3)		

Unlike the aforementioned, however, which is a coordination polymer with a 1D chain structure, compound **3** crystallizes as a 2D sheet structure (Figure 20). The close K···C contact distances are shorter than those described in $\{K(thf)[Ca(N(SiMe_3)_2)_3]\}_\infty$, and the absence of coordinated THF allows for the extra dimension of the 2D structure. Each two dimensional sheet expands in the crystallographic *xy* plane; the sheets are separated by van der Waals contact distances among the methyl groups in the *z* direction.

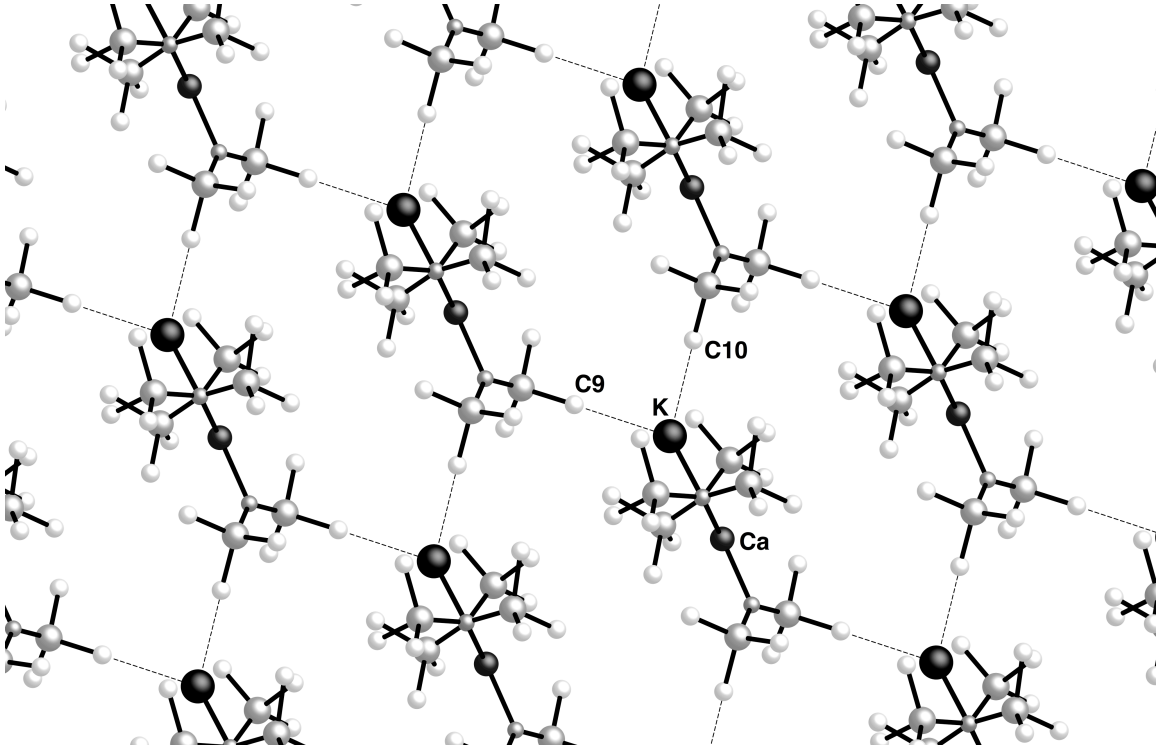

Figure 20. Rendering of the 2D sheet structure of $\{K[Ca(N(SiMe_3)_2)_3]\}_\infty$. Close C···K contacts are denoted with dashed lines (see Table 4).

The K atom in **3** resides roughly in the CaN_3 plane (N2–Ca–K angle = 176.73°). This is in contrast to $\{K(thf)[Ca(N(SiMe_3)_2)_3]\}_\infty$, where the equivalent angle is only 173.80°, and the potassium is bent below the CaN_3 plane. This is likely due to the incorporation of the THF solvent molecule: the K(thf) moiety is bent below the plane to relieve any steric congestion between the THF and the trimethylsilyl groups.

The very low solubility of CaI_2 in aromatic solvents ensures that $K[N(SiMe_3)_2]$ will always be in excess in solution in a reaction conducted in toluene, thus contributing to calciate formation. The solubility of CaI_2 in THF at room temperature is 12.4 g L^{-1};[110] it probably has a comparable solubility in Et_2O. However, it is still likely that the potassium compound will be in excess in the early stages of the reaction. After recrystallization from toluene and then hexane, the product isolated from the metathesis of CaI_2 and $K[N(SiMe_3)_2]$ in Et_2O was ostensibly pure by ICP analysis. Nevertheless, a sample prepared by the same method displays two peaks in its ^{1}H NMR spectrum in toluene-d_8 at 22 °C (δ = 0.27, 0.31 ppm). There is currently no simple explanation for the apparent discrepancy with the results reported here.

Computational study. The structures of **1**, **2**, and **3** were optimized at the B3PW91/cc-pVDZ level (triple zeta on the metals). The potassium calciate was initially derived from the known structure of $K(thf)[Ca(N(SiMe_3)_2)_3]$ by removing the coordinated THF ligand;[96b] the other two used the crystal structures of the compounds as starting geometries.[93,111] The bond lengths and angles for $K[N(SiMe_3)_2]$ and $Ca[N(SiMe_3)_2]_2$ are within 0.05 Å and 2°, respectively, of the experimentally determined values. Even given that these are gas-phase energies and that solvation effects may play an

important role, the proposed aggregation reaction (Figure 21) is exothermic by 7 kcal mol–1 ($\Delta H°$), and has a free energy of approximately -8 kcal mol^{-1}. The ease of aggregation could explain why separate resonances from **1** and **2** are not observed in NMR spectra until the amount of **2** becomes quite high. In this context, it is interesting to note that at a comparable level of theory, the reaction of $Mg[N(SiMe_3)_2]_2$ and **1** to produce $CaMg[N(SiMe_3)_2]_4$ was found to be essentially thermoneutral, helping to explain the appearance of all three species in NMR spectra of $CaMg[N(SiMe_3)_2]_4$.[101]

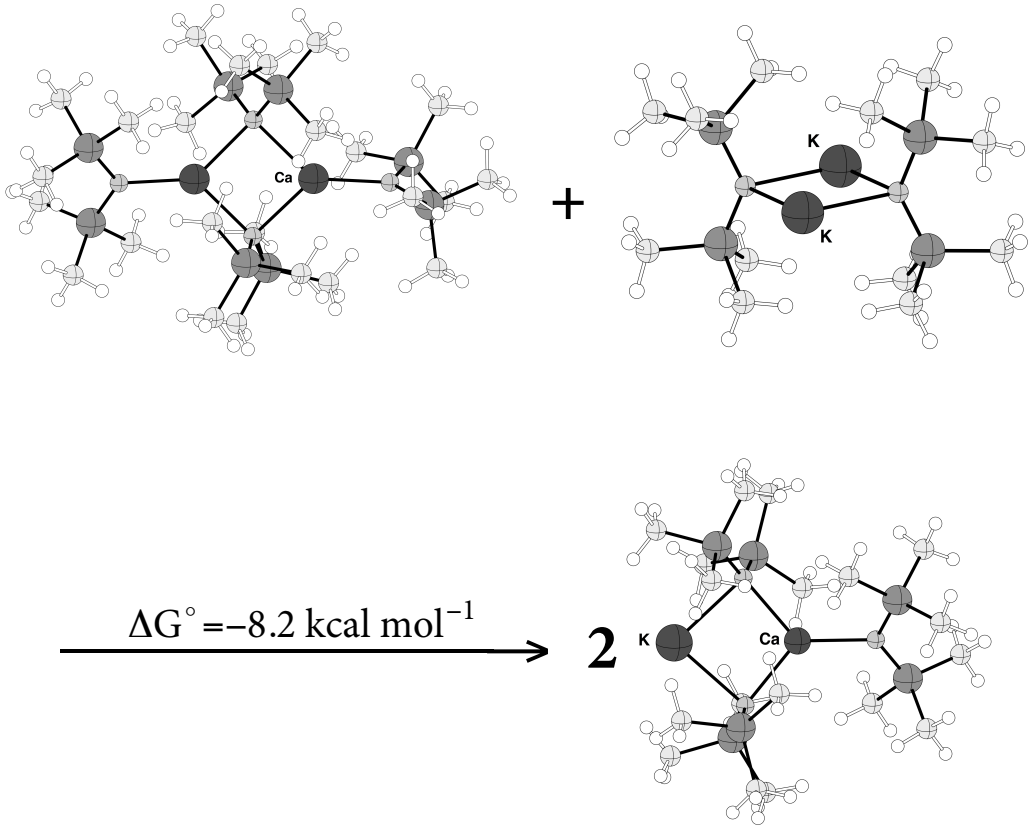

Figure 21. Optimized structures and reaction of **1** and **2** to produce $K[Ca\{N(SiMe_3)_2\}_3]$.

Conclusion

In summary, essentially potassium-free **1** is isolated in high yield from the room temperature reaction of $Ca(CH_2Ph)_2(THF)$ and $HN(SiMe_3)_2$ in toluene. In contrast, we have no evidence that the reaction of CaI_2 and **2** in toluene ever yields **1**; the formation of potassium calciates, particularly **3**, appears to be unavoidable in this solvent. That this fact has gone undetected for as long as it has indicates that for many synthetic purposes a species such as $K[Ca\{N(SiMe_3)_2\}_3]$ is an effective replacement for **1**, but this can hardly be assumed to be always the case. The use of ethers as reaction solvents for the metathetical preparation of **2** may be less problematic, but still should be approached with caution. It might be noted that related halide metathetical preparations have been described for the analogous barium[105] and strontium[97,112] amides. They should be used with care until the purity of the products is reconfirmed.

CHAPTER IV

INFLUENCE OF RING METHYLATION IN GROUP 15 TETRAMETHYLCYCLOPENTADIENYL COMPLEXES, $M(C_5Me_4H)_nI_{3-n}$ (M = As, Sb)

Introduction

In contrast to the near ubiquity of *pentahapto*-bonded cyclopentadienyl rings in transition metal chemistry, cyclopentadienyl complexes of the main group elements possess a range of bonding modes from η^1 to η^5, contained in an astonishing array of monomers, dimers, coordination polymers, and molecular aggregates.[4b,4c,61b,113] Cyclopentadienyl derivatives of the heavy Group 15 elements (As, Sb, Bi) have been isolated that display many of these features despite having extra experimental demands placed on their synthesis; i.e., in addition to the air- and moisture-sensitivity that is common to most main-group Cp complexes, many heavy Group 15 species have limited thermal stability, and some exhibit light sensitivity as well.

The tris(cyclopentadienyl) compounds MCp_3 (M = As, Sb, Bi) exemplify these difficulties. First synthesized by Fischer in 1957,[114] they have been reinvestigated several times,[115] in part for their potential use as precursors in MOCVD processes.[116] The arsenic and bismuth derivatives decompose at room temperature, forming insoluble, presumably polymeric solids. All three molecules are fluxional in solution, and 1,2-metallotropic shifts render the protons equivalent on the NMR timescale even at –70 °C (for $SbCp_3$ and $BiCp_3$). Both $SbCp_3$ and $BiCp_3$ have been characterized in the solid state,[115c,115d] and the

X-ray crystal structure of the latter displays close intermolecular Bi···Cp′ contacts that are probably responsible for its partially reversible thermochromic behavior.[115d]

Our long-standing interest in the chemistry of cyclopentadienyl main-group complexes[4b] and the possibilities for ligand design in Group 15 $[R_2ECp'_2]^-$ species[98] lead us to reexamine the corresponding MCp'_3 complexes. In particular, we were interested in preparing derivatives with substituted rings, which often confer kinetic and thermodynamic stability on their associated complexes.[4b,4c,61b,113] Despite the range of cyclopentadienyl ligands found in other Group 15 complexes (e.g., C_5H_5, C_5Me_5, $C_5(i\text{-}Pr_3)Me_2$, $C_5(i\text{-}Pr)_4H$, and $C_5(t\text{-}Bu)_3H_2$),[4c,61b,115d,117] only C_5H_5 has ever been successfully used with the MCp'_3 complexes. Fisher briefly reported the use of $[C_5MeH_4]^-$ in the preparation of MCp'_3 complexes,[115a] but the compounds were not fully characterized, and Lorberth obtained only intractable oils in attempting to form $Sb(C_5MeH_4)_3$.[116] We report here the first crystal structure of a tris(cyclopentadienyl)arsenic complex, its antimony analogue, and a mixed antimony iodide compound. We also report the result of density functional theory calculations that illuminate features of the structures and their facile rearrangements in solution.

Experimental

General Considerations. All manipulations were performed with the rigorous exclusion of air and moisture using high vacuum, Schlenk, or glovebox techniques. Proton and carbon ($^{13}C\{^1H\}$) NMR spectra were obtained at 25 °C (or above) on a Bruker DRX-400 spectrometer at 400 and 100.1 MHz, respectively, and were referenced to the

residual proton and ^{13}C resonances of C_6D_6 (δ 7.15 and 128.0). Low temperature ^1H NMR spectra were obtained on a Bruker DRX-500 instrument at 500 MHz. Elemental analyses were performed by Desert Analytics, Tucson, AZ; the often unsatisfactory values may be the result of high air sensitivity. Melting points were determined in sealed capillaries.

Materials. AsI_3 and SbI_3 were purchased from Aldrich and were visibly contaminated with purple iodine crystals. The triiodides were subsequently rinsed with hexane and the remaining dark orange solids were dried under vacuum and used without further purification. $C_5Me_4H_2$ and $Na[N(SiMe)_2]$ were purchased from Aldrich and Strem and used as received. $Na[C_5Me_4H]$ was prepared from the reaction of $C_5Me_4H_2$ and $Na[N(SiMe)_2]$ in toluene and dried under vacuum before use. THF, toluene, and hexane were distilled under nitrogen from potassium benzophenone ketyl. C_6D_6 and tol-d_8 were vacuum distilled from Na/K (22/78) alloy and stored over type 4A molecular sieves prior to use.

Synthesis of $As(C_5Me_4H)_3$ (1). AsI_3 (1.00 g, 2.19 mmol) was slurried in THF (40 mL). $Na[C_5Me_4H]$ (0.949 g, 6.58 mmol) was dissolved in THF (25 mL) and added dropwise over 30 min at 0 °C to the suspension of AsI_3. The mixture darkened to a deep red and eventually lightened to reveal a translucent yellow solution. The reaction was stirred for 1 h at 0 °C after which the solvent was removed under vacuum to yield a light yellow solid. The solid was extracted with hexanes (15 mL) and filtered through a medium porosity frit. The bright yellow filtrate was placed under vacuum to afford 0.590 g (61%) of **1** as a bright yellow, air-sensitive solid, mp 142-146 °C. X-ray quality crystals

were obtained by slow evaporation of a hexane solution of **1**. Anal. Calcd (%) for $C_{27}H_{39}As$: C, 73.95; H, 8.96; As, 17.08. Found: C, 68.5; H, 8.26; As, 16.8; the low values for carbon and hydrogen may be the result of high air-sensitivity. ^{1}H NMR (400 MHz, C_6D_6, 298 K): δ 3.52 (br s, 3H, C_5Me_4H); 1.96 (s, 18H, C_5Me_4); 1.73 (s, 18H, C_5Me_4); (500 MHz, tol-d_8, 203 K): δ 3.42 (br s, 3H, C_5Me_4H); 2.11 (s, 9H, C_5Me_4); 1.87 (s, 9H, C_5Me_4); 1.79 (s, 9H, C_5Me_4); 1.72 (s, 9H, C_5Me_4). $^{13}C\{^{1}H\}$ NMR (100 MHz, C_6D_6, 298 K): δ 136.6 (s, C_5Me_4); 134.6 (s, C_5Me_4); 55.6 (s, As-C_5Me_4); 14.1 (s, C_5Me_4); 11.2 (s, C_5Me_4).

Synthesis of $Sb(C_5Me_4H)_3$ (2). A procedure similar to that for **1**, employing SbI_3 (1.00 g, 2.00 mmol) and $Na[C_5Me_4H]$ (0.861 g, 6.00 mmol) afforded **2** as a bright yellow, air-sensitive solid (76%), mp 92 °C (dec). X-ray quality crystals were obtained by slow evaporation of a hexane solution of **2**. Elemental analysis was unsatisfactory, perhaps because of high air-sensitivity. ^{1}H NMR (400 MHz, C_6D_6, 298 K): δ 3.64 (br s, 3H, C_5Me_4H); 1.97 (s, 18H, C_5Me_4); 1.81 (s, 18H, C_5Me_4); (500 MHz, tol-d_8, 203 K): δ 3.52 (br s, 3H, C_5Me_4H); 2.14 (s, 9H, C_5Me_4); 1.93 (s, 9H, C_5Me_4); 1.86 (s, 9H, C_5Me_4); 1.78 (s, 9H, C_5Me_4). $^{13}C\{^{1}H\}$ NMR (100 MHz, C_6D_6, 298 K): d 135.5 (s, C_5Me_4); 132,4 (s, C_5Me_4); 58.8 (s, Sb-C_5Me_4); 13.8 (s, C_5Me_4); 11.2 (s, C_5Me_4).

Synthesis of $Sb(C_5Me_4H)I_2$ (3). A procedure similar to that for **2**, employing SbI_3 (1.00 g, 2.00 mmol) and $Na[C_5Me_4H]$ (0.287 g, 2.00 mmol), afforded **3** as bright orange, air-sensitive X-ray quality crystals (87%), mp 58-62 °C. Anal. Calcd (%) for $C_9H_{13}I_2Sb$: C,

21.76; H, 2.64; Sb, 24.51. Found: C, 22.3; H, 2.78; Sb, 20.8. ^{1}H NMR (400 MHz, C_6D_6, 298 K): δ 5.46 (br s, 1H, C_5Me_4H); 1.74 (s, 6H, C_5Me_4); 1.45 (s, 6H, C_5Me_4).

General Procedures for X-ray Crystallography. A suitable crystal of each sample was located, attached to a glass fiber, and mounted on a Bruker diffractometer for data collection at 173(2) K. Data collection and structure solutions for all molecules were conducted at the X-ray Crystallography Facility at the University of California, San Diego. The intensity data were corrected for absorption and decay (SADABS). All calculations were performed using the current SHELXTL suite of programs. Final cell constants were calculated from a set of strong reflections measured during the actual data collection. Relevant crystal and data collection parameters for each of the compounds are given in Appendix B.

The space groups were determined based on systematic absences (where appropriate) and intensity statistics. A direct-methods solution was calculated that provided most of the non-hydrogen atoms from the E-map. Several full-matrix least squares/difference Fourier cycles were performed that located the remainder of the non-hydrogen atoms. All non-hydrogen atoms were refined with anisotropic displacement parameters. All hydrogen atoms were placed in ideal positions and refined as riding atoms with relative isotropic displacement parameters.

Computational Details. Calculations were performed using the GAUSSIAN 03W suite of programs.[67] For the basic geometry optimizations, the B3PW91 functional, which incorporates Becke's three-parameter exchange functional[71] with the 1991 gradient-corrected correlation functional of Perdew and Wang,[72] was used. This hybrid functional

has previously been shown to provide realistic geometries for organometallic species.[73] The correlation-consistent double zeta basis set cc-pVDZ was used for optimization and final energy calculations.[106b]

For the transition energy calculations, Truhlar's BB1K functional was used;[68] this is a one-parameter hybrid based on the BB95 functional that is expressly designed for thermochemical kinetics. The QST2 program was used to identify the transition structures for the $M(C_5H_5)_3$ complexes; for the tetramethylcyclopentadienyl compounds, the QST3 approach was used.[118] For basis sets, the correlation-consistent double zeta basis sets cc-pVDZ were used for C and H. For As and Sb, the effective core potentials aug-cc-pVDZ-PP were used; the valence electrons are constructed from the contraction (9s,8p,8d)/[5s,4p,3d]. The nature of the stationary points (minima or transition structures) was determined with analytical frequency calculations. Atomic coordinates for all optimized structures are given in Appendix C.

Results and Discussion

Synthesis of the Complexes. The tris(tetramethylcyclopentadienyl) complexes of arsenic and antimony are readily prepared in good yields by the straightforward salt metathesis reaction of the element triiodides with three equivalents of $Na[C_5Me_4H]$ (eq 1). This is directly analogous to the method originally used by Fischer to make the unsubstituted $M(C_5H_5)_3$ counterparts.[114,115b]

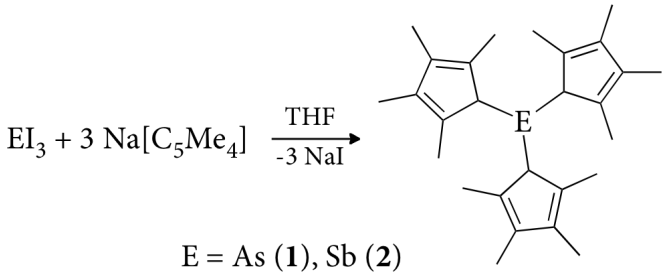

(1)

Both bright yellow compounds are highly air-sensitive; the arsenic compound displays no photosensitivity, but within a day the antimony derivative darkens to green and eventually black on exposure to ambient light. Unlike the thermally unstable $As(C_5H_5)_3$,[115b] **1** can be kept indefinitely in an inert atmosphere at room temperature, and it melts at 142-146 °C without decomposition.

The related cyclopentadienyl antimony diiodide $Sb(C_5Me_4H)I_2$ (**3**) was prepared in 87% yield by the salt metathesis reaction of antimony triiodide and one equivalent of $Na[C_5Me_4H]$ (eq 2). This method parallels the formation of $Sb(C_5Me_5)Cl_2$ and $Sb[C_5(i\text{-}Pr)_4H]Cl_2$ from $SbCl_3$ and the appropriate alkali metal cyclopentadienides,[119] but is different from the way the parent $Sb(C_5H_5)I_2$ has been made, i.e., by the reaction of

$SbCp_3$ with either SbI_3 or I_2.[116] The effect of the ring methylation on the physical properties of the $SbCp'X_2$ species is substantial, as unlike $Sb(C_5H_5)I_2$, which is light-sensitive and decomposes at low temperatures, **3** and the other substituted-ring dihalides are stable at room temperature, and display no photosensitivity.

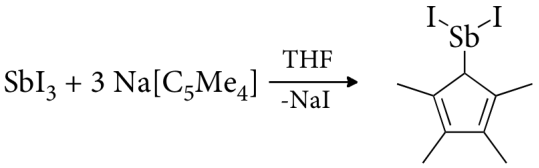

(2)

NMR Spectra. All protons are equivalent in the solution NMR spectra for $M(C_5H_5)_3$ (M = As, Sb, Bi) at room temperature, presumably as a result of 1,2-sigmatropic shifts.[113b,115b] For $Sb(C_5H_5)_3$ and $Bi(C_5H_5)_3$, a single peak is observed at all temperatures down to -70 °C. For $As(C_5H_5)_3$, the singlet resonance splits into two peaks in a 4:1 ratio by –30 °C, but then undergoes no further splitting down to –70 °C. A fully resolved static spectrum of a σ-bonded cyclopentadienyl ring would contain 3 peaks in a 2:2:1 ratio (as found, for example, in $As(C_5H_5)Cl_2$ at -95 °C),[120] but it is possible that near degeneracies obscure the resolution of the peaks, since the $As(C_5H_5)_3$ spectrum was recorded at 60 MHz, and the separation between the two ring proton resonances in the related $As(C_5H_5)H_2$ is only 4 Hz, and barely resolved on a 400 MHz instrument. Without further data, it is impossible to be definitive about the issue, but if the spectrum of $As(C_5H_5)_3$ at -30 °C is in fact essentially static, a simple two-site exchange mechanism would lead to an

approximate $\Delta G^{\ddagger}$ for ring rotation of 11 kcal mol^{-1};[121] this is in fact roughly similar to the value calculated for $As(C_5H_5)Cl_2$ (10.2 kcal mol^{-1}) and $As(C_5H_5)H_2$ (15.7 kcal mol^{-1}).[120]

At room temperature, both **1** and **2** display solution NMR spectra with 3 peaks in a 1:6:6 ratio, representing the unique hydrogen on the ring and the two sets of equivalent methyl groups. No change is observed in the spectrum of **1** at 100 °C, but on cooling, the peaks for the methyl resonances for both **1** and **2** gradually split into two each, leaving spectra with 5 peaks. The two methyl peaks observed at room temperature split at different rates; 4 peaks are first observed at about –42 °C for **1**, and –48 °C for **2**; at -70 °C, the resonances have stabilized into a 1:3:3:3:3 pattern. This behavior is different from that observed in $Al(C_5Me_4H)_3$, which displays a 1:6:6 patterns of resonances in its ^1H NMR spectra down to –90 °C.[122] Evidently, the activation barrier for the ring rearrangements in the aluminum complex is considerably lower than for the As and Sb counterparts.

Crystallographic Results

$As(C_5Me_4H)_3$ (1) and $Sb(C_5Me_4H)_3$ (2). Crystals of **1** and **2** were isolated from concentrated hexane solutions as yellow plates. Compound **1** represents the first structurally authenticated homoleptic cyclopentadienyl complex of arsenic. Both molecules are monomeric, with three sigma-bonded rings situated around the metal in an irregular paddlewheel arrangement; as they are isostructural and are numbered the same, they will be discussed together. A depiction of **1** is given in Figure 22; a corresponding plot for **2** is given in Figure 23. Selected bond lengths and angles are given in Table 5 (for **1**) and Table 6 (for **2**).

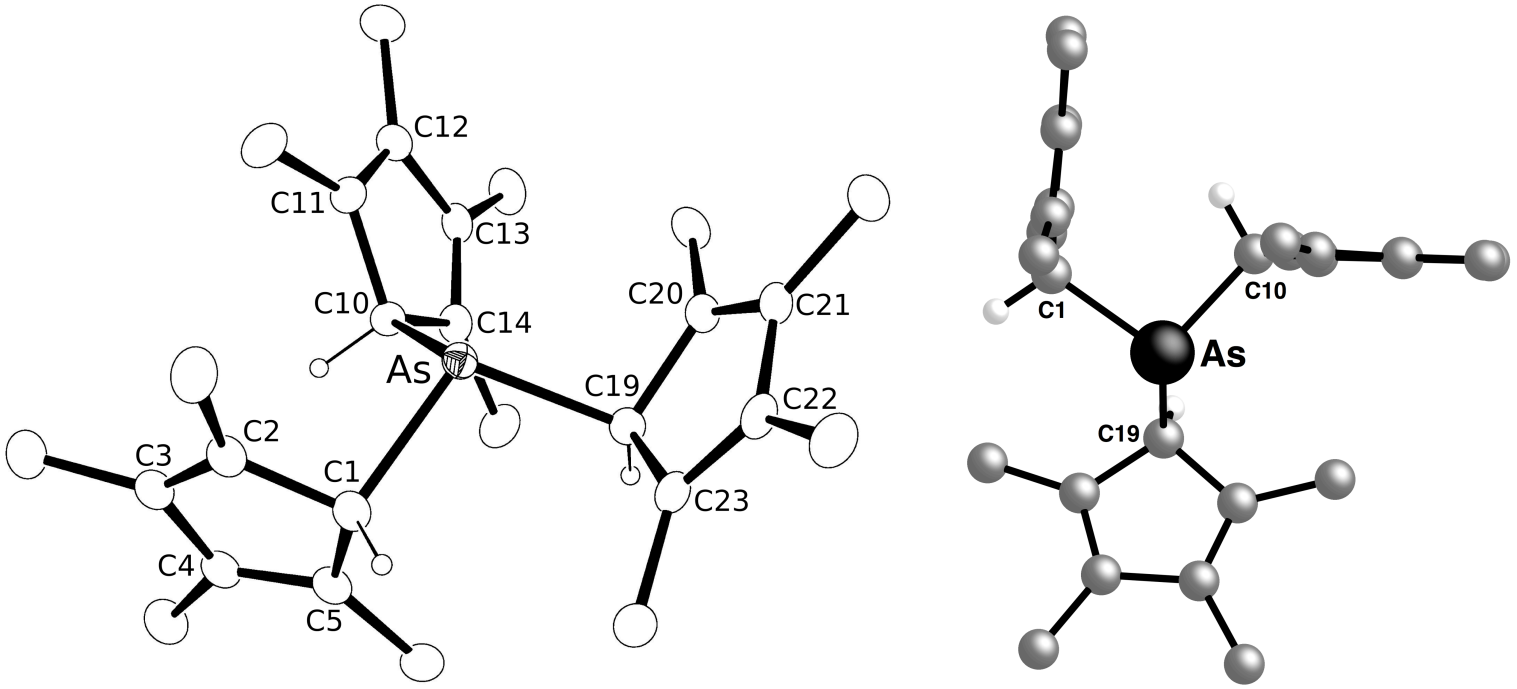

Figure 22. ORTEP (left) and ball-and stick plot (right) of $As(C_5Me_4H)_3$, illustrating the numbering scheme used in the text. Thermal ellipsoids are shown at the 50% level; for clarity, hydrogen atoms on the methyl groups have been removed. The ball-and-stick plot is rotated to illustrate the twisted orientation of the C19 ring.

Table 5. Selected bond distances and angles for $As(C_5Me_4H)_3$.

atoms	distance (Å)	atoms	angle (°)
As1–C19	2.027(2)	C19–As1–C10	109.32(9)
As1–C10	2.031(2)	C19–As1–C1	105.81(9)
As1–C1	2.042(2)	C10–As1–C1	96.39(9)
C1–C2	1.501(3)	C2–C1–As1	103.21(15)
C1–C5	1.491(3)	C5–C1–As1	116.54(16)
C2–C3	1.347(4)	C11–C10–As1	107.16(15)
C3–C4	1.471(3)	C14–C10–As1	121.64(16)
C4–C5	1.349(3)	C20–C19–As1	102.64(15)
C10–C11	1.507(3)	C23–C19–As1	105.93(15)
C10–C14	1.500(3)		
C11–C12	1.352(3)		
C12–C13	1.470(3)		
C13–C14	1.351(3)		
C19–C23	1.501(3)		
C19–C20	1.509(3)		
C20–C21	1.350(3)		
C21–C22	1.466(3)		
C22–C23	1.356(3)		

The average arsenic-carbon bond length of 2.033(3) Å falls within the range (2.026–2.056 Å) found for related pentamethylcyclopentadienyl structures of the general form $(C_5Me_5)_nAsX_{3-n}$.[119b,123] The average Sb–C bond length of 2.238(6) Å in **2** agrees well with that for $Sb(C_5H_5)_3$ (2.249 Å).[115c] The cyclopentadienyl rings display localized bonding; i.e., the formal double and single carbon-carbon bond lengths average to 1.35 and 1.49 Å, respectively, in **1**; the corresponding distances in **2** are 1.36 Å and 1.48 Å. The coordination around the metals is strongly pyramidalized, as indicated by the C–As–C′ angle sum of 311.5° and the C–Sb–C′ sum of 304.2°; the smaller value for the latter reflects the diminishing importance of bond hybridization in the heavier Sb.[124]

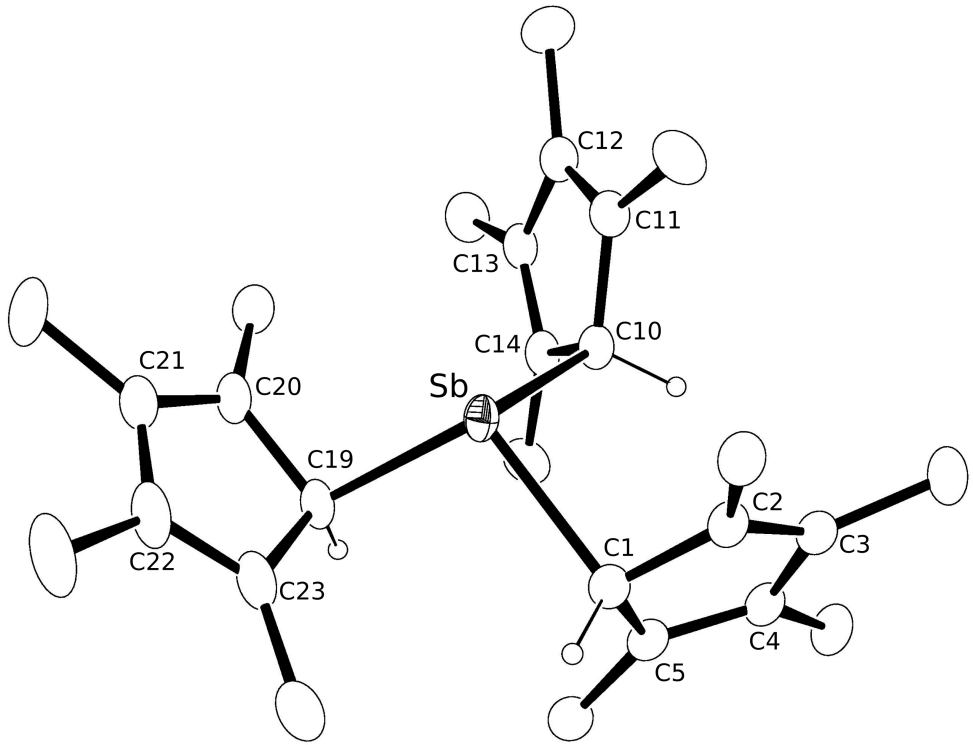

Figure 23. ORTEP of $Sb(C_5Me_4H)_3$ illustrating the numbering scheme used in the text. Thermal ellipsoids are shown at the 50% level; for clarity, hydrogen atoms on the methyl groups have been removed.

Table 6. Selected bond distances and angles for $Sb(C_5Me_4H)_3$.

atoms	distance (Å)	atoms	angle (°)
Sb1–C19	2.234(3)	C19–Sb1–C10	107.68(12)
Sb1–C10	2.229(3)	C19–Sb1–C1	102.94(13)
Sb1–C1	2.252(4)	C10–Sb1–C1	93.60(13)
C1–C2	1.491(4)	C2–C1–Sb1	101.1(2)
C1–C5	1.484(5)	C5–C1–Sb1	113.0(2)
C2–C3	1.354(5)	C11–C10–Sb1	105.1(2)
C3–C4	1.467(5)	C14–C10–Sb1	116.7(2)
C4–C5	1.364(5)	C20–C19–Sb1	103.1(2)
C10–C11	1.502(5)	C23–C19–Sb1	101.8(2)
C10–C14	1.497(5)		
C11–C12	1.348(5)		
C12–C13	1.467(5)		
C13–C14	1.353(5)		
C19–C23	1.498(5)		
C19–C20	1.497(5)		
C20–C21	1.367(5)		
C21–C22	1.448(6)		
C22–C23	1.362(5)		

The orientation of the C_5 ring planes relative to the C19–C1–C10 plane varies sharply, with angles of 46.3, 83.7, and 62.4° for the rings containing C19, C1, and C10, respectively (corresponding angles in **2** are (46.2, 80.2, and 63.1°). Despite the absence of substituents on the cyclopentadienyl rings (and the shorter element–carbon bonds in **1**), a related pattern of ring tilts relative to the central C_3 plane is also observed in $Sb(C_5H_5)_3$, i.e., 40.2, 80.9, and 46.1°, which suggests that the arrangements in **1** and **2** are not imposed solely by crystal packing forces. Even $Bi(C_5H_5)_3$ displays a set of widely varying ring tilt angles (55.2, 86.5, 44.0°), although close intermolecular contacts probably influence the angles in this case.[115d]

$Sb(C_5Me_4H)I_2$ (**3**). Orange plates of **3** were grown from hexane. The pyramidalized molecule consists of a η^3-bound cyclopentadienyl ring and two terminal iodides bonded

to the antimony (Figure 24); these units are connected into a coordination polymer. Selected bond lengths and angles are given in Table 7. Within error, the Sb–C_{ipso} distance of 2.267(9) Å is indistinguishable from the 2.271(8) Å distance observed in the unsubstituted $Sb(C_5H_5)Cl_2$,[125] or the pentamethylated $Sb(C_5Me_5)Cl_2$ (2.254(9) Å),[126] but is considerably shorter than that in the substituted $Sb[(C5(i\text{Pr})_4H]Cl_2$ (2.331(7) Å).[119b] Interestingly, the average Sb–C_β bond lengths in all these molecules are similar (2.62 Å, 2.59 Å, 2.61 Å, and 2.56 Å for **3**, $Sb(C_5H_5)Cl_2$, $Sb(C_5Me_5)Cl_2$, and $Sb[(C_5(i\text{Pr})_4H]Cl_2$, respectively), indicating that the cyclopentadienyl rings can be viewed as tilting around the C_β-$C_{\beta'}$ axis. The $[C_5Me_4H]^-$ ring in **3** shows a significant localization of π-electron density, as evidenced by the range of bond lengths (1.38–1.49 Å, ΔC–C = 0.11 Å); the range of C–C bond lengths in $Sb(C_5H_5)Cl_2$ (ΔC–C = 0.05 Å), $Sb(C_5Me_5)Cl_2$ (ΔC–C = 0.06 Å), and $Sb[(C_5(i\text{Pr})_4H]Cl_2$ (ΔC-C = 0.06 Å) is narrower, pointing to greater delocalization in the ring. Taken together, the short Sb–C_{ipso} bond length and the localization of the π-bonds in **3** point to somewhat more σ interaction between the Sb and the cyclopentadienyl ring in **3** than in the related complexes.

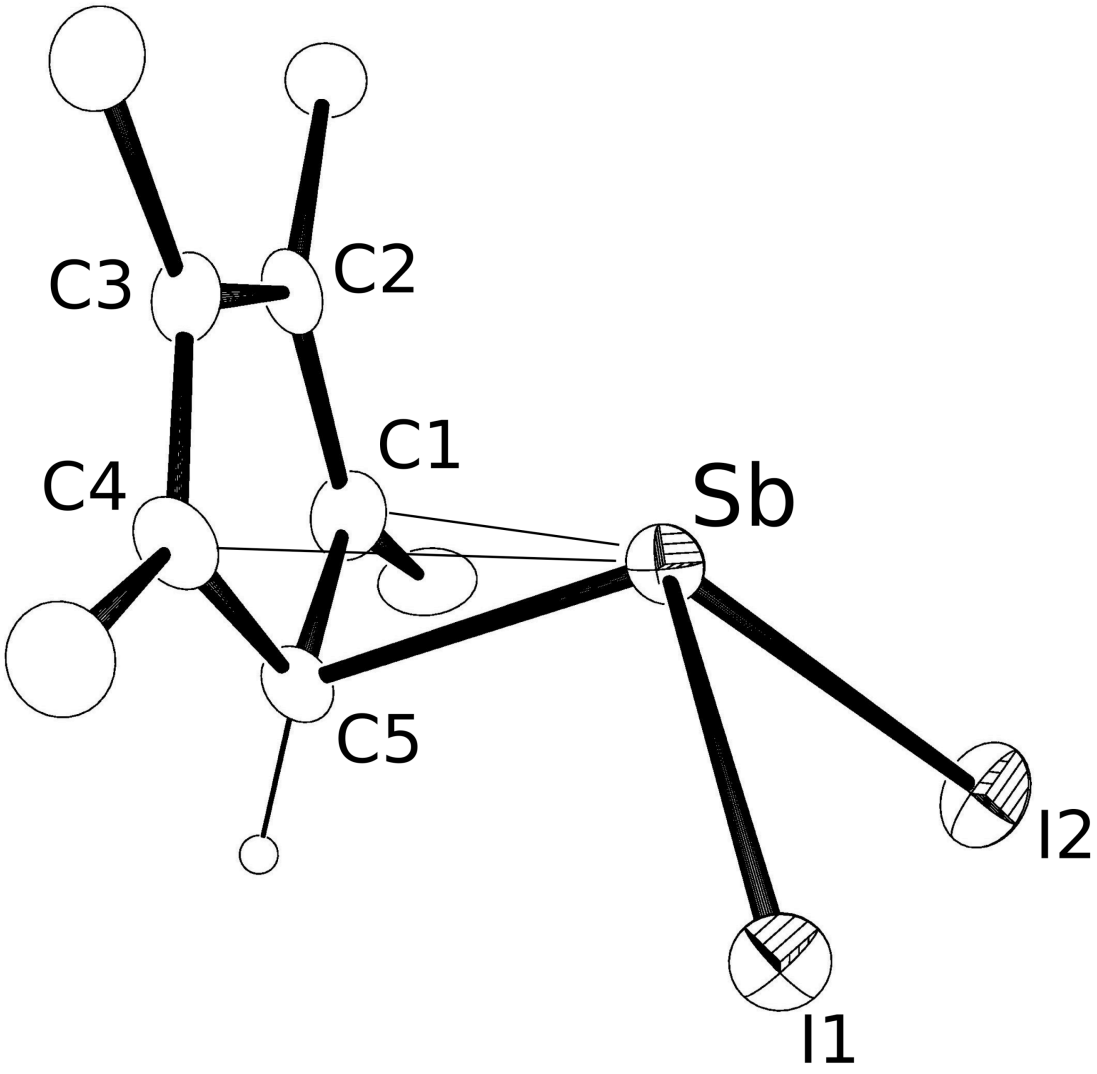

Figure 24. ORTEP of $Sb(C_5Me_4H)I_2$ (**3**), illustrating the numbering scheme used in the text. Thermal ellipsoids are shown at the 50% level.

Table 7. Selected bond distances and angles for $Sb(C_5Me_4H)I_2$.

atoms	distance (Å)	atoms	angle (°)
Sb1–C5	2.267(9)	I2–Sb1–I1	89.81(4)
Sb1–C1	2.616(11)	C5–Sb1–I1	101.5(2)
Sb1–C4	2.626(9)	C1–Sb1–I1	135.3(2)
Sb1–I2	2.8416(10)	C4–Sb1–I1	96.1(2)
Sb1–I1	2.8763(10)	C5–Sb1–I2	105.0(2)
C1–C2	1.403(14)	C1–Sb1–I2	95.2(2)
C1–C5	1.485(13)	C4–Sb1–I2	138.76(19)
C2–C3	1.435(11)	C4–C5–C1	106.0(8)
C3–C4	1.378(14)	C4–C5–Sb1	86.7(5)
C4–C5	1.463(12)	C1–C5–Sb1	85.7(6)

The I1–Sb–I2 angle of 89.81(4)° in **3** indicates the use of pure *p* orbitals in the bonding, and the Sb–I bond lengths (2.859(1) Å, avg) are in a typical range. They match the "short" Sb–I distances found in solid SbI_3 (2.87 Å),[127] but are longer than the same distances in the related $SbEI_2$ compounds (e.g., 2.799 Å in $SbMeI_2$[128] and 2.753 Å in $SbPhI_2$[129]). These are "soft" distances, however, and easily distorted by intermolecular interactions. In the case of **3**, there are van der Waals interactions between adjacent iodides (I2···I2′ = 3.92 Å) (Figure 25) that are on the order of I···I′ interatomic distances within a layer of crystalline iodine (3.50 and 3.97 Å),[130] and help to order the molecules into a coordination polymer. These interactions are associated with paired cyclopentadienyl rings, with a $Cp'_{centroid}\cdots Cp'_{centroid}$ distance of 3.60 Å. Adjacent Cp rings are staggered, and corresponding Me···Me′ contact distances are within the range for van der Waals interactions (3.68-3.99 Å).[131] There are also Me···Me′ contacts between the chains (not shown) at distances of 3.57 Å (C9···C9′) and 3.72 Å (C6···C7′), also clearly within van der Waals contact.

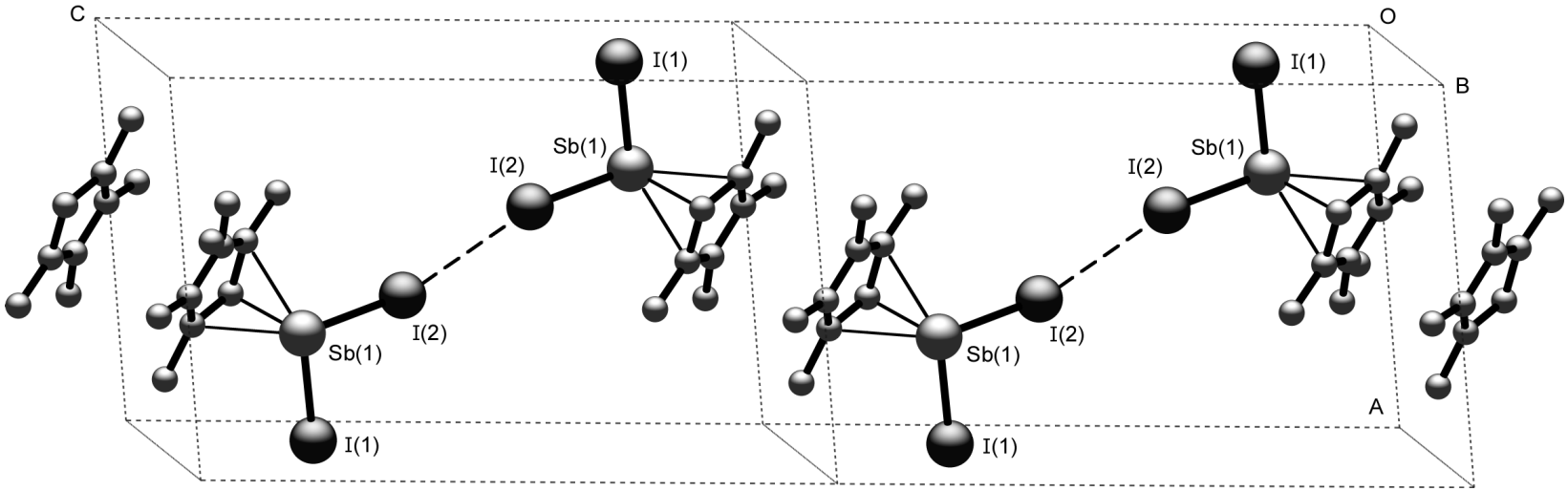

Figure 25. Packing in the unit cells of $Sb(C_5Me_4H)I_2$illustrating the I···I′ interactions and stacking of the cyclopentadienyl rings.

Computational Results

The similarities of the structure of **1**, **2** and $Sb(C_5H_5)_3$ suggested that a computational investigation of the structure of $As(C_5H_5)_3$ would be of interest. Calculations have been reported for the cyclopentadienyl arsines $As[(C_5(iPr)_4H]Cl_2$ (semiempirical methods),[125] $As(C_5H_5)H_2$ (HF, MP2,[132] DFT[120,133] and coupled cluster methods[120]) and $As(C_5H_5)Cl_2$ (DFT and coupled cluster methods[120]); we are not aware of previous calculations on the tris(cyclopentadienyl)arsines themselves.

Not surprisingly, we find the parent $As(C_5H_5)_3$ to be a conformationally flexible species. Two geometries were initially examined for its structure with DFT methods; one modeled on the ring arrangements in **1** (Figure 26a), and one with imposed C_3 symmetry (Figure 26b). The average As–C bond distances in 26a are within 0.006 Å of the distance in **1**, and those of 26b match the distances in **1**; the presence of the methyl groups evidently have little effect on this structural feature. The orientation of the C_5 ring planes relative to the C11–C1–C6 plane in 26a mimics that in **1**, with angles of 40.8°, 83.9, and 72.4° for the rings containing C11, C1, and C6, respectively. Both structures are local minima on the potential energy surface ($N_{imag} = 0$), and 26a is lower in energy than 26b by only 2.2 kcal mol^{-1} ($\Delta G°$).

An analogous set of calculations was performed on **1**. The presence of the methyl groups does not affect the relative energies of the structure modeled on **1** (Figure 26c), compared to one with imposed C_3 symmetry (Figure 26d). The average As–C bond distances of both in are within 0.006 Å of each other, and are approximately 0.03 Å longer than in the crystal structure. The energies of the two forms are virtually indistinguishable

(+2.4 kcal mol^{-1} higher in $\Delta H°$ for 26d than 26c, but < 0.1 kcal $mole^{-1}$ difference in $\Delta G°$); evidently the energetic cost of σ-bond ring rotation is negligible.

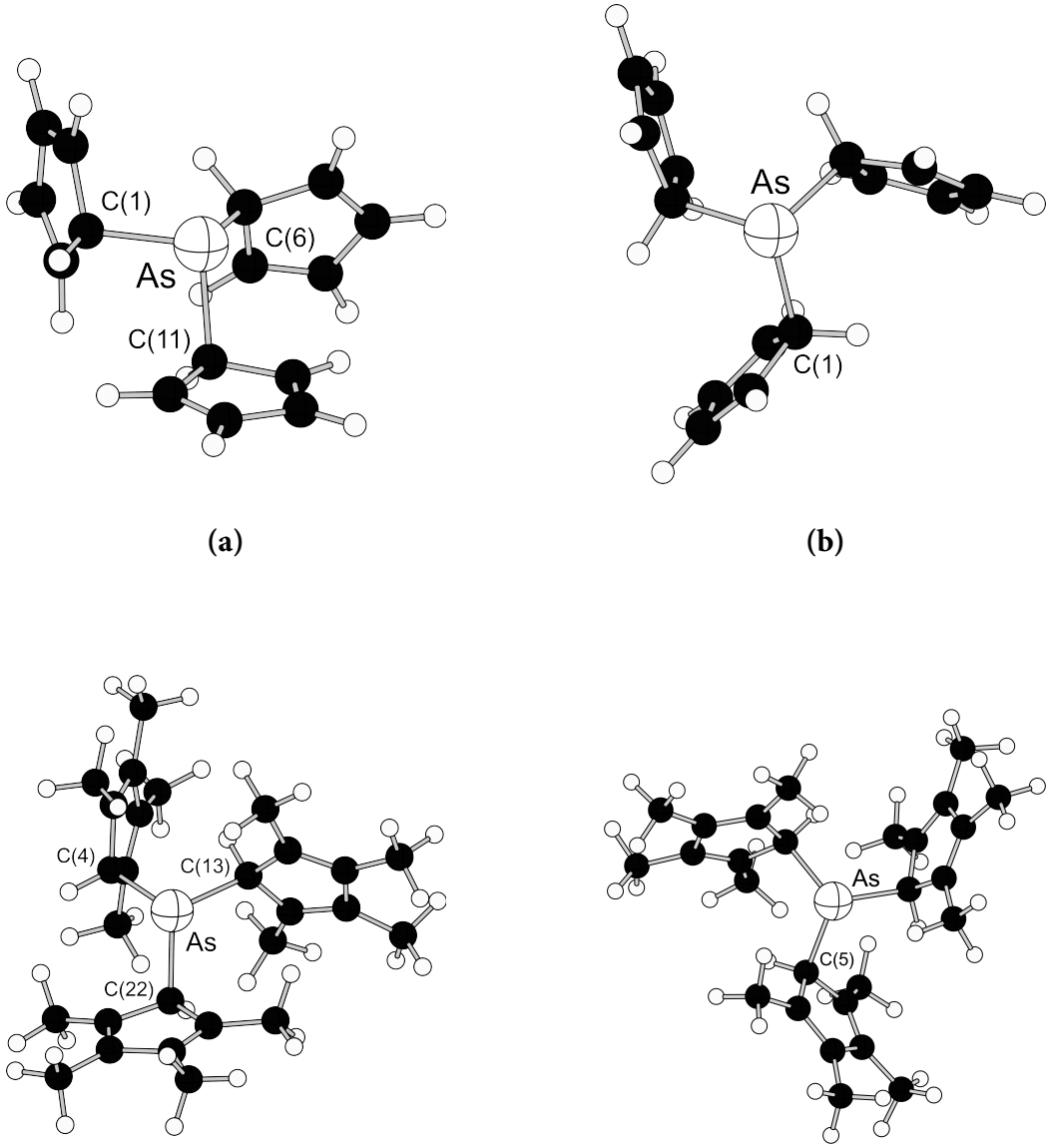

(a) **(b)**

(c) **(d)`**

Figure 26. Calculated structures of $As(C_5Me_nH_{5-n})_3$ (B3PW91/cc-pVDZ). (**a**) $As(C_5H_5)_3$, C_1 symmetry; As–C = 2.039 Å (av); C–As–C = 98.2–101.5°. (**b**) $As(C_5H_5)_3$, C_3 symmetry, As–C = 2.033 Å; C–As–C = 101.8°. (**c**) $As(C_5Me_4H)_3$, C_1 symmetry; As–C = 2.058 Å (av); C–As–C = 97.0–107.8°. (**d**) $As(C_5Me_4H)_3$, C_3 symmetry, As–C = 2.064 Å; C–As–C = 105.1°.

To examine the transition geometry for metallotropic rearrangements, the geometry of $As(C_5H_5)_3$ and **1** were reoptimized with the BB1K functional, which is specifically designed for estimation of transition state energetics.[68] The ground state structure of $As(C_5H_5)_3$ (Figure 27a) was based on that in Figure 26a; the transition geometry (ν = -232 cm^{-1}) is illustrated in Figure 27b, and lies 12.0 kcal mol^{-1} ($\Delta G°$) above the ground state. This is in good agreement with the estimated experimental value of $\Delta G^{‡}$ = 11 kcal mol^{-1} calculated from variable temperature solution NMR data (see above). A related set of calculations was also performed on $Sb(C_5H_5)_3$, and a transition geometry (ν = –107 cm^{-1}) was found 5.1 kcal mol^{-1} ($\Delta G°$) above the ground state; this low value is consistent with the inability to freeze out ring rotation in solution NMR spectra even at –70 °C.

Similar calculations was performed on **1** (Figure 28), including a model in which a C_5Me_4H ring has been rotated so that the arsenic is bonded to a methyl-bearing carbon (28c). Both 28a and 28c are minima on the potential energy surface (N_{imag} = 0), with 28c higher in energy by 4.4 kcal mol^{-1}. The transition geometry (N_{imag} = –166 cm^{-1}) is illustrated in Figure 28b, and lies 14.6 kcal mol^{-1} ($\Delta G°$) above the ground state. This is a modest increase in the barrier compared to that for the unsubstituted compound, and indicates that there is comparatively little additional steric congestion because of the methyl groups.

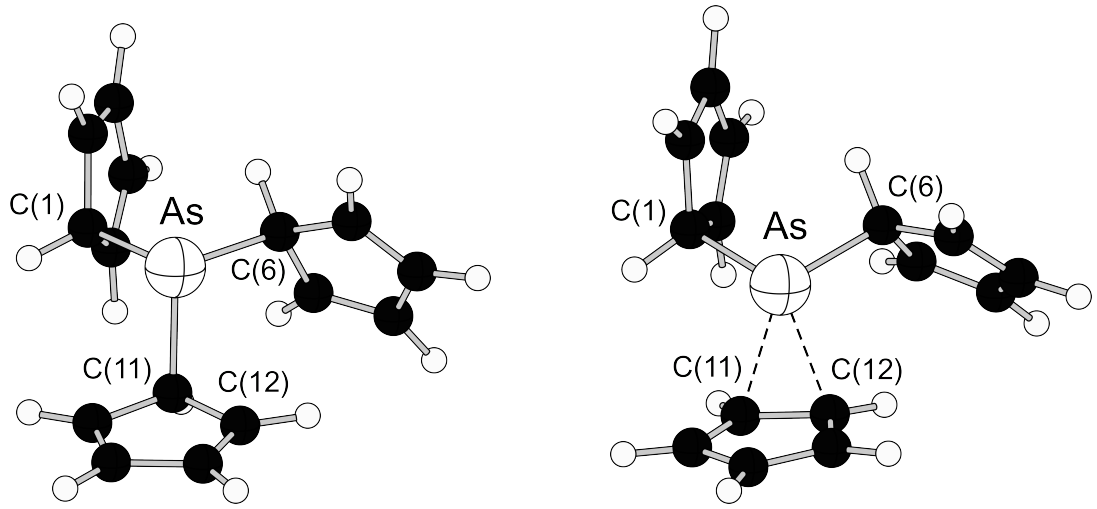

Figure 27. Calculated structures of $As(C_5H_5)_3$ (BB1K/aug-cc-pVDZ-PP (As), cc-pVDZ (C,H)). (**a**) As–C(11) = 2.014 Å (av); C–As–C = 97.3–100.6°. (**b**) As···C(11) = 2.302 Å; As···C(12) = 2.203 Å; As–C(1) = 2.065 Å; As–C(6) = 2.031 Å; C(1)–As–C(6) = 95.6°.

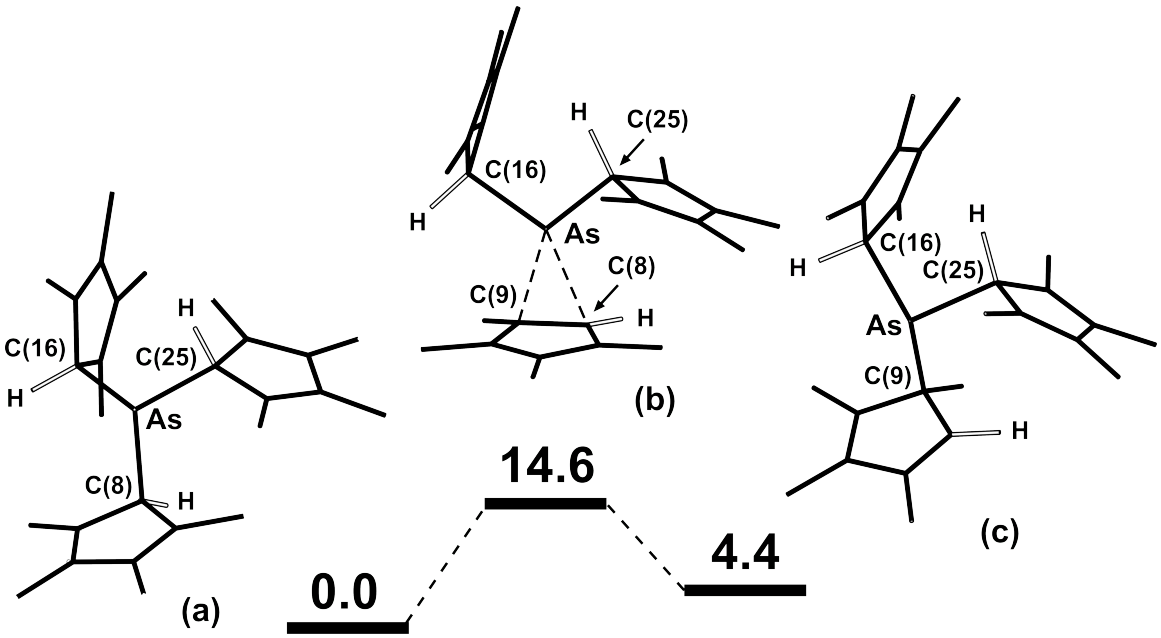

Figure 28. Free-energy profile (kcal mol^{-1}) for the 1,2-haptotropic bonding shift in $As(C_5Me_4H)_3$ with hydrogens on the methyl groups removed for clarity (BB1K/aug-cc-pVDZ-PP (As), cc-pVDZ (C,H)). Selected bond distances (Å) and angles (°): (a) As–C = 2.027 Å (av); C–As–C = 97.3–100.6°. (b) As···C(8) = 2.309 Å; As···C(9) = 2.228 Å; As–C(16) = 2.114 Å; As–C(25) = 2.036 Å; C(16)–As–C(25) = 95.7°. (c) As–C(9) = 2.055 Å; As–C(16) = 2.065 Å; As–C(25) = 2.023 Å; C(16)–As–C(25) = 98.6°; C(16)–As–C(9) = 114.5°.

Conclusion

Increasing the number of methyl groups on a cyclopentadienyl ring is a well-known method for tuning the physiochemical properties of transition metal complexes. Additional methyl groups systematically reduce the reduction potential of ferrocenes, for example, and progressively stabilize low-spin magnetic states in manganocenes.[4a] In main group complexes, where the balance between σ- and π-bonding is often delicate,[126] the modification in properties may not be as smooth. In particular, the change from a tetramethylated to a permethylated cyclopentadienyl ring can induce a disproportionally large alteration in properties. The η^5/η^1 'slip-sandwich' geometry of unsubstituted beryllocene, $Be(C_5H_5)_2$,[62b] for instance, is maintained even in its octamethyl $Be(C_5Me_4H)_2$ counterpart; yet the rings shift in decamethylberyllocene ($Be(\eta^5\text{-}C_5Me_5)_2$) to form a classically symmetric sandwich structure.[61f]

As to whether tetramethylcyclopentadienyl rings will substantially modify the properties of a main-group complex, such as in the case of $Sb(C_5H_5)_3$, which is already a monomeric, thermally stable compound (mp 53 °C), the additional methyl groups of **2** raises the melting point of the compound by about 40 °C, but other features, including its solid state structure, are largely unchanged. In addition, the synthesis of **2** via salt metathesis is accomplished exactly as for $Sb(C_5H_5)_3$. Interestingly, the discontinuity in properties that can be effected with pentamethylcyclopentadienyl rings is also observed with these compounds; the reaction of SbI_3 with $Na[C_5Me_5]$ does not yield $Sb(C_5Me_5)_3$, but rather the product of an apparent disproportionation process, *cyclo*-[σ-$Sb(C_5Me_5)]_4$.[116,134]

With **1**, in contrast, the increase in kinetic stability is such that the polymerization and decomposition observed at room temperature in $As(C_5H_5)_3$ is suppressed, making the substituted compound much more tractable. The thermal stability of **3** is also improved compared to $Sb(C_5H_5)I_2$, and in addition, **3** is no longer light-sensitive. The improvement in photostability does not extend to **2**, which may be a consequence of its larger number of electron-rich cyclopentadienyl rings.

The influence of ring methylation in cyclopentadienyl complexes of the Group 15 elements cannot be simply summarized, as it varies with the metal, the number of rings, and the presence of auxiliary ligands. The mix of covalent and ionic bonding found in these compounds makes controlling their chemistry especially challenging.

CHAPTER V

s-Block Metal Complexes of Phosphonium Ylides

Introduction

Distinctive electronic, structural, and configurational properties can be incorporated into *ansa*-metallocenes, $[ZCp'_2]MX_n$, by varying the identity of the *ansa*-bridge *Z*.[135] Most commonly this is done while leaving the net charge of the $[ZCp'_2]_n$ ligand at –2, as found not only in the catalytically important silyl bridged species $[R_2SiCp'_2]MX_2$,[136] but also in complexes with *Z* = R_2E (E = C, Ge, Sn), and *Z* = RE′ (E′ = B, P(III), As(III)).[137] In principle, *ansa* bridges with different charges could expand the range complexes available from a given oxidation state of a metal, allowing the preparation of isostructural complexes from different metal families; e.g., $[R_2SiCp'_2]M(III)X$ ~ $[R_2PCp'_2]M(II)X$ ~ $Cp'_2M(III)X$ (Figure 29). This same rationale can be applied to similar ligand systems using the 1,3-bis(trimethylsilyl)allyl anion $[1,3\text{-}(SiMe_3)_2C_3H_3]^-$ (A′) or the (trimethylsilyl)allyl anion $[(SiMe_3)C_3H_4]^-$ (A″) in place of either both Cp′ ligands or both Cp′ ligands and an additional R group (i.e., $[R_2PA'_2]^-$, $[RPA'_3]^-$, etc).

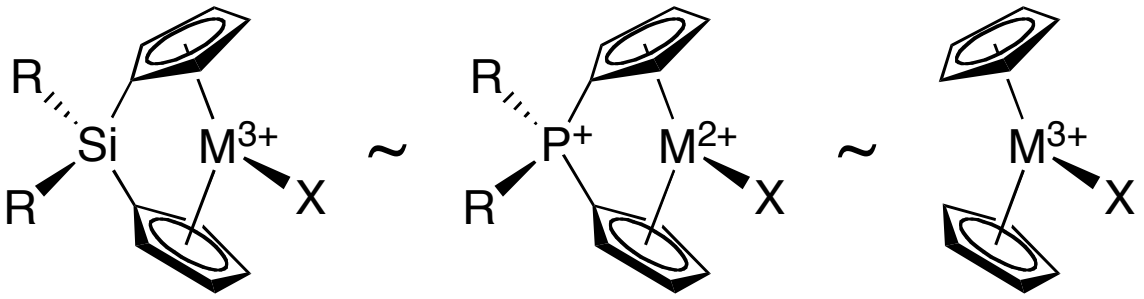

Figure 29. Isostructural silyl- and phosphonium-bridged metallocenes containing metals in different oxidation states. There is a formal similarity to unbridged bis(cyclopentadienyl) complexes (at right).

The extent to which such analogies have been studied varies with the *ansa*-bridge. In the case of phosphonium-bridged complexes, Brintzinger has used the ligand $[Me_2P(2\text{-}Me\text{-}4\text{-}t\text{-}Bu\text{-}C_5H_2)_2]^-$ ($[Me_2PCp''_2]^-$) to prepare a series of Group 1 and 2 *ansa*-metallocenes.[138] Among these, the complex $Me_2PCp''BaN(SiMe_3)_2$ is formally similar to $Cp'_2LnN(SiMe_3)_2$ compounds, and even though the barium complex has not been structurally authenticated, it does not undergo Schlenk redistribution to $(Me_2PCp''_2)_2Ba$ and $Ba[N(SiMe_3)_2]_2$ in solution, as is common in heavy Group 2 cyclopentadienyl complexes.[4b] Parkin has prepared the phosphonium bridged complexes $[\{Me_2P(C_5Me_4)_2\}MCl_2]^+I^-$ (M = Zr, Hf), and studied their reaction with methylating agents and CO.[139] These are compositionally related to the niobium(V) and tantalum(V) species $[(C_5H_5)_2MCl_2]^+X^-$ (M = Nb, X = I; M = Ta, X = Br, I), although reactions of the latter have not been extensively studied.[140]

In some cases, however, comparisons between phosphonium-bridged species and other complexes cannot be made at all. For example, calcium and barium both prefer to remain solvated with neutral oxygen donor ligands rather than bind to the phosphonium diylide $[Me_2P(fluorenyl)_2]^-$.[97] In contrast, although the metal-ligand coordination is sometimes considerably distorted, bis(fluorenyl) complexes such as $(fluorenyl)_2Ba(NH_3)_4$,[141] $(fluorenyl)_2BaLn$ (L = thf, dme, pyridine),[142] and [9-$(Me_3Si)_3Si$-fluorenyl)]$M(thf)_2$ (M = Ca, Sr) can be isolated,[143] as can complexes with the silyl bridged $[Me_2Si(fluorenyl)_2]^{2-}$ dianion.[11]

Ansa-bridged allyl complexes containing a Si bridge are widely known. In addition, Layfield has synthesized the *ansa*-bridged tripodal allyl complex K(thf)[(1,3-

$(SiMe_3)_2C_3H_3)_3Sn]$ which contains a bridging tin atom.[29] That same work outlines the synthesis of a tripodal mono(trimethylsilyl)allyl complex containing a silicon *ansa* bridge. However, unlike the Cp analog, *ansa*-bridged compounds containing either two or three mono- or bis(trimethylsilylated)allyl anions with a phosphorus bridging atom have yet to be synthesized.

The kinetic stability offered by a chelating $[R_2PCp'_2]^-$, $[R_2PA''_2]^-$, or $[RPA''_3]^-$ ligand is an attractive feature for complexes of highly electropositive metals, where ligand redistribution reactions are common. What follows is the attempted synthesis and structural characterization of a phosphonium-bridged alkaline-earth allyl complex that can be directly compared with trivalent lanthanide species, and density functional theory studies of bending in *ansa*-bridged cyclopentadienyl and allyl ligands.

Experimental

General Considerations. All manipulations were performed with the rigorous exclusion of air and moisture using high vacuum, Schlenk, or glovebox techniques. Proton (^{1}H and ^{1}H{^{31}P}), carbon (^{13}C{^{1}H}) and phosphorus (^{31}P{^{1}H}) NMR spectra were obtained at 25 °C on a Bruker DPX-400 spectrometer at 400, 100.6 and 161.9 MHz, respectively, and were referenced to the residual proton or ^{13}C resonances of THF-d_8 (δ 3.58 (^{1}H), 67.4 (^{13}C)), C_6D_6 (δ 7.15 (^{1}H)), CD_2Cl_2 or for ^{31}P NMR, an external standard of H_3PO_4. Elemental analyses were performed by Desert Analytics, Tucson, AZ. Melting points were determined in sealed capillaries.

Materials. Anhydrous calcium iodide was a commercial sample (Cerac, 95%) and was heated under vacuum (150 °C, 10^{-4} Torr) to ensure complete removal of water and residual amounts of free iodine. $Ca[N(SiMe_3)_2]_2$ was prepared as described previously.[144] Potassium hydride was purchased from Strem and washed with hexanes in a glovebox prior to use. $C_5Me_4H_2$, $K[N(SiMe_3)_2]$, *t*-$BuPCl_2$, PCl_3, CD_2Cl_2, MeOTf, $[Me_3O][BF_4]$, and MeI were purchased from Strem, Acros or Aldrich and used as received. $K[C_5Me_4H]$ was made by the reaction of $C_5Me_4H_2$ with $K[N(SiMe_3)_2]$. $K[1,3\text{-}(SiMe_3)_2C_3H_3]$[33] was prepared following the published procedures. The compounds $[Me(t\text{-}Bu)P(C_5Me_4Li)_2]I$, $K[Me(t\text{-}Bu)P(C_5Me_4)_2](thf)$, and $[Me(t\text{-}Bu)P(C_5Me_4)_2]CaN(SiMe_3)_2$ were synthesized previously and repeated for spectroscopic and elemental analysis according to published literature procedures.[98] Butyllithium was purchased from Aldrich as a 2.5 M solution in hexanes. THF, toluene, and hexanes were distilled under nitrogen from potassium

benzophenone ketyl. C_6D_6 and THF-d_8 were vacuum distilled from Na/K (22/78) alloy and stored over type 4A molecular sieves prior to use.

Attempted Synthesis of {(Me)(*t*-Bu)P[(SiMe$_3$)$_2$C$_3$H$_3$]$_2$}I (1). A THF solution of KA′ (7.21 g, 32.1 mmol) was added via cannula to a cold (-78 °C) hexane solution of (*t*-Bu)PCl_2 (2.55 g, 16.1 mmol). This was allowed to warm to room temperature and stir for 12 h. All volatiles were removed from the suspension and the resulting yellow waxy solid was extracted with hexane and filtered over a medium porosity frit. The filtrate was then cooled to 0 °C and treated with MeI (1.1 mL). These were allowed to react at room temperature for 24 h, after which time no visual change occurred. ^{1}H NMR confirmed the presence of unreacted (*t*-Bu)PA'_2 and MeI.

Synthesis of {(Me)(*t*-Bu)P[(SiMe$_3$)C$_3$H$_4$]$_2$}I (2). A THF solution of KA″ (5.35 g, 35.1 mmol) was added via cannula to a cold (-78 °C) hexane solution of (*t*-Bu)PCl_2 (2.79 g, 17.5 mmol). This was allowed to warm to room temperature and stir for 12 h. All volatiles were removed from the suspension and the resulting yellow waxy solid was extracted with hexane and filtered over a medium porosity frit. The filtrate was then cooled to 0 °C and treated with MeI (1.1 mL). These were allowed to react at room temperature for 24 h, after which time a copious amount of white powder was obtained. This powder was isolated via filtration over a medium porosity frit, washed with hexane (3 × 20 mL) and dried under vacuum to afford **2**. ^{1}H NMR (THF-d_8): δ 6.41 (m, 2H, P-γ-C*H*, $^4J_{PH}$ = 4.1 Hz), 6.21 (m, 2H, P-β-C*H*, $^3J_{PH}$ = 3.7 Hz), 3.89 (m, 4H, P-α-CH_2, $^2J_{PH}$ = 7.0 Hz), 2.26 (d, 3H, *Me*-P, $^2J_{PH}$ = 12.9 Hz), 1.44 (d, 9H, *t-Bu*-P, $^3J_{PH}$ = 16.1 Hz). ^{31}P NMR (THF-d_8): δ 35.7.

General Procedure for Attempted Synthesis of {(Me)P[(SiMe$_3$)C$_3$H$_4$]$_3$}X (X = I, OTf, and BF$_4$). A toluene suspension of KA″ was heated to reflux until all KA″ had dissolved. The resulting hot, dark red solution was treated with a toluene solution of PCl_3 (ratio of KA″:PCl_3 = 3:1). The resulting solution immediately lightened to yellow and, as it cooled to room temperature, white precipitate was evident. This was allowed to stir for 12 h at room temperature, after which time all volatiles were removed and the resulting residue was extracted with hexane (3 × 15 mL) over a medium porosity frit to afford a golden yellow filtrate of PA″$_3$. In an attempt to form the phosphonium salt, this filtrate was treated with MeI, MeOTf, and [Me$_3$O][BF$_4$]. The reaction with MeI showed only a trace amount of {(Me)P[(SiMe$_3$)C$_3$H$_4$]$_3$}I that could be detected by ^{1}H NMR, in addition to unreacted PA″$_3$ and MeI. However, neither MeOTf nor [Me$_3$O][BF$_4$] showed any sign of reaction, and ^{1}H NMR of each showed unreacted PA″$_3$ and MeOTf, or, in the case of [Me$_3$O][BF$_4$], a complicated spectrum (due to the loss of Me_2O).

Computational Details. Calculations involving the Cp compounds were performed using Gaussian 03W.[67] Geometry optimizations were carried out with the B3PW91 functional, which incorporates Becke's three–parameter exchange functional[71] with the 1991 gradient–corrected correlation functional of Perdew and Wang.[72] The standard 6-31+G(d,p) basis set was used for all computations; atomic charges were calculated with the Natural Population Analysis (NPA) method.[145] Displacements of the ring substituents were calculated under C_s symmetry. The bending angles graphed in Figure 30 are initial β values; because of puckering of the rings during optimization, they may differ from the

final β values by several degrees. Qualitative (and even semi-quantitative) conclusions about the energetics of bending are not affected by this.

Calculations involving allyl compounds were performed with the Amsterdam Density Functional suite (ADF)[146] using the gradient-generalized approximation of Becke[147] and Perdew.[148] Relativistic effects were included using the zeroth order relativistic approximation to the Dirac equation (ZORA). All-electron triple zeta double polarized (TZ2P) basis sets included with the ADF suite were employed. The ADF integration accuracy parameter was set to 5.0 for all calculations to ensure convergence for all numerical integrals. Atomic coordinates for all optimized structures are given in Appendix C.

Results and Discussion

Synthesis of Allyl Compounds

A general preparative route for the synthesis of bis- and tris(allyl)phosphonium compounds is given in Figure 30. A number of synthetic challenges were encountered in an attempt to isolate the various compounds, and they will be discussed below.

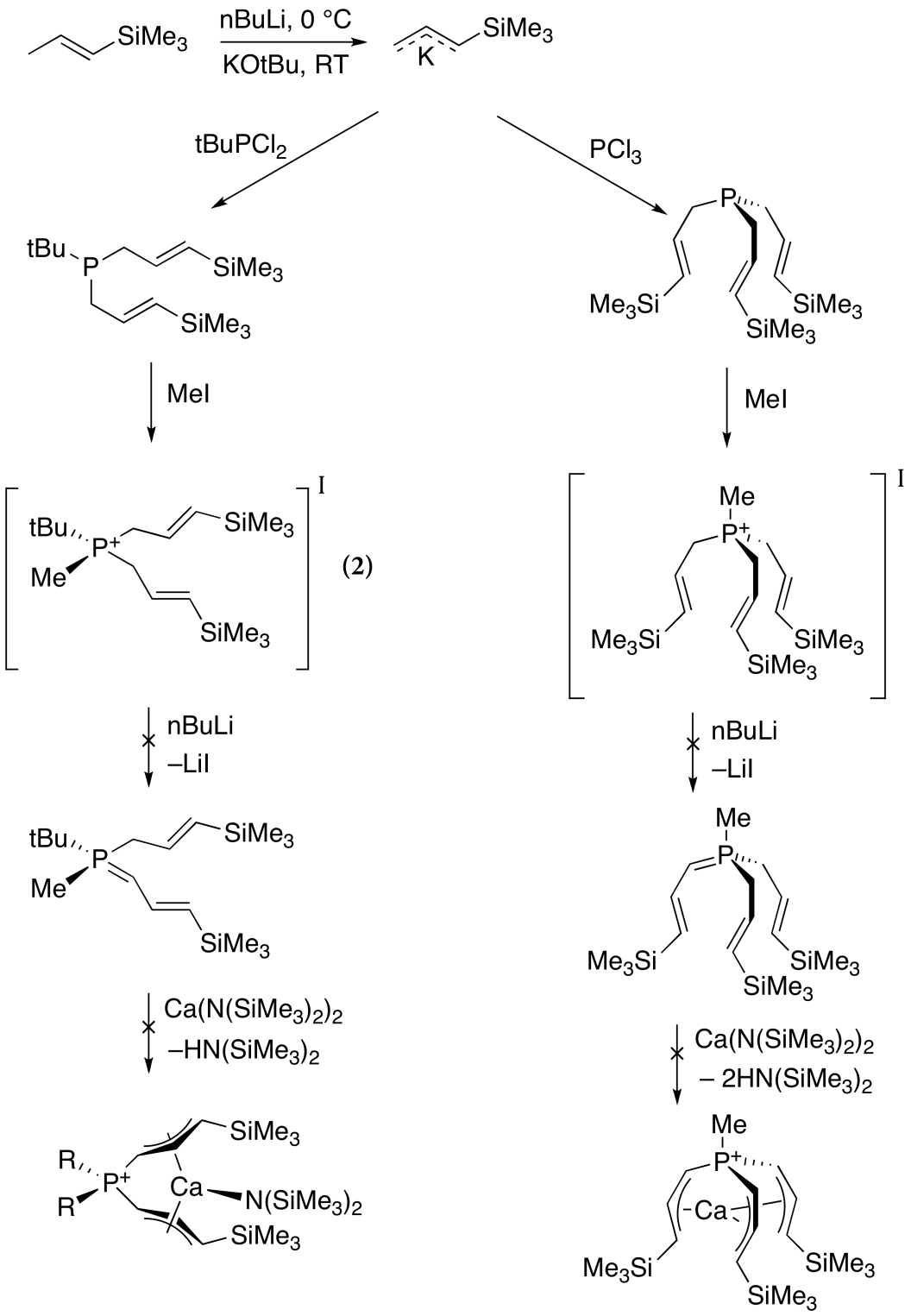

Figure 30. General preparative strategy for the attempted synthesis of bis- and tris(allyl)phosphonium compounds.

Synthesis of both (*t*-Bu)PA″$_2$ and PA″$_3$ proceed via the smooth reaction of either (*t*-Bu)PCl_2 or PCl_3 and either 2 or 3 equiv of KA″, respectively. Formation of the structurally similar (*t*-Bu)PA′$_2$ and PA′$_3$ is possible, but these phosphines are too bulky to react further to form the phosphonium salts (vide infra). Formation of the phosphonium iodide **2** is achieved by reaction of (*t*-Bu)PA″$_2$ and MeI in hexane: the ^{1}H and ^{1}H{^{31}P} spectra of **2** are shown in Figure 31.

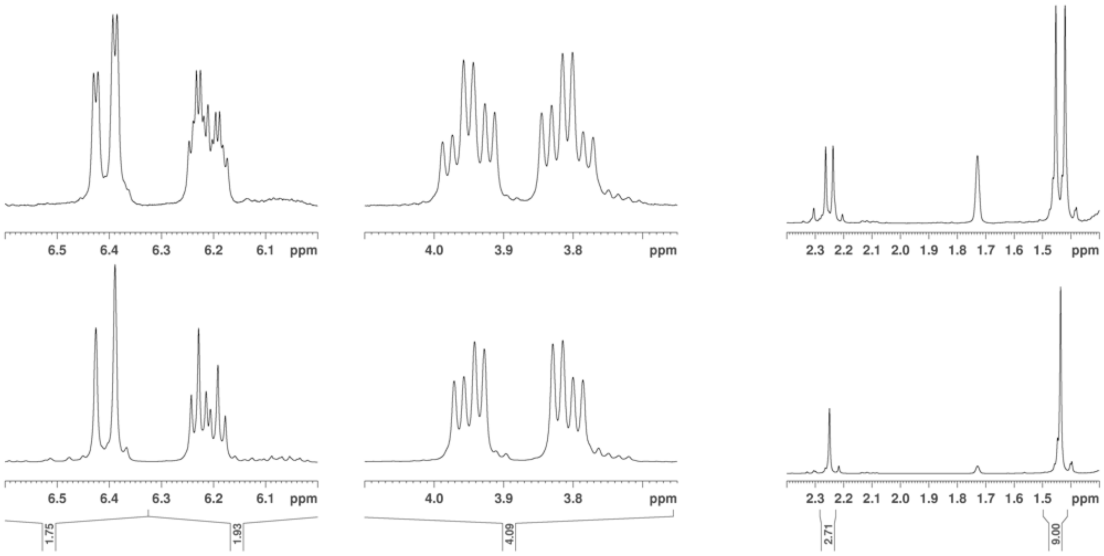

Figure 31. The ^{1}H (top) and ^{1}H{^{31}P} NMR spectra of {(Me)(*t*-Bu)P[(SiMe$_3$)C_3H_4]$_2$}I. Note that P–H coupling is evident even for those protons that are 4 bonds away from the phosphorus atom, and that the splitting patterns are less complex in the phosphorus-decoupled spectrum.

Because of the reactivity of the structurally related Cp phosphonium iodide, attempts were made to transform the allyl phosphonium iodide using the same methods.[98] However, these attempts were met with limited success. Unlike the Cp compound, which is readily deprotonated to form both the ylide and the lithium and potassium salts, the allyl compound undergoes a reaction with nBuLi or KH that yields an intractable dark purple solution with a highly complex ^{1}H NMR spectrum, which is inconsistent with either the neutral ylide or the K or Li salts.

With that in mind, attempts were made to synthesize a tripodal allyl phosphonium salt that contains three allyls and one methyl group bound to a central phosphorus. Such a molecule would have higher symmetry in solution, which would lead to a more easily interpreted ^{1}H NMR spectrum. Synthesis of PA″$_3$ is straightforward, however repeated attempts to form the phosphonium salt [(Me)PA″$_3$]X were met with limited success. Reaction of PA″$_3$ with MeI forms the expected [(Me)PA″$_3$]I only in trace yield; as a result, stronger methylating agents were employed. Reaction of PA″$_3$ with MeOTf to form [(Me)PA″$_3$]OTf were unsuccessful, despite the higher methylating power of MeOTf. In fact, reaction of PA″$_3$ with [Me$_3$O][BF$_4$] was also unsuccessful, despite the driving force of such a reaction due to the formation of the highly volatile Me$_2$O ether and the ostensibly high crystal-packing force supplied by the BF_4^- counter ions. The resulting ^{1}H NMR spectra of all three reactions showed unreacted starting materials or, in the case of [Me$_3$O][BF$_4$], a complex mixture, possibly due to the loss of Me$_2$O.

Computational Results: Cyclopentadienyl Ligands

C- and especially Si-bridged *ansa* metallocenes have been the subject of repeated computational investigations;[11,149] phosphonium-bridged counterparts, in contrast, have received much less attention. The $[Me_2P(C_5H_4)_2]^-$ anion has been studied with DFT methods (B3PW91/6-31+G(d)) as a model for $[Me_2P(\text{fluorenylidene})_2]^-$.[97] It was found that the calculated P–C distance (1.746 Å) and the C–P–C′ angle (115.9°) in the free $[Me_2P(C_5H_4)_2]^-$ anion were not greatly different from that of the substituted, complexed $[Me_2P(2\text{-Me-4-}(t\text{-Bu})\text{-}C_5H_2)_2]^-$ anion;[138] e.g., the P–C distances of the latter's potassium and barium derivatives average to 1.751 Å and 1.746 Å, respectively. The C–P–C′ angles in the two complexes (112.8(4)° in the K complex; 109.5(2)° in the barium compound) close somewhat to accommodate the metals. Recalculated values for $[Me_2P(C_5H_4)_2]^-$ with the slightly larger basis set 6-31+G(d,p), along with the methylated derivative $[Me_2P(C_5Me_4)_2]^-$ and the $[Me_2P(\text{fluorenylidene})_2]^-$ anion are reported in Table 9. Little change in the P–C distance or the C–P–C′ angle occurs on methylation or on substitution of the fluorenyl moiety for the cyclopentadienyl ring.

Table 8. Selected bond distance and angles for [Me(*t*-Bu)P(C_5Me_4)$_2$]CaN($SiMe_3$)$_2$.

atoms	distance (Å)	atoms	angle (°)
Ca(1)–C(1)	2.712(2)	C(1)–P(1)–C(10)	107.59(11)
Ca(1)–C(2)	2.682(2)	C(19)–P(1)–C(20)	99.64(14)
Ca(1)–C(3)	2.793(2)	C(1)–P(1)–C(19)	108.30(13)
Ca(1)–C(4)	2.873(2)	C(10)–P(1)–C(19)	106.94(13)
Ca(1)–C(5)	2.826(2)	C(1)–P(1)–C(20)	116.55(12)
Ca(1)–cent	2.501	C(10)–P(1)–C(20)	116.85(12)
Ca(1)···Si(1)	3.270(1)	N(1)–Si(1)–C(24)	107.1(11)
Ca(1)···Si(2)	3.448	N(1)–Si(1)–C(25)	114.2(14)
P(1)–C(1)	1.789(2)	N(1)–Si(1)–C(26)	115.6(14)
P(1)–C(19)	1.812(3)	N(1)–Si(2)–C(27)	114.95(14)
N(1)–Si(1)	1.679(2)	N(1)–Si(2)–C(28)	113.87(13)
Si(1)–C(24)	1.893(3)	N(1)–Si(2)–C(29)	109.64(12)
Si(1)–C(25)	1.878(3)	Ca(1)–N(1)–Si(1)	109.84(10)
Si(1)–C(26)	1.885(3)	Ca(1)–N(1)–Si(2)	119.56(11)
Ca(1)–N(1)	2.293(2)		
Ca(1)–C(10)	2.702(2)		
Ca(1)–C(11)	2.716(2)		
Ca(1)–C(12)	2.781(2)		
Ca(1)–C(13)	2.815(2)		
Ca(1)–C(14)	2.767(2)		
Ca(1)–cent	2.477		
Ca(1)···C(24)	3.035		
Ca(1)···C(29)	3.450		
P(1)–C(10)	1.796(2)		
P(1)–C(20)	1.896(3)		
N(1)–Si(2)	1.681(2)		
Si(2)–C(27)	1.880(3)		
Si(2)–C(28)	1.871(3)		
Si(2)–C(29)	1.875(3)		

The distortions in bond angles that accompany the coordination of *ansa*-bridged ligands to metals are well known.[137a,139] These can be categorized by reference to various angles (see Figure 32), and have been tabulated for structurally authenticated phosphonium bridged species in Table 9.

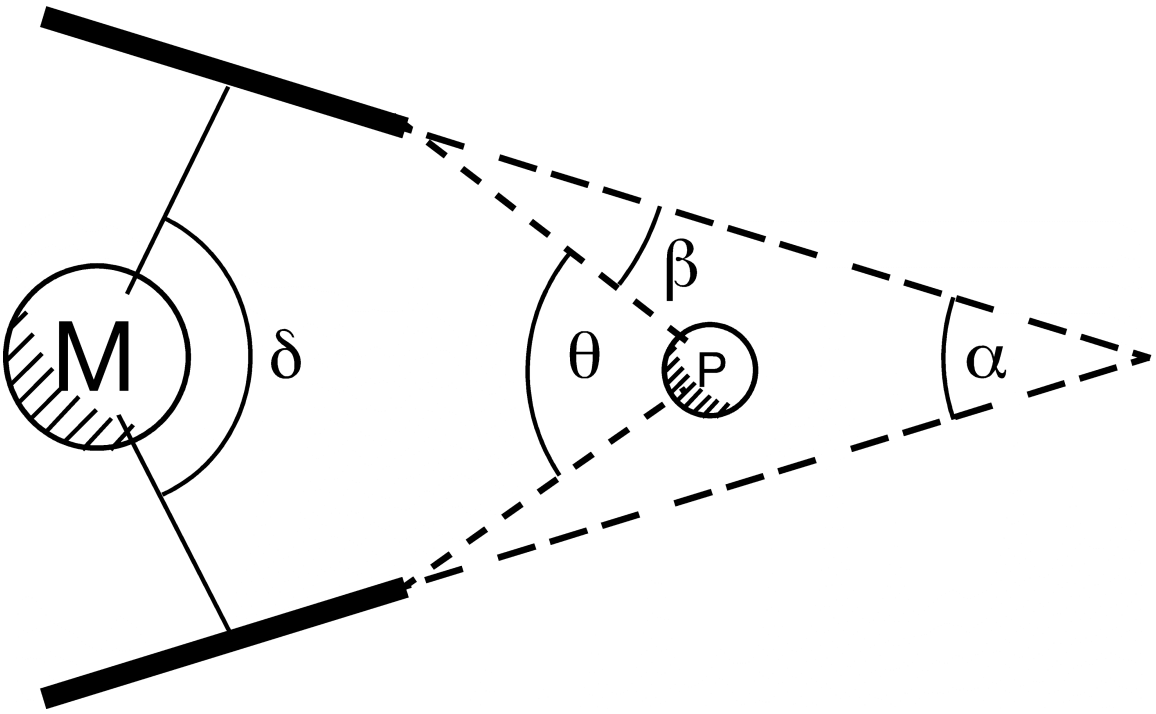

Figure 32. Geometric parameters in a phosphonium-bridged *ansa* metallocene. The angles are as follows: α = angle between the ring planes (ring tilt); β = tilt of the Cp ring relative to the P–C_{ipso} bond (ideally, β = (θ – α)/2); δ = ring centroid–M–ring centroid angle; θ = angle at phosphorus.

Table 9. Structural parameters for crystallographically characterized phosphonium-bridged metallocenes.[a]

Compound	*d*(M–cent)	*d*(M–C)	α	β	δ	θ	ref
[{$Me_2P(C_5Me_4)_2$}$ZrCl_2$]I	2.240	0.158	63.1	17.7	126.0	98.3	[139]
[{$Me_2P(C_5Me_4)_2$}$HfCl_2$]I	2.225	0.143	62.1	18.7	126.2	98.7	[139]
[{Me(Ph)P$(C_5H_4)_2$}Fe]OTf	2.240	0.158	24.4	37.9	163.6	99.8	[150]
[Me_2P(2-Me-4-*t*-Bu-$C_5H_2)_2$Ba$(thf)_3$]BPh_4	2.833	0.227	85.7	12.8	103.8	109.5	[138]
[Me(t-Bu)P$(C_5Me_4)_2$]$CaN(SiMe_3)_2$	2.489	0.191	68.8	19.8	118.2	107.5	this work

[a] d(M–Cp_{cent}) = metal–ring centroid distance (Å); $d(M–C)_{range}$ = range of M-C distances (Å); α, β, δ, θ, as defined in Figure 32 (in deg).

The angles at phosphorus (θ) are close to the tetrahedral ideal in the two alkaline-earth complexes, whereas the smaller metal centers of the transition metal compounds display roughly 10° of compression. The tilting of the Cp ring relative to the P–C_{ipso} bond (β) varies from a low of 13° in $[Me_2P(2\text{-}Me\text{-}4\text{-}t\text{-}Bu\text{-}C_5H_2)_2Ba(thf)_3]BPh_4$ to almost 38° in the highly distorted $[\{Me(Ph)P(C_5H_4)_2\}Fe]^+$ cation. Harder has shown with the aid of Hartree-Fock calculations that the energy required to bend a silyl group on the Cp anion is approximately half that required for an alkyl group,[11] a consequence of diminished delocalization in the Cp ring. We were interested in determining the extent that this might be true for phosphonium substituents.

DFT methods, which provide an accounting for electron correlation effects,[73b,151] were used to complete a set of calculations similar to those performed by Harder. They confirm that compared to the alkylated $[H_3CCp]^-$ anion, the *ipso* carbon of the $[H_3SiCp]^-$ anion bears the most negative charge; this is also true for the phosphonium ligand (Figure 33). Progressive loss of delocalization is evident in the change from carbon to silicon to phosphorus, as revealed in the lengthening of C_{ipso}–C_α and C_β–C_β' bonds relative to the C_α–C_β bonds. This can be quantified in the ratio $\Delta_L = ½(C_{ipso}–C_\alpha + C_\beta–C_\beta')/(C_\alpha–C_\beta)$, which equals 0.998, 1.013, and 1.034 for C, Si, and P, respectively. Bending the H_3E substituent out of the plane increases the charge on the C_{ipso} atom by 35% in the case of E = C (HF calculations put the change at 60%),[11] but leaves the charge unchanged when E = Si, and decreases the charge slightly (13%) in the phosphonium ligand. The delocalization decreases further on bending, but the change in Δ_L for a 50° bend is greatest for C (3.0%); that for Si (0.9%) and P (0.6%) is small.

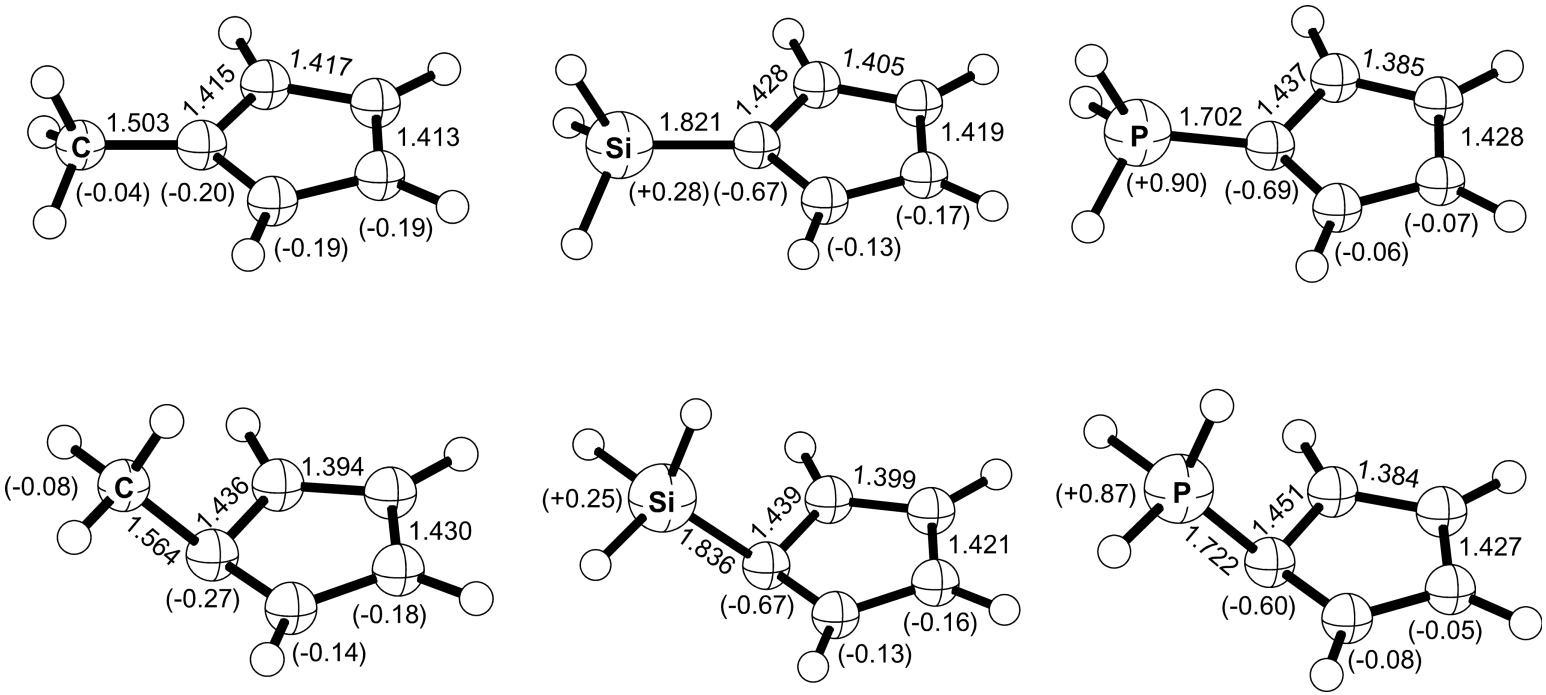

Figure 33. Geometries and group charges for undistorted and bent (β = 50°) $[H_3CCp]^-$, $[H_3SiCp]^-$, and $[H_3PCp]$ rings (left to right, respectively). Geometry optimization was carried out at the B3PW91/6-31+G(d,p) level of theory with C_s symmetry, and group charges are derived from NPA (in parenthesis).

The relative energetics of bending hold over a wide range of angles. The bending of a silyl group is always less costly than that of an alkyl, and in fact usually by substantially more than a factor of two (Figure 34). For a β angle of 30°, for example, the energetic cost of alkyl to silyl group bending is 3.5:1. The phosphonium ligand is even easier to bend, with an alkyl to phosphonium ratio of 8.7:1. Part of the reason for this is the previously mentioned loss of delocalization in the cyclopentadienyl rings in the Si- and P-based systems even prior to bending. In addition, the neutrality of the phosphonium-substituted ring (a consequence of the formal P(V) center) also makes the ring easier to bend, as less redistribution of charge is necessary.

NPA charges on the R_2P group relative to the rest of the molecule have been taken as a measure of the amount of delocalization in a diylide.[11] In $[Me_2P(C_5H_4)_2]^-$, the Me_2P/C_5H_4 difference is +1.16/-1.08 (Δ = 2.24); this amount of charge buildup is similar to that found for $[H_2P(CHPh)_2]^-$ (+1.09/-1.04; Δ = 2.13),[11] and reflects a similar loss of charge delocalization. Replacing the hydrogens on the cyclopentadienyl rings with methyl groups does not affect the charge buildup, as the Me_2P/C_5Me_4 ratio is +1.17/-1.08 (Δ = 2.25).

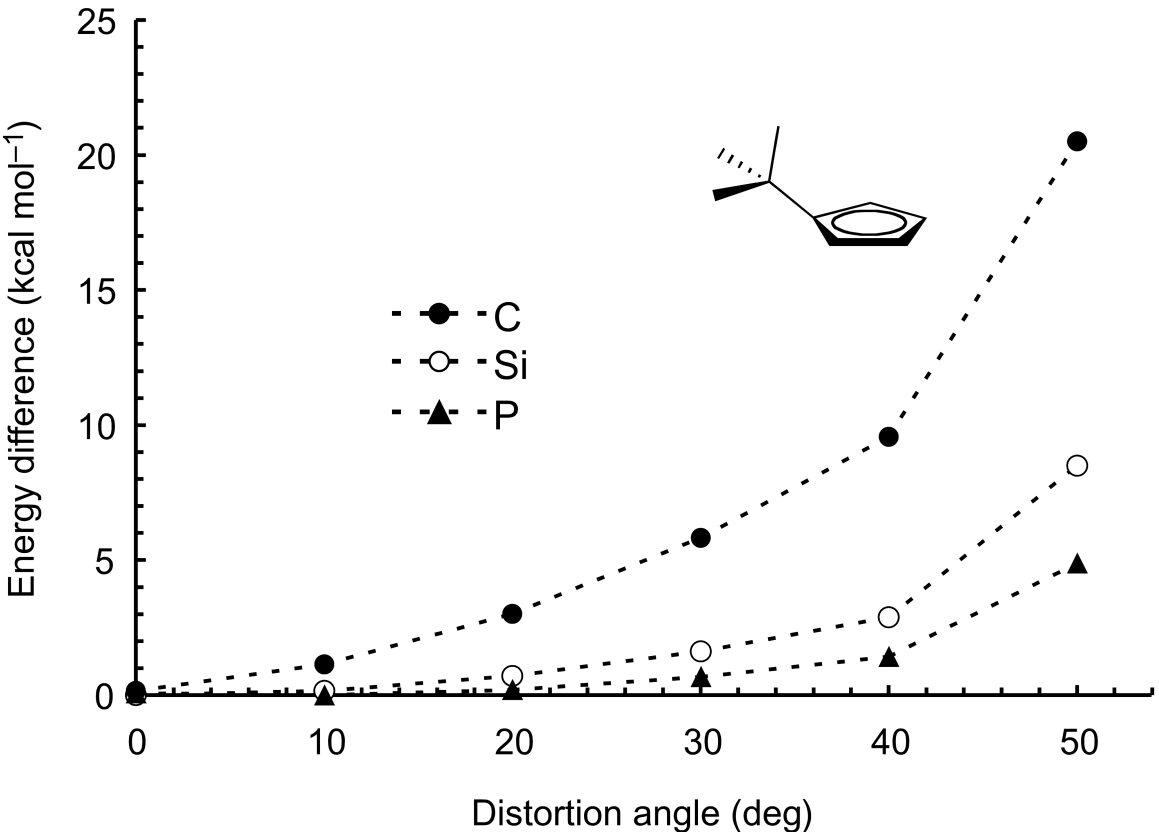

Figure 34. Relative energies (B3PW91/6-31+G(d,p)) as a function of bending the H_3E substituent out of the Cp ring plane for $[H_3CCp]^-$, $[H_3SiCp]^-$, and $[H_3PCp]$ rings.

Computational Results: Allyl Ligands

A systematic DFT investigation (PBE/TZ2P) of the triallyl phosphines was carried out. As is the case in the related cyclopentadienyl compound, the P–C bonds are quite flexible in triallyl phosphine (Figure 35). The structure with C_1 symmetry is a local minimum on the potential energy surface, whereby one of the allyl ligands is twisted out of a paddlewheel arrangement. However, the constrained C_3 structure is also a local minimum, with the difference in ΔE only 4.2 kcal mol^{-1}. This low-energy difference suggests that rotation about the P–C bond is quite facile. This behavior is similar to that in the related cyclopentadienyl compounds, in which bending has been shown to be easiest at a phosphorus bridging atom.

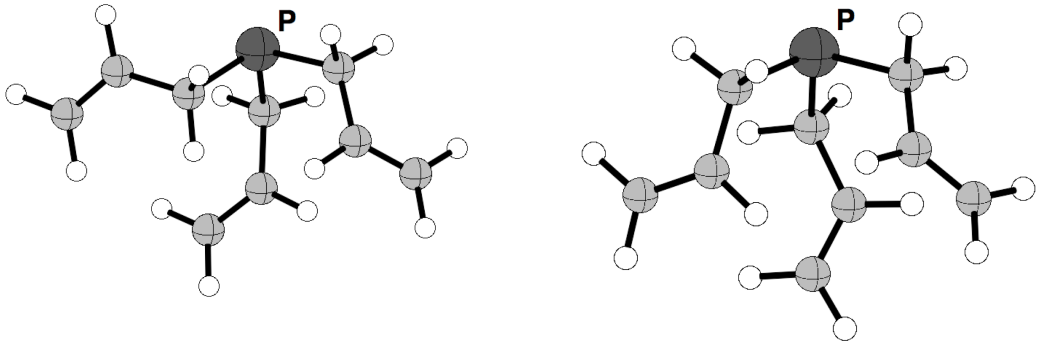

Figure 35. Calculated structures of triallylphosphine (PBE/TZ2P). The difference in ΔE between the C_1 (left) and C_3 (right) structures is 4.2 kcal mol^{-1}, which suggests a facile rotation about the P–C bond.

In order to understand difficulties in the synthesis of tripodal allyl phosphonium salts, a set of calculations (PBE/TZ2P) were performed on the related tris(allyl)phosphines. Space filling models of these phosphines (Figure 36) elucidate the steric congestion around the phosphorus atom in these compounds. Whereas addition of MeI to $P(C_3H_5)_3$ affords a smooth transition to the corresponding phosphonium iodide, the increased steric bulk around the P atom in PA''_3 and PA'_3 evidently hinders the methylation of these phosphines to form the corresponding phosphonium iodides. Evidently, this steric congestion dominates the coordination sphere of phosphorus enough to prevent reaction with stronger methylating agents like MeOTf and $[Me_3O][BF_4]$.

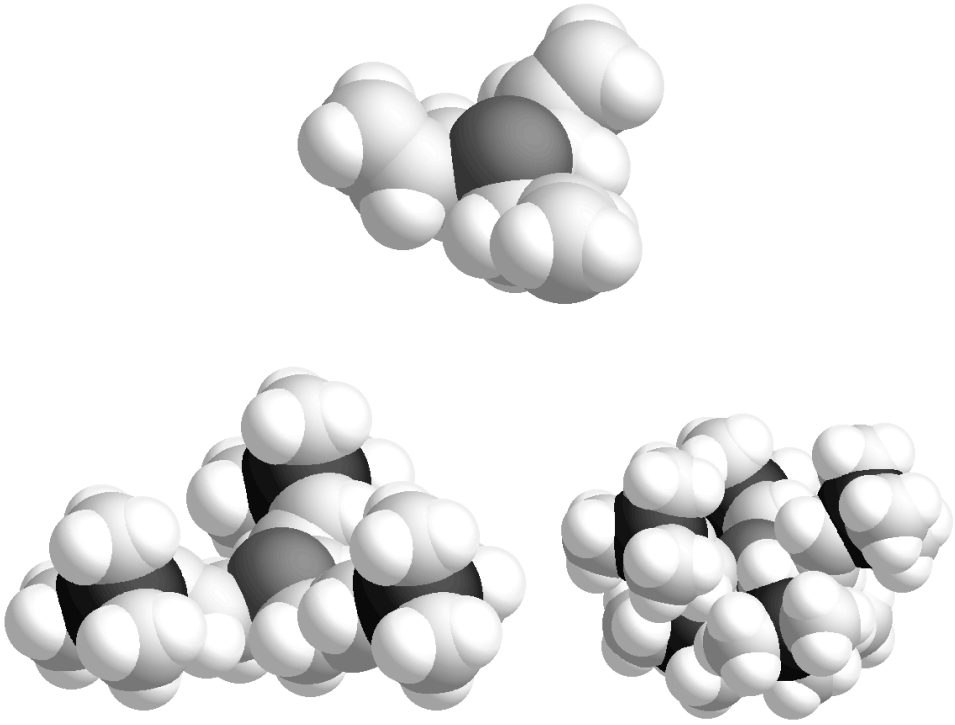

Figure 36. Space-filling models of $P(C_3H_5)_3$ (top), PA''_3 (bottom, left), and PA'_3 (bottom, right). The central P atom (dark gray) is protected from the surrounding environment by the successive addition of $SiMe_3$ groups to the corresponding allyls.

Conclusion

Phosphonium-bridged *ansa*-metallocenes, although not yet widely encountered in organometallic chemistry, display many of the features of their silyl-bridged counterparts, including a high degree of flexibility in bending at the C_{ipso} of the cyclopentadienyl ring. In the context of Group 2 metal chemistry, the $[R_2PCp'_2]^-$ anion offers a uninegative charge with the coordination environment of two cyclopentadienyl rings, opening possibilities for a range of Schlenk redistribution-resistant $[R_2PCp'_2]MX$ complexes, with intriguing parallels to organolanthanide species.

Analogous compounds using allyl ligands in place of cyclopentadienyl ligands should be isolable. The compound {(Me)(*t*-Bu)P[$(SiMe_3)_2C_3H_3]_2$}I can be prepared, but reactions to form s-block metal complexes with this molecule do not yield the desired products. Tripodal allyl phosphines are an attractive target, but the corresponding phosphonium iodides are yet to be isolated, likely due to the increased steric bulk around the phosphorus atom.

CHAPTER VI

SUMMARY AND FUTURE DIRECTIONS

The bulk of this work was dedicated to elucidating structure-function relationships among main-group organometallic complexes. The effects on the structure and reactivity of such complexes by increasing steric bulk on ligands were probed. First and foremost, it was determined that bulky substituents lead to more thermally stable complexes. This is most obvious in the case of the isolated tris(tetramethylcyclopentadienyl)arsenic and antimony compounds. Additional methyl groups on the cyclopentadienyl rings aid in isolation of a crystalline arsenic compound that is stable at room temperature, whereas the unsubstituted tri(cyclopentadienyl)arsenic has not been crystallographically characterized due to thermal instability. Interestingly enough, however, increased bulk is not a "magic bullet" for improving the handling characteristics of these compounds: e.g., the tris(tetramethylcyclopentadienyl)antimony remains highly light sensitive. Perhaps an investigation into other means of increasing bulk on the cyclopentadienyl ligands (e.g. $SiMe_3$ or isopropyl substituents or even various *ansa* bridges) is warranted in order to stabilize these complexes to a greater degree.

Steric bulk in and of itself does not necessarily provide a route to isolable complexes: *judicious* choice of bulky substituents, as is the case for the bis(1,3-bis(trimethylsilyl)allyl)beryllium diethyletherate, leads to the isolation of some main group complexes, due to the solubility enhancement provided by the trimethylsilyl groups. The unsubstituted diallyl beryllium has not been structurally authenticated,

possibly because it is polymeric in the solid state. However, the trimethylsilyl groups provide not only bulk to the allyl ligands, which help to stabilize the resulting compound, but also a marked increase in the solubility of the resulting beryllium complex. The parent diallyl beryllium is soluble only in ethers, whereas bis(1,3-bis(trimethylsilyl)allyl)beryllium diethylether is soluble in a wide variety of hydrocarbon solvents, including hexane, toluene, and benzene, in addition to THF and diethyl ether.

Bonding motifs in light alkaline-earth metal complexes were also investigated in this work. The idea of coordination sphere saturation can be thought of as somewhat related to steric bulk: these highly electropositive complexes will attract substituents in the form of negatively charged anions and electron pairs from Lewis bases to satisfy their coordination sphere. In the case of allyl ligands, and specifically the bulky 1,3-bis(trimethylsilyl)allyl, σ bonding was thought to be the preferred motif. However, this has been shown to be an artifact of the way that these compounds had been isolated. In fact, in the absence of coordinating Lewis bases, these complexes prefer π-bonding, just like their heavier counterparts. Astonishingly, the related beryllium complex shows very little energetic preference for sigma or pi bonding in the absence of coordinating bases, as both forms are minima on their potential energy surface.

Finally, the phosphonium-containing *ansa*-bridged cyclopentadienyl and allyl complexes represent a rare subset of widely-studied *ansa* complexes. However, the incorporation of a 4-coordinate ylidic phosphorus(V) in an *ansa* bridge has exciting implications in terms of electronic manipulation of potential polymerization catalysts as well as stereodirection of the resulting polymerization. The use of an ylide in these complexes allows for the incorporation of metal centers with a +2 charge (like alkaline

earth metals), and the resulting complexes would mimic the electronic composition of non-bridged complexes with metal centers containing a +3 charge (as is the case for rare-earth elements). The steric bulk the *ansa*-bridge imparts allows for limited access to the active metal center for a growing polymer chain.

There are a number of questions that this work addresses that lead to other potential avenues of research. First, allyl complexes of the light alkaline earth metals (magnesium and beryllium) represent somewhat of a watershed among those of the rest of Group 2. Allyl complexes of Ca and Sr contain π-bound ligands even with coordinated ethereal bases. Is it possible to force these allyl ligands into a σ-bonding mode by saturating the coordination sphere of these metals with more Lewis-basic electron pairs?

Additionally, this work details the limited successes with the *ansa*-bridged allyl complexes. Perhaps further investigation into these complexes will lead to a starting material that can be isolated and used to synthesize s-block metal complexes, as is the case for the phosphonium-bridge cyclopentadienyl complexes. And, as an interesting side-note, could the fact that the tris(tetramethylcyclopentadienyl)arsenic compound is thermodynamically stable signal that arsonium-bridged *ansa* complexes could be realized?

APPENDIX A:

SYNTHESIS AND STRUCTURAL CHARACTERIZATION OF ARSENIC TRIS(HEXAMETHYLDISILAZIDE)

Introduction

The coordination chemistry of the pnictogens (that is, elements of the nitrogen group) has been well studied, especially for those compounds containing nitrogen and phosphorus atoms. Compounds of the type ER_3 (E = As, Sb, Bi) have been recognized as good Lewis bases due to the presence of a chemically active lone pair of electrons, and numerous examples can be found in the open literature.[152] Structurally authenticated compounds containing an As–N bond are far less common, however, with fewer than fifty references of such compounds appearing in the Cambridge Structural Database. Homoleptic N-containing arsenic compounds are exceptionally rare: only the tris(morpholino)[153] and tris(pyrrolyl)[154] arsine compounds have been isolated. There is no example of a structurally authenticated homoleptic tris(amide) compound of arsenic.

This is especially surprising considering the wealth of organoarsenic chemistry. Alkali-metal salts of the hexamethyldisilazide ligand are widely used starting materials in organometallic chemistry, because they are not only strong bases (good deprotonating agents) but also highly soluble in a wide range of organic solvents due to the highly lipophilic trimethylsilyl moieties.[155] Additionally, transition-metal complexes of bis(trimethylsilyl)amine are typically highly reactive, low-coordinate, monomeric species due to the steric demands imposed by the bulky trimethylsilyl moieties.[152] Taken together, isolation of a homoleptic tris(amide) of arsenic is an attractive target because of its potential as a starting material for other organoarsine compounds as well as its potentially monomeric structure. Similar compounds containing one[156] and two[157] bis(trimethylsilyl)amido moieties have been isolated, but the homoleptic tris(amido)

complex of arsenic remains elusive. What follows is the synthesis and structural characterization of a homoleptic tris(amido) complex of arsenic.

Experimental

General Considerations. All manipulations were performed with the rigorous exclusion of air and moisture using high vacuum, Schlenk, or glovebox techniques. Proton NMR spectra were obtained at 25 °C on a Bruker DRX-400 spectrometer at 400 MHz and were referenced to the residual proton resonances of C_6D_6 (δ 7.15).

Materials. AsI_3 was purchased from Aldrich and was visibly contaminated with purple iodine crystals. This was subsequently rinsed with hexane and the remaining dark orange solid was dried under vacuum and used without further purification. $K[N(SiMe_3)_2]$ was purchased from Aldrich and used as received. Hexane and toluene were distilled under nitrogen from potassium benzophenone ketyl. C_6D_6 was vacuum distilled from Na/K (22/78) alloy and stored over type 4A molecular sieves prior to use.

Synthesis of $As[N(SiMe_3)_2]_3$. AsI_3 (0.503 g, 1.10 mmol) was dissolved in 70 mL of toluene. To this, a solution of $K[N(SiMe_3)]$ (0.661 g, 3.30 mml) in toluene was added via a dropping funnel over the course of 30 m at room temperature. The resulting light yellow, turbid solution was allowed to stir at room temperature for 2 h, after which time the reaction was filtered over a medium porosity frit. All volatiles were removed from the resulting light yellow filtrate to afford a waxy yellow solid (0.507 g, 82.9%). Slow-evaporation of a hexane solution of the above afforded X-ray quality crystals of $As[N(SiMe_3)_2]_3$. ^1H NMR (C_6D_6): δ 0.31 (s, 2H); 0.35 (s, 1H); 0.37 (s, 1H); 0.41 (s, 6H).

Results and Discussion

Arsenic tris(hexamethyldisilazide) $As[N(SiMe_3)_2]_3$ was synthesized by way of a salt elimination reaction in which one equivalent of arsenic triiodide was treated with three equivalents of potassium hexamethyldisilazide (eq 1):

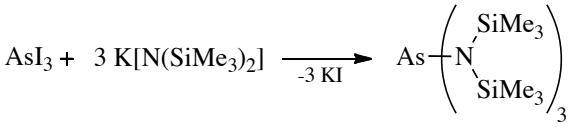

(1)

The yield of the amide is very good (83%). The compound is stable at room temperature and is soluble in polar and nonpolar organic solvents, due to the lipophilic character of the trimethylsilyl moieties. The yellow solid shows no signs of decomposition in an inert atmosphere after 6 weeks. The multiple signals in the ^1H NMR spectrum could be due to a complex monomer-dimer equilibrium in solution: a variable temperature study could elucidate the solution structure.

$As[N(SiMe_3)_2]_3$ crystallizes in the monoclinic space group $P2_1/c$, and suitable crystals were obtained from a concentrated hexane solution as colorless blocks. The molecule, depicted in Figure 37, is monomeric, with three bis(trimethylsilyl)amide moieties arranged around an As center. Selected bond distances and angles are given in Table 10.

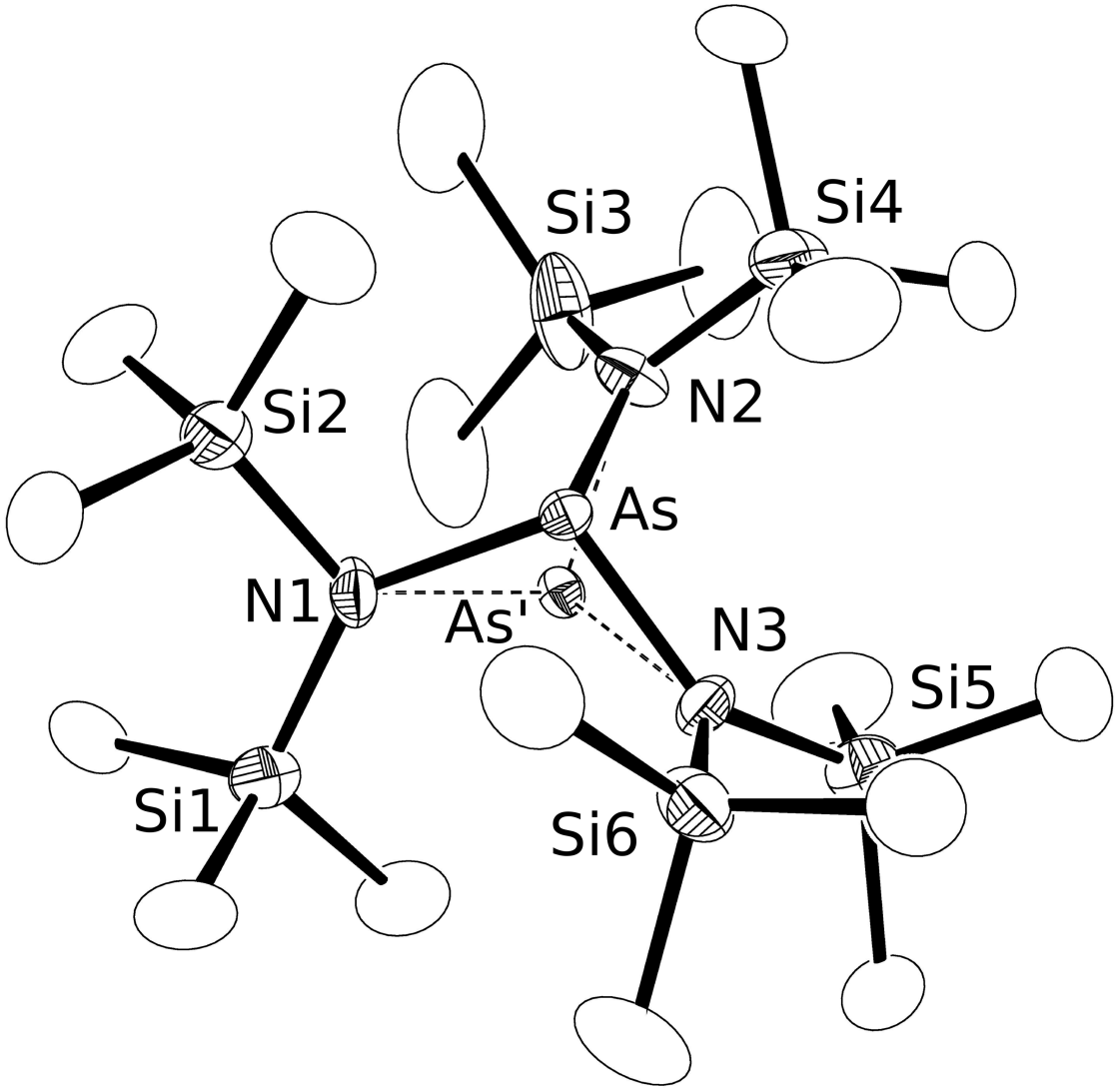

Figure 37. ORTEP of $As[N(SiMe_3)_2]_3$. There is a 55/45 disorder at the As center. Non-hydrogen atoms have been omitted for clarity.

Table 10. Selected bond distance and angles for $As[N(SiMe_3)_2]_3$.

atoms	distance (Å)	atoms	angle (°)
As–N1	1.879(2)	N1–As–N2	105.33(12)
As–N2	1.896(2)	N2–As–N3	102.92(12)
As–N3	1.956(3)	N1–As–N3	103.71(11)
As′–N1	1.917(2)	N1–As′–N2	102.70(11)
As′–N2	1.927(3)	N2–As′–N3	103.78(11)
As′–N3	1.903(3)	N1–As′–N3	104.36(12)
N1–Si1	1.749(3)		
N1–Si2	1.752(3)		
N2–Si3	1.762(3)		
N2–Si4	1.760(3)		
N3–Si5	1.758(3)		
N3–Si6	1.756(3)		

The average As–N bond length of 1.910(3) Å (1.916(2) Å for As′–N) is somewhat longer than that reported for the related compounds $HAs[N(SiMe_3)_2]_2$ (1.878(4) Å),[157] $Cp^*AsCl[N(SiMe_3)_2]$ (1.874(2) Å),[123b] and $AsCl_2[N(SiMe_3)_2]$ (1.802(3) Å).[156] This is likely attributed to the disorder at the As center in the crystal structure. The sum of the angles at each As center (311.96° at As and 310.84° at As′) indicates a strong pyramidalization caused by repulsion from the lone pair of electrons.

Conclusion

The homoleptic arsenic amido complex $As[N(SiMe_3)_2]_3$ is the first example of such a compound. It is stable at room temperature in an inert atmosphere indefinitely and is a promising precursor for other arsenic-containing organometallic complexes. Further work will be necessary to determine the reactivity of the complex, and investigations regarding the feasibility of isolating the heavier Sb and Bi congeners could prove interesting.

APPENDIX B:

CRYSTAL DATA, ATOMIC FRACTIONAL COORDINATES, AND ISOTROPIC THERMAL PARAMETERS FOR X-RAY STRUCTURAL DETERMINATIONS

Table 11. Crystal data and structure refinement for [BeA′$_2$(Et$_2$O)].

Empirical formula	C_{22} H_{52} Be O Si_4	
Formula weight	454.01	
Temperature	100.0(1) K	
Wavelength	0.71073 Å	
Crystal system	Triclinic	
Space group	$P\bar{1}$	
Unit cell dimensions	a = 9.6404(17) Å	α = 93.539(3)°
	b = 11.642(2) Å	β = 107.290(3)°
	c = 16.030(3) Å	γ = 114.379(3)°
Volume	1529.0(5) Å^3	
Z	2	
Density (calculated)	0.986 Mg/m^3	
Absorption coefficient	0.204 mm^{-1}	
F(000)	504	
Crystal color, morphology	colorless, block	
Crystal size	0.34 × 0.30 × 0.24 mm^3	
θ range for data collection	1.36 to 33.14°	
Index ranges	$-14 \le h \le 14$, $-17 \le k \le 17$, $-24 \le l \le 24$	
Reflections collected	29095	
Independent reflections	11568 [R_{int} = 0.0679]	
Observed reflections	7955	
Completeness to θ = 33.14°	99.1%	
Absorption correction	Multi-scan	
Max. and min. transmission	0.9526 and 0.9338	
Refinement method	Full-matrix least-squares on F^2	
Data / restraints / parameters	11568 / 0 / 292	
Goodness-of-fit on F^2	0.949	
Final R indices [$I>2\sigma(I)$]	R_1 = 0.0461, wR_2 = 0.0868	
R indices (all data)	R_1 = 0.0819, wR_2 = 0.0960	
Largest diff. peak and hole	0.467 and -0.442 e$^-$ Å^{-3}	

Table 12. Atomic coordinates ($\times 10^4$) and equivalent isotropic displacement parameters ($Å^2 \times 10^3$) for [BeA′$_2$(Et$_2$O)]. U_{eq} is defined as one third of the trace of the orthogonalized U_{ij} tensor.

atom	x	y	z	U_{eq}
Be1	7015(3)	2365(2)	2423(2)	20(1)
C1	5376(2)	1676(2)	1402(1)	20(1)
C2	4153(2)	402(2)	1432(1)	20(1)
C3	3787(2)	-768(2)	999(1)	23(1)
C4	7357(2)	2976(2)	3534(1)	20(1)
C5	6974(2)	4077(2)	3633(1)	20(1)
C6	7984(2)	5318(2)	4016(1)	22(1)
Si1	4422(1)	2729(1)	980(1)	21(1)
C7	6015(2)	4396(2)	1108(1)	31(1)
C8	3130(2)	2066(2)	-228(1)	30(1)
C9	3033(2)	2787(2)	1571(1)	29(1)
Si2	2287(1)	-2306(1)	1122(1)	21(1)
C10	1447(3)	-1997(2)	1976(1)	34(1)
C11	573(3)	-3153(2)	36(1)	38(1)
C12	3263(2)	-3377(2)	1444(1)	31(1)
Si3	6295(1)	1694(1)	4087(1)	20(1)
C13	4134(2)	1376(2)	3822(1)	26(1)
C14	6377(2)	165(2)	3736(1)	25(1)
C15	7301(2)	2226(2)	5329(1)	29(1)
Si4	7357(1)	6619(1)	3988(1)	22(1)
C16	5134(2)	5943(2)	3776(1)	33(1)
C17	7832(3)	7507(2)	3098(1)	35(1)
C18	8493(3)	7811(2)	5077(1)	36(1)
O1	8662(2)	2376(1)	2286(1)	25(1)
C19	10199(2)	4697(2)	2569(1)	27(1)
C20	10278(2)	3456(2)	2690(1)	28(1)
C21	8603(2)	1228(2)	1824(1)	25(1)
C22	9551(2)	678(2)	2440(1)	28(1)

Table 13. Crystal data and structure refinement for $[MgA'_2]_2$.

Empirical formula	C_{18} H_{42} Mg Si_4	
Formula weight	395.19	
Temperature	200(2) K	
Wavelength	1.54178 Å	
Crystal system	Monoclinic	
Space group	$P2_1$	
Unit cell dimensions	a = 10.7597(2) Å	α = 90°
	b = 12.9099(2) Å	β = 100.1650(10)°
	c = 19.7051(3) Å	γ = 90°
Volume	2694.21(8) $Å^3$	
Z	4	
Density (calculated)	0.974 g/cm^3	
Absorption coefficient	2.247 mm^{-1}	
F(000)	872	
Crystal size	0.40 × 0.32 × 28 mm^3	
Crystal color, habit	Colorless plates	
θ range for data collection	2.28 to 68.17°	
Index ranges	$-12 \le h \le 12$, $-14 \le k \le 10$, $-23 \le l \le 21$	
Reflections collected	15128	
Independent reflections	6694 [R_{int} = 0.0226]	
Completeness to θ = 58.00°	97.8 %	
Absorption correction	Multi-scan	
Refinement method	Full-matrix least-squares on F^2	
Data / restraints / parameters	6694 / 1 / 487	
Goodness-of-fit on F^2	0.997	
Final R indices [$I>2\sigma(I)$]	R_1 = 0.0273, wR_2 = 0.0695	
R indices (all data)	R_1 = 0.0292, wR_2 = 0.0711	
Absolute structure parameter	0.039(17)	
Largest diff. peak and hole	0.329 and -0.156 e^- $Å^{-3}$	

Table 14. Atomic coordinates ($\times 10^4$) and equivalent isotropic displacement parameters ($Å^2 \times 10^3$) for $[MgA'_2]_2$. U_{eq} is defined as one third of the trace of the orthogonalized U_{ij} tensor.

atom	x	y	z	U_{eq}
Mg(1)	7849(1)	4355(1)	3328(1)	35(1)
Mg(2)	7214(1)	3904(1)	1795(1)	35(1)
Si(1)	6674(1)	6655(1)	3716(1)	38(1)
Si(2)	7847(1)	4440(1)	6123(1)	40(1)
Si(3)	11508(1)	4290(1)	3976(1)	36(1)
Si(4)	9066(1)	5674(1)	1499(1)	42(1)
Si(5)	9100(1)	1349(1)	1391(1)	42(1)
Si(6)	6957(1)	2078(1)	3606(1)	36(1)
Si(7)	4045(1)	3571(1)	1256(1)	42(1)
Si(8)	6178(1)	3650(1)	-999(1)	44(1)
C(1)	5620(3)	6677(3)	2856(1)	66(1)
C(2)	8173(3)	7364(2)	3661(2)	60(1)
C(3)	5858(3)	7389(2)	4332(1)	57(1)
C(4)	6930(2)	5284(2)	3990(1)	35(1)
C(5)	7530(2)	5145(2)	4718(1)	35(1)
C(6)	7106(2)	4615(2)	5212(1)	43(1)
C(7)	6831(3)	5029(3)	6693(1)	66(1)
C(8)	9438(2)	5049(3)	6310(1)	55(1)
C(9)	8020(4)	3031(3)	6330(2)	76(1)
C(11)	12900(2)	5120(3)	3921(2)	63(1)
C(12)	11246(3)	4277(3)	4883(1)	56(1)
C(13)	11805(2)	2961(2)	3673(1)	53(1)
C(14)	10064(2)	4841(2)	3431(1)	37(1)
C(15)	9654(2)	4646(2)	2753(1)	34(1)
C(16)	8575(2)	5104(2)	2287(1)	35(1)
C(17)	10602(3)	6368(3)	1735(2)	80(1)
C(18)	9257(3)	4613(3)	885(1)	60(1)
C(19)	7835(3)	6598(3)	1091(2)	68(1)
C(21)	10703(2)	1669(3)	1867(2)	55(1)
C(22)	8997(4)	1675(3)	464(1)	77(1)

Table 14, continued

atom	x	y	z	U_{eq}
C(23)	8778(3)	-59(3)	1471(2)	70(1)
C(24)	7903(2)	2085(2)	1778(1)	38(1)
C(25)	8059(2)	2380(2)	2446(1)	35(1)
C(26)	7152(2)	2863(2)	2825(1)	34(1)
C(27)	5444(2)	2471(2)	3870(2)	55(1)
C(28)	8313(2)	2322(2)	4322(1)	50(1)
C(29)	6897(3)	674(2)	3389(1)	51(1)
C(31)	2689(2)	3889(3)	548(2)	72(1)
C(32)	3684(3)	4134(3)	2073(1)	62(1)
C(33)	4124(3)	2124(3)	1338(2)	65(1)
C(34)	5527(2)	4114(2)	1053(1)	36(1)
C(35)	5767(2)	3711(2)	383(1)	41(1)
C(36)	5950(2)	4227(2)	-174(1)	49(1)
C(37)	7777(3)	4009(3)	-1168(2)	77(1)
C(38)	6026(3)	2222(3)	-1007(2)	62(1)
C(39)	4970(3)	4209(3)	-1705(1)	71(1)

Table 15. Crystal data and structure refinement for $\{K[Ca(N(SiMe_3)_2)_3]\}_\infty$.

Empirical formula	$C_{18}\ H_{54}\ Ca\ K\ N_3\ Si_6$	
Formula weight	560.36	
Temperature	123(2) K	
Wavelength	0.71073 Å	
Crystal system	Triclinic	
Space group	$P\bar{1}$	
Unit cell dimensions	a = 8.6477(8) Å	α = 93.148(5)°
	b = 11.2357(9) Å	β = 91.419(2)°
	c = 19.398(2) Å	γ = 111.817(2)°
Volume	1745.0(3) Å^3	
Z	2	
Density (calculated)	1.066 g/cm^3	
Absorption coefficient	0.516 mm^{-1}	
F(000)	612	
Crystal size	0.32 × 0.28 × 0.24 mm^3	
Crystal color, habit	Colorless block	
θ range for data collection	1.96 to 27.01°	
Index ranges	$-11 \le h \le 10$, $-14 \le k \le 14$, $0 \le l \le 24$	
Reflections collected	25442	
Independent reflections	7444 [R_{int} = 0.0000]	
Completeness to θ = 25.00°	99.8 %	
Absorption correction	Multi-scan	
Refinement method	Full-matrix least-squares on F^2	
Data / restraints / parameters	7444 / 0 / 263	
Goodness-of-fit on F^2	1.062	
Final R indices [I>2σ(I)]	R_1 = 0.0327, wR_2 = 0.0794	
R indices (all data)	R_1 = 0.0422, wR_2 = 0.0840	
Largest diff. peak and hole	0.358 and -0.289 e$^-$ Å^{-3}	
Twinning		
Full rotational twin (50/50)		

Table 16. Atomic coordinates ($\times 10^4$) and equivalent isotropic displacement parameters ($Å^2 \times 10^3$) for $\{K[Ca(N(SiMe_3)_2)_3]\}_\infty$. U_{eq} is defined as one third of the trace of the orthogonalized U_{ij} tensor.

atom	x	y	z	U_{eq}
Ca(1)	6803(1)	8993(1)	2530(1)	17(1)
K(1)	5015(1)	5444(1)	2537(1)	21(1)
Si(1)	7697(1)	7904(1)	3960(1)	17(1)
Si(2)	3980(1)	7092(1)	3821(1)	18(1)
Si(3)	7321(1)	12036(1)	3080(1)	20(1)
Si(4)	9509(1)	11824(1)	1917(1)	21(1)
Si(5)	4668(1)	7733(1)	1090(1)	19(1)
Si(6)	7381(1)	6682(1)	1216(1)	18(1)
N(1)	5906(2)	7689(2)	3484(1)	16(1)
N(2)	8067(3)	11212(2)	2507(1)	20(1)
N(3)	6205(2)	7474(2)	1563(1)	16(1)
C(1)	9538(3)	9062(3)	3519(1)	23(1)
C(2)	7808(4)	8591(3)	4879(1)	30(1)
C(3)	8115(3)	6379(3)	4028(1)	26(1)
C(4)	3497(3)	8127(3)	4511(1)	30(1)
C(5)	3558(3)	5499(3)	4215(1)	31(1)
C(6)	2298(3)	6801(3)	3120(1)	24(1)
C(7)	5455(4)	10869(3)	3485(1)	30(1)
C(8)	8868(4)	12979(3)	3799(1)	36(1)
C(9)	6513(4)	13224(3)	2700(2)	34(1)
C(10)	11497(4)	13140(3)	2268(2)	40(1)
C(11)	8741(4)	12514(4)	1185(2)	51(1)
C(12)	10177(4)	10533(3)	1534(2)	47(1)
C(13)	4059(3)	8972(3)	1596(1)	25(1)
C(14)	5273(4)	8404(3)	228(1)	30(1)
C(15)	2707(3)	6252(3)	930(1)	28(1)
C(16)	9042(3)	6720(3)	1879(1)	25(1)
C(17)	6133(3)	4920(2)	955(1)	26(1)
C(18)	8519(4)	7302(3)	416(1)	31(1)

Table 17. Crystal data and structure refinement for $As(C_5Me_4H)_3$.

Empirical formula	$C_{27}\ H_{39}\ As$	
Formula weight	438.50	
Temperature	100(2) K	
Wavelength	0.71073 Å	
Crystal system	Triclinic	
Space group	$P\bar{1}$	
Unit cell dimensions	a = 10.5768(9) Å	α = 90.8240(10)°.
	b = 10.9950(10) Å	β = 106.3050(10)°.
	c = 11.1954(10) Å	γ = 110.2700(10)°.
Volume	1163.14(18) $Å^3$	
Z	2	
Density (calculated)	1.252 Mg/m^3	
Absorption coefficient	1.471 mm^{-1}	
F(000)	468	
Crystal size	0.25 × 0.25 × 0.08 mm^3	
θ range for data collection	1.91 to 26.00°.	
Index ranges	$-13 \le h \le 13$, $-13 \le k \le 13$, $-13 \le l \le 13$	
Reflections collected	12294	
Independent reflections	4549 [R_{int} = 0.0297]	
Completeness to θ = 26.00°	99.7 %	
Max. and min. transmission	0.8914 and 0.7100	
Refinement method	Full-matrix least-squares on F^2	
Data / restraints / parameters	4549 / 0 / 253	
Goodness-of-fit on F^2	1.042	
Final R indices [$I>2\sigma(I)$]	R_1 = 0.0332, wR_2 = 0.0877	
R indices (all data)	R_1 = 0.0387, wR_2 = 0.0910	
Largest diff. peak and hole	0.615 and -0.532 e^- $Å^{-3}$	

Table 18. Atomic coordinates ($\times 10^4$) and equivalent isotropic displacement parameters ($Å^2 \times 10^3$) for $As(C_5Me_4H)_3$. U_{eq} is defined as one third of the trace of the orthogonalized U_{ij} tensor.

atom	x	y	z	U_{eq}
As(1)	3702(1)	2811(1)	743(1)	16(1)
C(1)	4811(2)	1591(2)	973(2)	20(1)
C(2)	4747(3)	796(2)	2037(2)	22(1)
C(3)	6019(3)	1272(2)	2927(2)	22(1)
C(4)	6994(3)	2353(2)	2492(2)	22(1)
C(5)	6323(3)	2517(2)	1326(2)	21(1)
C(6)	3476(3)	-357(2)	2051(3)	27(1)
C(7)	6480(3)	789(3)	4166(2)	30(1)
C(8)	8497(3)	3092(3)	3258(3)	28(1)
C(9)	6910(3)	3421(3)	461(3)	28(1)
C(10)	4247(2)	3462(2)	2590(2)	17(1)
C(11)	3163(2)	3201(2)	3273(2)	19(1)
C(12)	3168(2)	4357(2)	3704(2)	19(1)
C(13)	4230(3)	5433(2)	3350(2)	21(1)
C(14)	4899(2)	4932(2)	2727(2)	19(1)
C(15)	2332(3)	1868(2)	3504(2)	25(1)
C(16)	2291(3)	4608(3)	4450(2)	27(1)
C(17)	4484(3)	6841(3)	3675(3)	28(1)
C(18)	6109(3)	5643(3)	2259(2)	26(1)
C(19)	1631(2)	1635(2)	138(2)	18(1)
C(20)	897(2)	2594(2)	-209(2)	19(1)
C(21)	449(2)	2513(2)	-1472(2)	20(1)
C(22)	770(2)	1482(2)	-2027(2)	20(1)
C(23)	1411(2)	919(2)	-1099(2)	19(1)
C(24)	808(3)	3523(2)	722(2)	23(1)
C(25)	-285(3)	3308(3)	-2264(2)	27(1)
C(26)	427(3)	1150(3)	-3408(2)	27(1)
C(27)	1791(3)	-250(2)	-1268(2)	26(1)

Table 19. Crystal data and structure refinement for $Sb(C_5Me_4H)_3$.

Empirical formula	C_{27} H_{39} As	
Formula weight	438.50	
Temperature	100(2) K	
Wavelength	0.71073 Å	
Crystal system	Triclinic	
Space group	$P\bar{1}$	
Unit cell dimensions	a = 10.5768(9) Å	α = 90.8240(10)°.
	b = 10.9950(10) Å	β = 106.3050(10)°.
	c = 11.1954(10) Å	γ = 110.2700(10)°.
Volume	1163.14(18) $Å^3$	
Z	2	
Density (calculated)	1.252 Mg/m^3	
Absorption coefficient	1.471 mm^{-1}	
F(000)	468	
Crystal size	0.25 × 0.25 × 0.08 mm^3	
θ range for data collection	1.91 to 26.00°.	
Index ranges	$-13 \le h \le 13$, $-13 \le k \le 13$, $-13 \le l \le 13$	
Reflections collected	12294	
Independent reflections	4549 [R_{int} = 0.0297]	
Completeness to θ = 26.00°	99.7 %	
Max. and min. transmission	0.8914 and 0.7100	
Refinement method	Full-matrix least-squares on F^2	
Data / restraints / parameters	4549 / 0 / 253	
Goodness-of-fit on F^2	1.042	
Final R indices [$I>2\sigma(I)$]	R_1 = 0.0332, wR_2 = 0.0877	
R indices (all data)	R_1 = 0.0387, wR_2 = 0.0910	
Largest diff. peak and hole	0.615 and -0.532 e^- $Å^{-3}$	

Table 20. Atomic coordinates ($\times 10^4$) and equivalent isotropic displacement parameters ($Å^2 \times 10^3$) for $Sb(C_5Me_4H)_3$. U_{eq} is defined as one third of the trace of the orthogonalized U_{ij} tensor.

atom	x	y	z	U_{eq}
Sb(1)	9477(1)	7749(1)	1604(1)	21(1)
C(1)	10352(3)	6389(4)	3253(3)	24(1)
C(2)	11696(3)	6323(4)	2617(3)	29(1)
C(3)	12476(3)	7168(4)	2798(4)	32(1)
C(4)	11737(4)	7725(4)	3613(4)	29(1)
C(5)	10479(3)	7261(4)	3927(3)	26(1)
C(6)	12098(4)	5457(4)	1927(4)	37(1)
C(7)	13898(4)	7475(5)	2273(4)	43(1)
C(8)	12321(4)	8635(4)	4071(4)	44(1)
C(9)	9388(4)	7555(4)	4761(4)	34(1)
C(11)	7352(3)	7591(3)	2263(3)	22(1)
C(12)	6864(3)	6802(3)	3659(3)	22(1)
C(13)	6382(3)	7674(3)	4151(3)	24(1)
C(14)	6470(3)	9050(4)	3128(3)	25(1)
C(15)	6984(3)	9012(3)	2013(3)	25(1)
C(16)	6884(3)	5289(4)	4324(4)	30(1)
C(17)	5845(4)	7337(4)	5520(4)	33(1)
C(18)	6010(4)	10269(4)	3338(4)	35(1)
C(19)	7151(4)	10135(4)	690(4)	33(1)
C(21)	9396(3)	6476(3)	532(3)	22(1)
C(22)	8503(3)	5261(3)	1249(3)	23(1)
C(23)	7412(3)	5512(3)	744(3)	24(1)
C(24)	7573(3)	6841(3)	-352(3)	24(1)
C(25)	8760(3)	7394(3)	-524(3)	22(1)
C(26)	8815(4)	3986(4)	2297(4)	28(1)
C(27)	6215(3)	4602(4)	1197(3)	28(1)
C(28)	6550(4)	7455(4)	-1127(4)	31(1)
C(29)	9377(4)	8706(4)	-1573(3)	27(1)

Table 21. Crystal data and structure refinement for $Sb(C_5Me_4H)I_2$.

Empirical formula	$C_9 H_{13} I_2 Sb$	
Formula weight	496.74	
Temperature	100(2) K	
Wavelength	1.54178 Å	
Crystal system	Monoclinic	
Space group	$P2_1/n$	
Unit cell dimensions	a = 9.7400(19) Å	α = 90°
	b = 8.7500(17) Å	β = 96.67(3)°
	c = 15.390(3) Å	γ = 90°
Volume	1302.7(4) $Å^3$	
Z	4	
Density (calculated)	2.533 g/cm^3	
Absorption coefficient	53.646 mm^{-1}	
F(000)	896	
Crystal size	0.24 × 0.10 × 0.06 mm^3	
θ range for data collection	5.12 to 67.99°	
Index ranges	$-11 \le h \le 11$, $-10 \le k \le 9$, $-18 \le l \le 14$	
Reflections collected	4946	
Independent reflections	2141 [R_{int} = 0.0228]	
Completeness to θ = 25.00°	98.8 %	
Absorption correction	Face-indexed	
Max. and min. transmission	0.1411 and 0.0273	
Refinement method	Full-matrix least-squares on F^2	
Data / restraints / parameters	2141 / 0 / 109	
Goodness-of-fit on F^2	1.177	
Final R indices [$I>2\sigma(I)$]	R_1 = 0.0534, wR_2 = 0.1414	
R indices (all data)	R_1 = 0.0571, wR_2 = 0.1447	
Largest diff. peak and hole	3.549 and -1.821 e^- $Å^{-3}$	

Table 22. Atomic coordinates ($\times 10^4$) and equivalent isotropic displacement parameters ($Å^2 \times 10^3$) for $Sb(C_5Me_4H)I_2$. U_{eq} is defined as one third of the trace of the orthogonalized U_{ij} tensor.

atom	x	y	z	U_{eq}
Sb(1)	8171(1)	1633(1)	7145(1)	16(1)
I(1)	5378(1)	690(1)	7291(1)	20(1)
I(2)	8979(1)	596(1)	8879(1)	28(1)
C(1)	10285(4)	440(5)	6489(3)	21(1)
C(2)	10360(4)	1742(5)	5964(2)	16(1)
C(3)	9099(4)	1869(5)	5388(3)	18(1)
C(4)	8229(5)	677(5)	5532(3)	20(1)
C(5)	8882(4)	-216(5)	6269(3)	16(1)
C(6)	11385(4)	-242(5)	7132(3)	24(1)
C(7)	11560(4)	2844(5)	5988(3)	20(1)
C(8)	8798(5)	3170(5)	4742(3)	27(1)
C(9)	6819(5)	349(6)	5069(3)	27(1)

Table 23. Crystal data and structure refinement for $As[N(SiMe_3)_2]_3$.

Empirical formula	$C_{18}\ H_{54}\ As\ N_3\ Si_6$	
Formula weight	556.10	
Temperature	100(2) K	
Wavelength	0.71073 Å	
Crystal system	Monoclinic	
Space group	$P2_1/c$	
Unit cell dimensions	a = 8.4874(4) Å	α = 90°
	b = 20.6151(9) Å	β = 93.2760(10)°
	c = 18.2372(8) Å	γ = 90°
Volume	3185.7(2) $Å^3$	
Z	4	
Density (calculated)	1.159 g/cm^3	
Absorption coefficient	1.303 mm^{-1}	
F(000)	1200	
Crystal size	0.30 × 0.25 × 0.20 mm^3	
Crystal color, habit	Colorless rod	
θ range for data collection	1.49 to 25.40°	
Index ranges	$-10 \le h \le 10$, $-24 \le k \le 24$, $-21 \le l \le 21$	
Reflections collected	23641	
Independent reflections	5817 [R_{int} = 0.0353]	
Completeness to θ = 25.00°	99.3 %	
Absorption correction	Multi-scan	
Max. and min. transmission	0.7806 and 0.6959	
Refinement method	Full-matrix least-squares on F^2	
Data / restraints / parameters	5817 / 0 / 263	
Goodness-of-fit on F^2	1.022	
Final R indices [$I>2\sigma(I)$]	R_1 = 0.0478, wR_2 = 0.1278	
R indices (all data)	R_1 = 0.0591, wR_2 = 0.1368	
Largest diff. peak and hole	0.927 and -0.608 e^- $Å^{-3}$	
Remarks	Disordered As (55/45)	

Table 24. Atomic coordinates ($\times 10^4$) and equivalent isotropic displacement parameters ($Å^2 \times 10^3$) for $As[N(SiMe_3)_2]_3$. U_{eq} is defined as one third of the trace of the orthogonalized U_{ij} tensor.

atom	x	y	z	U_{eq}
As(1)	3575(1)	5727(1)	7449(1)	17(1)
As(1′)	1690(1)	5753(1)	7399(1)	18(1)
Si(1)	3949(2)	4376(1)	7695(1)	57(1)
Si(2)	1269(1)	4587(1)	6596(1)	42(1)
Si(3)	3988(1)	6652(1)	8642(1)	35(1)
Si(4)	1456(1)	5694(1)	8956(1)	43(1)
Si(5)	1241(1)	6936(1)	6629(1)	38(1)
Si(6)	3904(1)	6222(1)	5980(1)	36(1)
N(1)	2618(3)	4918(1)	7257(2)	30(1)
N(2)	2701(3)	6032(1)	8318(1)	28(1)
N(3)	2601(3)	6293(1)	6691(1)	30(1)
C(1)	4843(7)	3828(3)	7017(3)	99(2)
C(2)	2965(8)	3825(3)	8356(3)	95(2)
C(3)	5633(5)	4769(4)	8211(3)	99(2)
C(4)	308(6)	3840(2)	6932(3)	75(2)
C(5)	2226(6)	4349(2)	5735(3)	73(2)
C(6)	-379(5)	5150(3)	6325(3)	83(2)
C(7)	2931(5)	7433(2)	8777(3)	54(1)
C(8)	5620(5)	6815(2)	8025(3)	54(1)
C(9)	4985(5)	6436(2)	9554(2)	55(1)
C(10)	505(6)	6332(2)	9506(3)	65(1)
C(11)	2559(7)	5145(2)	9620(3)	74(2)
C(12)	-206(5)	5222(3)	8517(3)	76(2)
C(13)	-321(5)	6889(2)	7305(3)	61(1)
C(14)	2245(6)	7744(2)	6764(3)	71(2)
C(15)	181(5)	6993(2)	5708(3)	57(1)
C(16)	4874(5)	7003(2)	5761(2)	53(1)
C(17)	2861(5)	5953(2)	5092(2)	60(1)
C(18)	5541(5)	5646(2)	6190(3)	72(2)

APPENDIX C:

ATOMIC FRACTIONAL COORDINATES FOR DENSITY FUNCTIONAL THEORY OPTIMIZED STRUCTURES

Table 25. Atomic coordinates for the optimized structures of [(C_3H_5)BeH].

atom	x	y	z
σ-bound			
Be	-0.11931	0.61395	-0.07202
C	-1.72285	1.10621	-0.18177
H	-1.88207	2.06345	0.30917
H	-1.97521	1.23525	-1.23368
C	-2.55801	0.04332	0.43118
H	-2.63633	0.06756	1.50962
C	-3.16419	-0.94439	-0.20682
H	-3.71992	-1.69580	0.32582
H	-3.13180	-1.02712	-1.28167
H	1.13997	0.20239	0.00958
π-bound			
C	0.13461	-0.19387	1.2148
H	1.21503	-0.16463	1.295
H	-0.40323	-0.30485	2.13526
C	-0.44644	-0.53906	0
C	0.13461	-0.19387	-1.2148
H	-0.40323	-0.30485	-2.13526
H	1.21503	-0.16463	-1.295
H	-1.50857	-0.73891	0
Be	0.13461	1.18708	0
H	0.40977	2.49033	0
transition structure			
Be	0.18939	1.62368	-0.67597
H	0.20649	2.89331	-0.28882
C	0.19388	0.00365	-1.11081
H	-0.35796	-0.29345	-1.99204
H	1.21899	-0.34863	-1.19320
C	-0.44282	-0.43914	0.15226
H	-1.51289	-0.59111	0.12039

Table 25, continued

atom	x	y	z
transition structure cont'd			
C	0.15802	-0.55197	1.33110
H	-0.39306	-0.81250	2.21697
H	1.22217	-0.41112	1.44012

Table 26. Atomic coordinates for the optimized structure of σ-[Be(1,3-$(SiH_3)_2C_3H_3)_2$].

atom	x	y	z
Be	0	0	0
C	1.23738	1.0506	-0.4497
H	1.25346	1.05765	-1.55611
C	-1.23738	-1.0506	0.4497
H	-1.25346	-1.05765	1.55611
C	2.53516	0.531	0.08407
H	2.65669	0.59693	1.17363
C	-2.53516	-0.531	-0.08407
H	-2.65669	-0.59693	-1.17363
C	3.54536	-0.00979	-0.62871
H	3.4323	-0.0705	-1.71859
C	-3.54536	0.00979	0.62871
H	-3.4323	0.0705	1.71859
Si	-5.12418	0.64307	-0.14829
Si	-0.87217	-2.82529	-0.12257
Si	0.87217	2.82529	0.12257
Si	5.12418	-0.64307	0.14829
H	-5.3328	2.10025	0.14166
H	-5.04783	0.44966	-1.63248
H	-6.32395	-0.0875	0.37759
H	-0.82206	-2.87415	-1.62094
H	-1.9252	-3.78477	0.34231
H	0.4558	-3.27152	0.40997
H	5.3328	-2.10025	-0.14166
H	5.04783	-0.44966	1.63248
H	6.32395	0.0875	-0.37759
H	1.9252	3.78477	-0.34231
H	0.82206	2.87415	1.62094
H	-0.4558	3.27152	-0.40997

Table 27. Atomic coordinates for the optimized structure of π-[Be(1,3-$(SiH_3)_2C_3H_3)_2$].

atom	x	y	z
C	0.55810	1.53375	0.96556
C	-1.22858	1.30811	-0.71254
C	1.22858	-1.30811	-0.71254
C	-0.01342	-1.77929	-0.31929
C	-0.55810	-1.53375	0.96556
C	0.01342	1.77929	-0.31929
H	-2.02022	1.16544	0.01626
H	0.71288	2.04558	-1.10847
H	-0.10014	1.56875	1.82818
H	2.02022	-1.16544	0.01626
H	-0.71288	-2.04557	-1.10847
H	0.10014	-1.56875	1.82818
Be	0	0	0.10527
H	1.52505	-1.35970	-1.75019
H	-1.58554	-1.81377	1.15005
H	1.58554	1.81377	1.15005
H	-1.52505	1.35970	-1.75019

Table 28. Atomic coordinates for the optimized structure of {Be(1,3-$(SiH_3)_2C_3H_3)_2[Et_2O]$}.

atom	x	y	z
Be	0.02335	-0.40674	1.05582
C	1.07081	0.98976	0.85580
C	2.26301	0.67662	0.02755
C	3.55997	0.67815	0.41990
C	-1.16401	-1.23856	0.07134
C	-2.34830	-0.41321	-0.27901
C	-3.63642	-0.64352	0.06706
C	-1.88184	-0.93785	3.53207
C	-0.70588	-1.85825	3.29887
C	1.68729	-1.55029	2.85965
C	2.01118	-2.95905	2.40934
H	1.39853	1.31510	1.86086
H	2.05533	0.40053	-1.01475
H	3.78560	0.98502	1.45017
H	-1.50093	-2.15562	0.58801
H	-2.13827	0.48657	-0.87084
H	-3.86141	-1.55338	0.63907
H	-2.64714	-1.47474	4.10827
H	-2.33903	-0.61731	2.58680
H	-1.57907	-0.05186	4.10398
H	-0.24705	-2.16266	4.24902
H	-0.99535	-2.76099	2.74557
H	1.81691	-1.42381	3.94368
H	2.31362	-0.81760	2.34090
H	3.06773	-3.16399	2.62715
H	1.86160	-3.07043	1.32807
H	1.40990	-3.71378	2.93242
O	0.32178	-1.15891	2.54809
Si	0.10205	2.44302	0.12873
Si	4.97700	0.23298	-0.70804
Si	-0.27767	-1.83226	-1.49453
Si	-5.04280	0.49044	-0.39732

Table 28, continued

atom	x	y	z
H	0.89409	3.71912	0.15763
H	-0.27362	2.17636	-1.29781
H	-1.16080	2.67624	0.90649
H	5.74697	-0.95354	-0.19811
H	4.44532	-0.09823	-2.06925
H	5.96574	1.35564	-0.83413
H	1.00951	-2.52307	-1.13663
H	-1.10103	-2.80818	-2.28434
H	0.05927	-0.68033	-2.39060
H	-4.51489	1.63033	-1.21411
H	-6.09670	-0.22575	-1.19177
H	-5.73304	1.05201	0.81382

Table 29. Atomic coordinates for the optimized structure of $[Mg(C_3H_5)_2]$.

atom	x	y	z
Mg	0.06588	-0.02497	-0.00034
C	-0.31122	0.12234	2.19335
C	1.08104	0.19153	1.96871
C	-1.17036	-0.88429	1.77277
H	-0.78476	-1.88599	1.5832
H	-2.23296	-0.80709	1.94987
H	-0.78477	1.04044	2.5415
H	1.63262	1.03948	2.34876
H	1.64302	-0.741	1.91232
C	-0.33412	0.1222	-2.18999
C	0.66464	-0.85305	-1.97781
C	-0.30653	1.44394	-1.76507
H	0.64777	1.9379	-1.58249
H	-1.15501	2.09093	-1.93222
H	-1.30032	-0.25032	-2.53064
H	0.51228	-1.85227	-2.35993
H	1.70397	-0.52731	-1.92976
H	-0.71288	-2.04557	-1.10847

Table 30. Atomic coordinates for the optimized structure of $[Mg\{(C_3(SiH_3)_2)H_3\}_2]$.

atom	x	y	z
Mg	0.23679	-0.08973	-0.00123
C	0.03706	0.09498	2.20356
C	1.41599	0.13779	1.91428
C	-0.86665	-0.91031	1.82829
H	-0.42414	-1.88425	1.58739
H	-0.40174	1.01615	2.59239
H	1.88374	-0.83083	1.70237
C	-0.05527	-0.08807	-2.20347
C	0.95157	-1.03496	-1.92662
C	-0.06237	1.26236	-1.82345
H	0.91662	1.69763	-1.58995
H	-0.99786	-0.48578	-2.5851
H	1.94568	-0.62029	-1.72233
Si	-1.44803	2.42905	-2.20636
H	-1.70681	3.3573	-1.06932
H	-1.18616	3.27826	-3.40507
H	-2.67966	1.62932	-2.46249
Si	0.86098	-2.80673	-2.45152
H	1.58125	-3.08847	-3.72795
H	1.45149	-3.70612	-1.41899
H	-0.57223	-3.17292	-2.63817
Si	2.52709	1.52285	2.43386
H	3.2648	1.2521	3.70269
H	3.55591	1.80861	1.39289
H	1.69824	2.74623	2.6323
Si	-2.67395	-0.86706	2.22785
H	-3.49325	-1.38679	1.09642
H	-3.0297	-1.68069	3.42704
H	-3.06392	0.54716	2.49242

Table 31. Atomic coordinates for the optimized structure of $[Mg(C_3H_5)_2(thf)]$.

atom	x	y	z
Mg	-0.13505	0.19235	-0.03211
O	-0.14064	0.30451	2.03503
C	2.73454	-0.46893	0.12034
C	3.50209	-0.09644	1.15762
C	1.88196	0.36115	-0.73012
H	2.17449	1.41539	-0.71644
H	1.87415	0.01243	-1.7664
H	2.7107	-1.53744	-0.10174
H	4.06777	-0.82135	1.72957
H	3.62233	0.94761	1.43186
C	-2.12915	0.0893	-1.09846
C	-2.12137	1.36476	-0.54398
C	-1.96659	-1.13648	-0.43368
H	-2.29004	-1.21984	0.60251
H	-1.99346	-2.05345	-1.00545
H	-2.03938	0.04925	-2.18466
H	-2.21218	2.2317	-1.18247
H	-2.38881	1.50584	0.50126
C	0.00332	-0.84718	2.90192
C	0.12708	-0.26816	4.29639
C	0.89912	1.02426	4.03606
C	0.31607	1.50095	2.71638
H	0.90588	-1.38769	2.60692
H	-0.87023	-1.48074	2.75494
H	-0.8599	-0.05563	4.7126
H	0.64596	-0.94456	4.97439
H	1.9628	0.81271	3.92136
H	0.77641	1.76408	4.8261
H	1.04621	1.99996	2.07879
H	-0.54983	2.15217	2.85397

Table 32. Atomic coordinates for the optimized structure of $[Mg(C_3H_5)_2(thf)_2]$.

atom	x	y	z
Mg	0	0	0.67626
O	0.68762	1.45764	-0.67803
O	-0.68762	-1.45764	-0.67803
H	-2.29301	1.57222	0.93065
H	-2.13869	-0.56621	3.12231
H	-4.3347	-0.04653	1.0574
H	2.29301	-1.57222	0.93065
H	2.13869	0.56621	3.12231
H	4.3347	0.04653	1.0574
H	2.1234	0.93786	-2.07777
H	2.68766	1.05955	-0.38265
H	3.11954	3.14497	-2.11581
H	2.64298	3.4561	-0.4428
H	0.8512	4.57771	-1.68611
H	0.80263	3.27778	-2.87973
H	-0.17843	3.20588	0.00398
H	-0.93945	2.48992	-1.42743
H	0.17843	-3.20588	0.00398
H	0.93945	-2.48992	-1.42743
H	-0.8512	-4.57771	-1.68611
H	-0.80263	-3.27778	-2.87973
H	-3.11954	-3.14497	-2.11581
H	-2.64298	-3.4561	-0.4428
H	-2.1234	-0.93786	-2.07777
H	-2.68766	-1.05955	-0.38265
H	-1.24202	1.56766	2.36501
H	-4.2978	-1.30113	2.41348
H	1.24202	-1.56766	2.36501
H	4.2978	1.30113	2.41348
C	-1.728	0.93103	1.61544
C	-2.57514	-0.0741	2.25103
C	-3.79271	-0.50619	1.87921
C	1.728	-0.93103	1.61544

Table 32, continued

atom	x	y	z
C	2.57514	0.0741	2.25103
C	3.79271	0.50619	1.87921
C	2.05723	1.51131	-1.14817
C	2.3349	2.98354	-1.37741
C	0.97034	3.50366	-1.82437
C	0.01479	2.71	-0.94917
C	-0.01479	-2.71	-0.94917
C	-0.97034	-3.50366	-1.82437
C	-2.3349	-2.98354	-1.37741
C	-2.05723	-1.51131	-1.14817

Table 33. Atomic coordinates for the optimized structure of $K[N(SiMe_3)_2]$.

atom	x	y	z
N	0.13183	0.03705	-2.05217
N	-0.12653	0.05237	2.05217
Si	1.72218	-0.15249	-2.66437
Si	-1.37407	0.13656	-2.86673
Si	1.38058	-0.02671	2.86673
Si	-1.72813	0.05201	2.66437
K	-0.10683	-1.80234	0.00000
C	-2.31486	-1.54371	-2.89419
H	-2.52349	-1.93724	-1.87784
H	-3.29471	-1.46054	-3.40183
H	-1.72692	-2.31015	-3.43476
C	-1.36959	0.75302	-4.67686
H	-0.86580	0.04032	-5.35366
H	-2.40274	0.89153	-5.04840
H	-0.84819	1.72396	-4.77118
C	1.91676	-0.62505	-4.50715
H	2.97627	-0.83131	-4.75051
H	1.33423	-1.53233	-4.75333
H	1.57248	0.18240	-5.17753
C	2.79260	1.42782	-2.41355
H	2.31882	2.30610	-2.89367
H	2.96020	1.66982	-1.34437
H	3.79657	1.31176	-2.86456
C	2.67481	-1.53244	-1.70626
H	2.22119	-2.53313	-1.86181
H	3.71798	-1.60679	-2.06762
H	2.74171	-1.34244	-0.61572
C	-2.55399	1.34337	-1.93609
H	-2.69700	1.07253	-0.87089
H	-2.19304	2.39167	-1.98470
H	-3.56082	1.34267	-2.39431
C	-2.83711	-1.20575	1.70626
H	-3.88175	-1.15635	2.06762

Table 33, continued

atom	x	y	z
H	-2.88110	-1.00917	0.61572
H	-2.50486	-2.25301	1.86181
C	-1.97717	-0.39426	4.50715
H	-3.05363	-0.47391	4.75051
H	-1.50590	-1.36400	4.75333
H	-1.53993	0.36688	5.17753
C	-2.60439	1.74770	2.41355
H	-2.03018	2.56387	2.89367
H	-2.74222	2.00781	1.34437
H	-3.61504	1.75105	2.86456
C	2.11630	-1.80635	2.89419
H	2.27699	-2.22177	1.87784
H	3.09911	-1.83950	3.40183
H	1.44194	-2.49797	3.43476
C	2.69479	1.03227	1.93609
H	2.46021	2.11587	1.98470
H	3.69449	0.91264	2.39431
H	2.80481	0.74644	0.87089
C	1.44895	0.58596	4.67686
H	1.04589	1.61170	4.77118
H	0.86450	-0.06223	5.35366
H	2.49123	0.60147	5.04840
K	0.11110	1.87437	0.00000

Table 34. Atomic coordinates for the optimized structure of $Ca[N(SiMe_3)_2]_2$.

atom	x	y	z
C	2.32215	-3.10023	-1.27121
C	0.18250	-1.71721	-3.00055
C	-0.38963	-4.35905	-1.63508
C	-1.25426	-4.02121	1.63690
C	-1.39438	-1.14074	2.55167
C	1.28280	-2.62874	2.57120
C	-0.63143	3.56585	2.39391
C	1.68138	1.63517	2.27300
C	1.76862	4.16888	0.61197
C	-1.76613	4.23133	-0.98968
C	-1.96216	1.57718	-2.42982
C	0.48668	3.31094	-2.81255
C	3.15938	0.74412	-2.54220
C	5.80351	-0.69968	-2.29803
C	5.54125	2.21536	-1.36805
C	5.41405	-2.48723	1.23520
C	6.88863	0.18201	1.30399
C	4.56522	-0.26376	3.14348
C	-3.55720	-2.00958	-2.09542
C	-5.39937	-2.87849	0.17144
C	-6.33249	-0.80032	-1.86380
C	-6.44894	0.15134	2.05158
C	-3.92768	1.83134	2.35194
C	-5.82965	2.36830	0.04072
Ca	1.76018	0.06710	-0.07420
Ca	-1.80365	0.01565	-0.04438
N	-0.03745	-1.67209	-0.02036
N	-0.05790	1.80197	-0.13295
N	4.03872	-0.00658	0.14893
N	-4.06764	-0.12215	0.11887
Si	0.46828	-2.68711	-1.38790
Si	-0.31029	-2.38204	1.57710
Si	0.60367	2.78564	1.19027

Table 34, continued

atom	x	y	z
Si	-0.74108	2.71600	-1.49545
Si	4.67448	0.52621	-1.38425
Si	5.15531	-0.60730	1.36745
Si	-4.83618	-1.36745	-0.83609
Si	-5.04189	0.97528	1.07172
H	2.48702	-3.85018	-0.47995
H	2.99351	-2.25410	-1.03716
H	2.67234	-3.54194	-2.21945
H	-0.88582	-1.72567	-3.26895
H	0.50892	-0.66473	-2.96787
H	0.72985	-2.19793	-3.82833
H	-0.08366	-5.09964	-0.88171
H	-1.48746	-4.29378	-1.62781
H	-0.08718	-4.75087	-2.62139
H	-1.56910	-4.21376	2.67643
H	-2.15799	-4.00212	1.00901
H	-1.45400	-1.47112	3.60130
H	-0.98961	-0.11202	2.58876
H	-2.44236	-1.10160	2.19601
H	1.95794	-3.34013	2.06983
H	1.84318	-1.69258	2.72361
H	-0.07058	4.17901	3.11958
H	-1.19202	2.80934	2.96381
H	-1.35841	4.22351	1.89513
H	1.94297	2.18578	3.19064
H	2.65915	1.34919	1.83785
H	1.15423	0.72603	2.61642
H	2.24781	4.63775	1.48771
H	2.57138	3.78427	-0.03750
H	1.24023	4.96416	0.06305
H	-1.15710	5.02391	-0.52772
H	-2.57019	3.96661	-0.28527
H	-2.23839	4.66368	-1.88784

Table 34, continued

atom	x	y	z
H	-2.27000	2.10816	-3.34546
H	-2.90855	1.35532	-1.89873
H	-1.50597	0.63300	-2.77686
H	-0.04259	3.97722	-3.51436
H	1.32227	3.88163	-2.37940
H	0.90605	2.48060	-3.40091
H	2.42670	1.49795	-2.19881
H	2.63865	-0.20765	-2.75117
H	3.50066	1.11468	-3.52227
H	6.74199	-0.88246	-1.75160
H	5.30391	-1.67213	-2.43684
H	6.07290	-0.30958	-3.29425
H	6.48420	2.17885	-0.80138
H	4.90217	2.98123	-0.89912
H	5.77826	2.54818	-2.39279
H	6.13193	-2.84083	1.99459
H	4.47066	-3.03596	1.38750
H	5.80564	-2.76738	0.24394
H	6.84133	1.26940	1.47824
H	7.51815	-0.25454	2.09788
H	7.40751	0.01353	0.34723
H	5.28588	-0.71370	3.84734
H	4.52552	0.81644	3.35811
H	3.57852	-0.69402	3.37473
H	-3.96028	-2.87196	-2.65181
H	-2.62974	-2.36428	-1.61204
H	-3.29654	-1.23832	-2.83937
H	-6.18848	-2.60918	0.89100
H	-4.56387	-3.31166	0.74562
H	-5.80184	-3.66662	-0.48759
H	-7.17836	-0.49313	-1.22783
H	-6.07231	0.05170	-2.51267
H	-6.68788	-1.62199	-2.50863

Table 34, continued

atom	x	y	z
H	-6.96454	0.89826	2.67885
H	-7.20608	-0.29964	1.38978
H	-6.06579	-0.64121	2.71500
H	-3.53500	1.11903	3.09631
H	-4.48567	2.60904	2.89910
H	-3.07280	2.33519	1.87156
H	-6.38309	3.07316	0.68434
H	-6.53584	1.96978	-0.70444
H	1.05365	-3.03454	3.57064
H	-0.63365	-4.87198	1.31871
H	-5.06248	2.94383	-0.50378

Table 35. Atomic coordinates for the optimized structure of $K\{Ca[N(SiMe_3)_2]_3\}$.

atom	x	y	z
N	-1.61860	0.97841	-1.21809
N	0	0	2.75086
N	1.61860	-0.97841	-1.21809
Si	-1.34644	2.69682	-1.13422
Si	-3.12245	0.32707	-1.81042
Si	1.50563	0.25277	3.56477
Si	-1.50563	-0.25277	3.56477
Si	3.12245	-0.32707	-1.81042
Si	1.34644	-2.69682	-1.13422
Ca	0	0	0.38663
K	0	0	-3.33751
C	-3.45110	0.75675	-3.66378
H	-2.70638	0.33599	-4.37261
H	-4.43073	0.34933	-3.97904
H	-3.48237	1.84856	-3.83741
C	-4.71316	0.83627	-0.88993
H	-4.95657	1.90495	-1.01877
H	-5.57286	0.25111	-1.26832
H	-4.63235	0.64175	0.19449
C	-2.82760	3.80141	-0.66645
H	-2.49473	4.84796	-0.53203
H	-3.61155	3.80473	-1.44545
H	-3.29710	3.47512	0.27873
C	0.00283	3.05118	0.18788
H	-0.27024	2.70359	1.20572
H	1.00659	2.65344	-0.06636
H	0.14513	4.14492	0.27307
C	-0.65127	3.42294	-2.77633
H	-1.33798	3.24171	-3.62547
H	-0.51548	4.51853	-2.69951
H	0.34340	3.01104	-3.04313
C	-3.09382	-1.58646	-1.74950
H	-2.22875	-2.05088	-2.26239

Table 35, continued

atom	x	y	z
H	-3.09439	-1.95697	-0.70731
H	-4.00344	-1.99176	-2.23215
C	0.65127	-3.42294	-2.77633
H	0.51548	-4.51853	-2.69951
H	-0.34340	-3.01104	-3.04313
H	1.33798	-3.24171	-3.62547
C	2.82760	-3.80141	-0.66645
H	2.49473	-4.84796	-0.53203
H	3.61155	-3.80473	-1.44545
H	3.29710	-3.47512	0.27873
C	-0.00283	-3.05118	0.18788
H	0.27024	-2.70359	1.20572
H	-1.00659	-2.65344	-0.06636
H	-0.14513	-4.14492	0.27307
C	3.45110	-0.75675	-3.66378
H	2.70638	-0.33599	-4.37261
H	4.43073	-0.34933	-3.97904
H	3.48237	-1.84856	-3.83741
C	3.09382	1.58646	-1.74950
H	3.09439	1.95697	-0.70731
H	4.00344	1.99176	-2.23215
H	2.22875	2.05088	-2.26239
C	4.71316	-0.83627	-0.88993
H	4.63235	-0.64175	0.19449
H	4.95657	-1.90495	-1.01877
H	5.57286	-0.25111	-1.26832
C	1.45990	1.50590	5.00977
H	0.81736	1.15386	5.83836
H	2.47157	1.67143	5.42698
H	1.06691	2.48589	4.68142
C	2.29150	-1.35159	4.25004
H	3.28065	-1.16521	4.71050
H	1.64761	-1.81695	5.01847

Table 35, continued

atom	x	y	z
H	2.43128	-2.09844	3.44559
C	2.76611	0.95208	2.29504
H	2.88170	0.28690	1.41484
H	2.47282	1.95769	1.93592
H	3.77328	1.04985	2.74237
C	-2.76611	-0.95208	2.29504
H	-2.88170	-0.28690	1.41484
H	-2.47282	-1.95769	1.93592
H	-3.77328	-1.04985	2.74237
C	-2.29150	1.35159	4.25004
H	-3.28065	1.16521	4.71050
H	-1.64761	1.81695	5.01847
H	-2.43128	2.09844	3.44559
C	-1.45990	-1.50590	5.00977
H	-0.81736	-1.15386	5.83836
H	-2.47157	-1.67143	5.42698
H	-1.06691	-2.48589	4.68142

Table 36. Atomic coordinates for the optimized structure of $As(C_5H_5)_3$, C_1 symmetry.

atom	x	y	z
As1	0.06307	0.38108	0.74616
C1	-1.96254	0.55402	0.49308
C2	-2.49836	0.00238	-0.77760
C3	-2.99131	1.02159	-1.52896
C4	-2.84703	2.27078	-0.78880
C5	-2.27230	2.00904	0.41427
C6	0.63908	0.98499	-1.11069
C7	0.66008	-0.03564	-2.19400
C8	1.92689	-0.15702	-2.66538
C9	2.79613	0.77114	-1.94568
C10	2.05464	1.45985	-1.04286
C11	0.24041	-1.63733	0.58732
C12	1.70563	-1.86737	0.71210
C13	1.96206	-2.38621	1.94293
C14	0.70523	-2.58232	2.64886
C15	-0.32182	-2.17945	1.85314
H1	-2.04346	2.72767	1.20149
H2	-3.16245	3.25032	-1.15086
H3	-3.42672	0.93403	-2.52530
H4	-2.48528	-1.05404	-1.04469
H5	-1.38412	-2.21800	2.09387
H6	0.61281	-2.98925	3.65681
H7	2.94743	-2.61975	2.34797
H8	2.42738	-1.60719	-0.06078
H9	2.40927	2.22817	-0.35569
H10	3.86656	0.88758	-2.12095
H11	2.25373	-0.82792	-3.46132
H12	-0.22310	-0.56398	-2.54877
H13	-2.33482	0.06133	1.40718
H14	-0.22968	-1.95206	-0.35376
H15	-0.08964	1.79685	-1.29493

Table 37. Atomic coordinates for the optimized structure of $As(C_5H_5)_3$, C_3 symmetry.

atom	x	y	z
As1	-0.00731	0.00283	1.02089
C1	1.32690	1.24744	0.12514
C2	0.41526	-1.77310	0.12698
C3	-0.35794	-2.80088	0.88785
C4	-1.19368	-3.44366	0.03345
C5	-0.98336	-2.92770	-1.31613
C6	-0.03008	-1.96184	-1.27866
C7	-1.74471	0.52665	0.10515
C8	2.59718	1.09962	0.89819
C9	3.57877	0.68843	0.05616
C10	3.03804	0.59863	-1.29712
C11	1.72470	0.94161	-1.27414
C12	-2.25819	1.70859	0.86176
C13	-2.38579	2.75549	0.00775
C14	-2.02641	2.31813	-1.33813
C15	-1.66706	1.00956	-1.29860
H1	-2.33551	-0.39826	0.23321
H2	0.81963	2.22127	0.24853
H3	2.68361	1.27043	1.97133
H4	4.61130	0.46949	0.33186
H5	3.61079	0.30935	-2.17938
H6	1.05039	1.01237	-2.12474
H7	-2.45826	1.70915	1.93331
H8	1.51054	-1.82095	0.26467
H9	-0.26733	-2.96333	1.96194
H10	-1.90308	-4.22895	0.29825
H11	-1.50861	-3.27728	-2.20608
H12	0.37946	-1.41150	-2.12283
H13	-2.71466	3.76196	0.27031
H14	-2.05486	2.94962	-2.22724
H15	-1.38414	0.38145	-2.14042

Table 38. Atomic coordinates for the optimized structure of $As(C_5Me_4H)_3$, C_1 symmetry.

atom	x	y	z
As1	-0.54344	-0.00898	0.54342
C1	-0.13074	-3.78063	3.43310
C2	3.40151	0.32215	-0.35145
C3	-2.89596	-2.56940	-0.69789
C4	-1.86548	0.83613	-0.80468
C5	-1.46132	0.86204	-2.24115
C6	-1.19223	2.15675	-2.58373
C7	-1.48006	3.03492	-1.43511
C8	-1.93071	2.27723	-0.39395
C9	-1.48531	-0.33317	-3.13765
C10	-0.73007	2.68323	-3.90580
C11	-1.32958	4.52221	-1.49280
C12	-2.46309	2.72844	0.92748
C13	1.15731	0.89573	-0.17144
C14	1.85739	-2.31457	1.40702
C15	-2.95486	-3.88462	2.20064
C16	3.22896	1.13551	0.86404
C17	1.92056	1.49392	0.98030
C18	1.94577	-0.48237	-2.29229
C19	4.73382	-0.20069	-0.78692
C20	4.36694	1.49780	1.76530
C21	1.29066	2.36585	2.01598
C22	-0.42375	-2.00628	0.09691
C23	0.38599	-2.52080	1.25456
C24	-0.45833	-3.16511	2.11001
C25	-1.80610	-3.20318	1.52762
C26	-1.79591	-2.57647	0.31497
C27	2.19817	0.16748	-0.97192
H1	2.25021	-2.88235	2.26262
H2	2.12417	-1.25610	1.56166
H3	2.40277	-2.64488	0.50762
H4	0.93579	-3.68919	3.67911
H5	-0.38928	-4.85297	3.45716

Table 38, continued

atom	x	y	z
H6	-0.69922	-3.30192	4.24906
H7	-3.88384	-3.81033	1.61923
H8	-3.15149	-3.44520	3.19339
H9	-2.74851	-4.95567	2.36781
H10	-3.75304	-3.16594	-0.35489
H11	-2.55622	-3.00725	-1.65231
H12	-3.27712	-1.56487	-0.93869
H13	-1.04595	-0.11545	-4.12169
H14	-2.52138	-0.67339	-3.31321
H15	-0.94207	-1.19144	-2.71608
H16	-0.55831	1.87979	-4.63521
H17	0.21110	3.25059	-3.80855
H18	-1.46916	3.37574	-4.34436
H19	-1.56954	4.99893	-0.53251
H20	-1.98981	4.96557	-2.25808
H21	-0.29998	4.81375	-1.76092
H22	-2.32497	3.80828	1.08049
H23	-1.98243	2.20168	1.76898
H24	-3.54508	2.52037	1.00962
H25	0.68552	1.68686	-0.78598
H26	2.88486	-0.67860	-2.82974
H27	1.32117	0.15838	-2.93396
H28	1.42089	-1.44940	-2.20489
H29	4.67494	-0.75390	-1.73432
H39	-2.79356	0.28177	-0.59556

Table 38, continued

atom	x	y	z
H30	5.16178	-0.88465	-0.03342
H31	5.46600	0.61401	-0.92013
H32	4.04273	2.11671	2.61317
H33	5.14963	2.05768	1.22509
H34	4.85527	0.59907	2.17998
H35	2.03688	2.78627	2.70501
H36	0.54931	1.81459	2.62087
H37	0.75106	3.20994	1.55321
H38	0.00887	-2.17281	-0.89917

Table 39. Atomic coordinates for the optimized structure of $As(C_5Me_4H)_3$, C_3 symmetry.

atom	x	y	z
As1	-0.00147	0.00083	0.45442
C1	-2.31574	0.99574	-1.24372
C2	-3.48492	1.19755	-0.57259
C3	-3.20552	1.87166	0.71063
C4	-1.86688	2.08914	0.81636
C5	-1.18947	1.46966	-0.37795
C6	-2.14832	0.51539	-2.64881
C7	-4.87255	0.87566	-1.02913
C8	-4.28121	2.25952	1.67477
C9	-1.11646	2.80605	1.88911
C10	2.02815	1.50768	-1.23064
C11	2.78318	2.41929	-0.55461
C12	3.21903	1.84022	0.73142
C13	2.73738	0.57218	0.83400
C14	-0.67683	-1.76701	-0.37036
C15	1.53749	1.60292	-2.63891
C16	3.20115	3.78197	-1.00842
C17	4.08655	2.57783	1.70118
C18	2.97614	-0.43620	1.90826
C19	0.29954	-2.51022	-1.22884
C20	0.70715	-3.61991	-0.55022
C21	-0.02051	-3.70789	0.73115
C22	-0.87850	-2.65676	0.82826
C23	0.63639	-2.13285	-2.63496
C24	1.68119	-4.66321	-0.99782
C25	0.17828	-4.82802	1.70217
C26	-1.87805	-2.35939	1.89613
C27	1.86989	0.29530	-0.36593
H1	-4.85899	1.38092	2.00949
H2	-5.00552	2.95489	1.21659
H3	-3.87520	2.74819	2.57110
H4	-0.33229	2.16806	2.33324
H5	-1.77744	3.13920	2.70170

Table 39, continued

atom	x	y	z
H6	-0.60465	3.69871	1.48815
H7	3.49588	-1.32575	1.51060
H8	2.02871	-0.79634	2.34630
H9	3.58992	-0.03038	2.72483
H10	-1.83873	-3.09388	2.71294
H11	-2.90572	-2.36471	1.49186
H12	-1.71905	-1.35884	2.33524
H13	-1.61747	-1.48829	-0.87139
H14	-0.47456	2.14494	-0.87438
H15	2.10044	-0.66144	-0.86092
H16	-3.06296	0.03993	-3.03216
H17	-1.32917	-0.21089	-2.75359
H18	-1.91216	1.35383	-3.32932
H19	-0.20559	-2.35132	-3.31702
H20	1.50670	-2.68933	-3.01240
H21	0.85615	-1.06090	-2.74498
H22	0.49963	1.25665	-2.75038
H23	2.14988	0.97920	-3.31553
H24	1.58550	2.63276	-3.02192
H25	2.15442	-4.40714	-1.95572
H26	1.19155	-5.64472	-1.12260
H27	2.48554	-4.80833	-0.25676
H28	2.92226	4.55522	-0.27254
H29	2.74590	4.05845	-1.96936

Table 39, continued

atom	x	y	z
H30	4.29639	3.84799	-1.13001
H31	-5.40516	0.25160	-0.29151
H32	-4.88125	0.33784	-1.98713
H33	-5.47694	1.79046	-1.15776
H34	-0.06030	-5.80550	1.24863
H35	-0.45083	-4.71577	2.59585
H36	1.22697	-4.88723	2.04063
H37	4.30098	1.98184	2.59888
H38	3.61239	3.51748	2.03290
H39	5.05383	2.85743	1.24922

Table 40. Atomic coordinates for the transition structure of $As(C_5H_5)_3$.

atom	x	y	z
As1	-0.34484	0.01819	0.68325
C1	-1.75504	0.88852	-0.54821
C2	-1.35617	1.01196	-1.95544
C3	-1.14236	2.31489	-2.24186
C4	-1.43791	3.10540	-1.06447
C5	-1.83211	2.27913	-0.06941
C6	1.25187	0.94972	-0.15700
C7	1.78241	0.38345	-1.41200
C8	3.02111	-0.10106	-1.19017
C9	3.37635	0.12963	0.19752
C10	2.36161	0.77628	0.80532
C11	-0.96477	-2.02883	-0.16805
C12	0.42769	-2.00213	0.26311
C13	0.45640	-2.53019	1.57286
C14	-0.84466	-2.83143	1.94878
C15	-1.72020	-2.52187	0.89570
H1	0.85998	1.96844	-0.25712
H2	-1.35399	4.18355	-1.00204
H3	-0.79458	2.71319	-3.18689
H4	-1.23114	0.17544	-2.63105
H5	-2.79653	-2.62777	0.90850
H6	-1.14725	-3.19933	2.92096
H7	1.34289	-2.62055	2.18466
H8	1.27788	-1.85462	-0.38960
H9	2.32639	1.09335	1.83985
H10	4.31084	-0.16566	0.65862
H11	3.65595	-0.58464	-1.92259
H12	1.24572	0.38543	-2.34889
H13	-2.62053	0.25883	-0.33461
H14	-1.30501	-1.83299	-1.17598
H15	-2.13620	2.56630	0.92897

Table 41. Atomic coordinates for the transition structure of $As(C_5Me_4H)_3$.

atom	x	y	z
As1	0.00000	0.00000	-0.00000
C1	3.55638	-0.71805	-0.51639
C2	2.72211	-0.04761	0.30773
C3	1.72540	1.32837	-3.08024
C4	4.08422	-0.84201	-3.04974
C5	4.64058	-1.67871	-0.15765
C6	2.64420	-0.06029	1.79737
C7	0.14379	-2.75692	-0.29404
C8	0.20934	-1.85637	-1.35760
C9	-1.11661	-1.22989	-1.48488
C10	-1.94383	-1.83899	-0.48909
C11	-1.17655	-2.75137	0.22518
C12	1.28827	-3.50667	0.30097
C13	-1.61166	-3.55030	1.41076
C14	3.28847	-0.31351	-1.90247
C15	-1.63740	-0.49223	-2.67481
C16	-1.07181	1.81687	-0.13303
C17	-0.31829	2.96438	-0.67032
C18	0.28133	3.60313	0.36864
C19	-0.13208	2.97470	1.62161
C20	-1.00268	1.96610	1.34943
C21	-0.40028	3.44127	-2.08389
C22	1.19503	4.78310	0.32494
C23	0.36417	3.43838	2.95010
C24	-1.77008	1.11555	2.30573
C25	1.80105	0.78989	-0.52544
C26	2.27715	0.58275	-1.91839
C27	-3.38320	-1.49620	-0.29169
H1	-3.53931	-0.41738	-0.33720
H2	-3.74183	-1.84266	0.67528
H3	-4.00675	-1.95238	-1.06337
H4	-2.17960	-1.17811	-3.32996
H5	-2.32231	0.30351	-2.38344

Table 41, continued

atom	x	y	z
H6	-0.82166	-0.05831	-3.24692
H7	0.46356	4.04515	-2.35494
H8	-1.29247	4.05924	-2.21079
H9	-0.47045	2.62056	-2.78911
H10	1.44026	5.05806	-0.69888
H11	2.12948	4.57231	0.84882
H12	0.73804	5.64992	0.80608
H13	-0.06601	2.85790	3.76268
H14	0.11784	4.48886	3.11428
H15	-1.56548	1.40493	3.33426
H16	-1.52420	0.05627	2.19599
H17	-2.84197	1.22208	2.12978
H18	1.45098	3.34524	3.00795
H19	2.27228	1.10173	-3.99335
H20	1.77880	2.40519	-2.90374
H21	0.67728	1.08611	-3.24132
H22	1.69998	1.83207	-0.22294
H23	3.74965	-0.42289	-3.99589
H24	4.00079	-1.92897	-3.11333
H25	5.14232	-0.60351	-2.92886
H26	4.71956	-1.80155	0.92072
H27	5.60491	-1.33267	-0.53328
H28	4.45156	-2.66030	-0.59490
H29	3.54151	-0.49130	2.23785
H30	1.78272	-0.63630	2.14928

Table 41, continued

atom	x	y	z
H31	2.52293	0.95828	2.17108
H32	1.01168	-1.73071	-2.06013
H33	-2.02024	1.55376	-0.59339
H34	0.93204	-4.34922	0.89190
H35	1.87732	-2.85857	0.94969
H36	1.94981	-3.88905	-0.47481
H37	-0.86271	-3.50889	2.20143
H38	-1.76063	-4.59829	1.14524
H39	-2.54816	-3.17446	1.81709

REFERENCES

(1) Elschenbroich, C. *Organometallics*; VCH Publishers: Weinheim, 2006.

(2) Hegedus, L. S. *Transition Metals in the Synthesis of Complex Organic Molecules*; 2nd ed.; University Science Books: Sausalito, California, 1999.

(3) Wilke, G.; Bogdanovic, B.; Hardt, P.; Heimbach, P.; Keim, W.; Kroner, M.; Oberkirch, W.; Tanaka, K.; Walter, D. *Angew. Chem., Int. Ed. Engl.* **1966**, *5*, 151.

(4) (a) Hays, M. L.; Hanusa, T. P. *Adv. Organomet. Chem.* **1996**, *40*, 117. (b) Hanusa, T. P. *Organometallics* **2002**, *21*, 2559. (c) Jutzi, P.; Burford, N. *Chem. Rev.* **1999**, *99*, 969.

(5) Grosselin, J. M.; Dixneuf, P. H. *J. Organomet. Chem.* **1986**, *314*, C76.

(6) Schott, A.; Schott, H.; Wilke, G.; Brandt, J.; Hoberg, H.; Hoffmann, E. G. *Liebigs Ann. Chem.* **1973**, 508.

(7) (a) Fraenkel, G.; Chow, A.; Winchester, W. R. *J. Am. Chem. Soc.* **1990**, *112*, 1382. (b) Fraenkel, G.; Chow, A.; Winchester, W. R. *J. Am. Chem. Soc.* **1990**, *112*, 2582. (c) Boche, G.; Fraenkel, G.; Cabral, J.; Harms, K.; van Eikema Hommes, N. J. R.; Lohrenz, J.; Marsch, M.; Schleyer, P. v. R. *J. Am. Chem. Soc.* **1992**, *114*, 1562.

(8) Fraenkel, G.; Winchester, W. R. *Organometallics* **1990**, *9*, 1314.

(9) Ray, B.; Neyroud, T. G.; Kapon, M.; Eichen, Y.; Eisen, M. S. *Organometallics* **2001**, *20*, 3044.

(10) Comment145 *These volumes were calculated at the B3LYP/6-31+G(d) level, using the MacSpartan program (t. Hanusa, unpublished results).*

(11) Harder, S.; Lutz, M.; Straub, A. W. G. *Organometallics* **1997**, *16*, 107.

(12) Carlson, C. N.; Smith, J. D.; Hanusa, T. P.; Brennessel, W. W.; Young, V. G., Jr. *J. Organomet. Chem.* **2003**, *683*, 191.

(13) Quisenberry, K. T.; Smith, J. D.; Voehler, M.; Stec, D. F.; Hanusa, T. P.; Brennessel, W. W. *J. Am. Chem. Soc.* **2005**, *127*, 4376.

(14) Carlson, C. N.; Hanusa, T. P.; Brennessel, W. W. *J. Am. Chem. Soc.* **2004**, *126*, 10550.

(15) Gren, C. K.; Hanusa, T. P.; Rheingold, A. L. *Main Group Chem.* **2009**, *8*, 225.

(16) Smith, J. D.; Hanusa, T. P.; Young, V. G., Jr. *J. Am. Chem. Soc.* **2001**, *123*, 6455.

(17) (a) Smith, J. D.; Quisenberry, K. T.; Hanusa, T. P.; Brennessel, W. W. *Acta Crystallogr., Sect. C.* **2004**, *60*, m507. (b) Schormann, M.; Garratt, S.; Bochmann, M. *Organometallics* **2005**, *24*, 1718.

(18) Kuehl, C. J.; Simpson, C. K.; John, K. D.; Sattelberger, A. P.; Carlson, C. N.; Hanusa, T. P. *J. Organomet. Chem.* **2003**, *683*, 149.

(19) Woodman, T. J.; Schormann, M.; Hughes, D. L.; Bochmann, M. *Organometallics* **2003**, *22*, 3028.

(20) Hanusa, T. P.; Carlson, C. N. In Encyclopedia of Inorg. Chem.-II; King, R. B., Ed.; Wiley: 2005; Vol. 9, p 5690.

(21) Caro, C. F.; Lappert, M. F.; Merle, P. G. *Coord. Chem. Rev.* **2001**, *219-221*, 605.

(22) Sudupe, M.; Cano, J. s.; Royo, P.; Herdtweck, E. *Eur. J. Inorg. Chem.* **2004**, *2004*, 3074.

(23) Strohmann, C.; Lehmen, K.; Dilsky, S. *J. Am. Chem. Soc.* **2006**, *128*, 8102.

(24) (a) Fernandez-Galan, R.; Hitchcock, P. B.; Lappert, M. F.; Antinolo, A.; Rodriguez, A. M. *Dalton* **2000**, 1743. (b) Woodman, T. J.; Schormann, M.; Bochmann, M. *Organometallics* **2003**, *22*, 2938.

(25) Hitchcock, P. B.; Lappert, M. F.; Leung, W.-P.; Liu, D.-S.; Mak, T. C. W.; Wang, Z.-X. *J. Chem. Soc., Dalton Trans.* **1999**, 1257.

(26) White, R. E.; Hanusa, T. P.; Kucera, B. E. *J. Am. Chem. Soc.* **2006**, *128*, 9622.

(27) (a) Fraenkel, G.; Qiu, F. *J. Am. Chem. Soc.* **1996**, *118*, 5828. (b) Fraenkel, G.; Qiu, F. *J. Am. Chem. Soc.* **1997**, *119*, 3571. (c) Fraenkel, G.; Duncan, J. H.; Wang, J. *J. Am. Chem. Soc.* **1998**, *121*, 432. (d) Fraenkel, G.; Chow, A.; Fleischer, R.; Liu, H. *J. Am. Chem. Soc.* **2004**, *126*, 3983. (e) Fraenkel, G.; Cabral, J.; Chen, X.; Chow, A. *J. Org. Chem.* **2009**, *74*, 2311.

(28) Winchester, W. R.; Bauer, W.; Schleyer, P. v. R. *Chem. Commun.* **1987**, 177.

(29) Solomon, S. A.; Muryn, C. A.; Layfield, R. A. *Chem. Commun.* **2008**, 3142.

(30) Praesang, C.; Sahin, Y.; Hofmann, M.; Geiseler, G.; Massa, W.; Berndt, A. *Eur. J. Inorg. Chem.* **2004**, 3063.

(31) Boche, G.; Etzrodt, H.; Marsch, M.; Massa, W.; Baum, G.; Dietrich, H.; Mahdi, W. *Angew. Chem. Int. Ed.* **1986**, *25*, 104.

(32) Layfield, R. A.; Garcia, F.; Hannauer, J.; Humphrey, S. M. *Chem. Commun.* **2007**, 5081.

(33) Simpson, C. K.; White, R. E.; Carlson, C. N.; Wrobleski, D. A.; Kuehl, C. J.; Croce, T. A.; Steele, I. M.; Scott, B. L.; Hanusa, T. P.; Sattelberger, A. P.; John, K. D. *Organometallics* **2005**, *24*, 3685.

(34) Quisenberry, K. T.; Gren, C. K.; White, R. E.; Hanusa, T. P.; Brennessel, W. W. *Organometallics* **2007**, *26*, 4354.

(35) Harvey, M. J.; Hanusa, T. P.; Pink, M. *J. Chem. Soc., Dalton Trans.* **2001**, 1128.

(36) Hill, E. A.; Boyd, W. A.; Desai, H.; Darki, A.; Bivens, L. *J. Organomet. Chem.* **1996**, *514*, 1.

(37) Harvey, M. J.; Hanusa, T. P.; Young, V. G., Jr. *Angew. Chem. Int. Ed.* **1999**, *38*, 217.

(38) Williams, R. A.; Hanusa, T. P.; Huffman, J. C. *Organometallics* **1990**, *9*, 1128.

(39) (a) Smith, A. E. *Inorg. Chem.* **1972**, *11*, 165. (b) Murrall, N. W.; Welch, A. J. *J. Organomet. Chem.* **1986**, *301*, 109.

(40) Woodman, T. J.; Schormann, M.; Bochmann, M. *Isr. J. Chem.* **2002**, *42*, 283.

(41) White, R. E.; Hanusa, T. P. *Organometallics* **2006**, *25*, 5621.

(42) Shannon, R. D. *Acta Crystallogr., Sect A.* **1976**, *32*, 751.

(43) Kawalec, M.; Smiga-Matuszowicz, M.; Kurcok, P. *Eur. Polymer J.* **2008**, *44*, 3556.

(44) Woodman, T. J.; Sarazin, Y.; Garratt, S.; Fink, G.; Bochmann, M. *J. Mol. Catal. A: Chem.* **2005**, *235*, 88.

(45) (a) Hitchcock, P. B.; Lappert, M. F.; Wang, Z. X. *Chem. Commun.* **1996**, 1647. (b) Boche, G.; Fraenkel, G.; Cabral, J.; Harms, K.; van Eikema Hommes, N. J. R.; Lohrenz, J.; Marsch, M.; Schleyer, P. v. R. *J. Am. Chem. Soc.* **1992**, *114*, 1562. (c) Praesang, C.; Sahin, Y.; Hofmann, M.; Geiseler, G.; Massa, W.; Berndt, A. *Eur. J. Inorg. Chem.* **2004**, 3063. (d) Marr, F.; Frˆhlich, R.; Hoppe, D. *Tetrahedron: Asymmetry* **2002**, *13*, 2587. (e) Wilkes, J. B. *J Org Chem* **1967**, *32*, 3231.

(46) Halstead, G. W.; Baker, E. C.; Raymond, K. N. *J. Am. Chem. Soc.* **1975**, *97*, 3049.

(47) (a) Gren, C. K.; Hanusa, T. P.; Brennessel, W. W. *Polyhedron* **2006**, *25*, 286. (b) Gren, C. K.; Hanusa, T. P.; Rheingold, A. L. *Organometallics* **2007**, *26*, 1643. (c) Cheon, J.; Dubois, L. H.; Girolami, G. S. *Chemistry of Materials* **1994**, *6*, 2279.

(48) Hanusa, T. P. *Coordin Chem Rev* **2000**, *210*, 329.

(49) Harvey, M. J.; Hanusa, T. P.; Young, V. G., Jr. *Angew. Chem., Int. Ed.* **1999**, *38*, 217.

(50) (a) Alexander, J. S.; Ruhlandt-Senge, K. *Chem. Eur. J.* **2004**, *10*, 1274. (b) Westerhausen, M. *Coordin Chem Rev* **2008**, *252*, 1516.

(51) Clark, T.; Rohde, C.; Schleyer, P. V. *Organometallics* **1983**, *2*, 1344.

(52) Cotton, F. A. *Advanced inorganic chemistry / F. Albert Cotton ... [et al.]*; 6th ed.; Wiley: New York, 1999.

(53) (a) Coates, G. E.; Francis, B. R. *J. Chem. Soc. A* **1971**, 1308. (b) Coates, G. E.; Morgan, G. L. *Advances in Organometallic Chemistry*; Academic Press: New York, 1970; Vol. 9. (c) Whitt, C. D.; Atwood, J. L. *J. Organomet. Chem.* **1971**, *32*, 17.

(54) (a) Morosin, B.; Howatson, J. *J. Organomet. Chem.* **1971**, *29*, 7. (b) Bell, N. A.; Nowell, I. W.; Coates, G. E.; Shearer, H. M. M. *J. Organomet. Chem.* **1984**, *273*, 179.

(55) (a) Ruhlandt-Senge, K.; Bartlett, R. A.; Olmstead, M. M.; Power, P. P. *Inorg. Chem.* **1993**, *32*, 1724. (b) Clyburne, J. A. C.; McMullen, N. *Coord. Chem. Rev.* **2000**, *210*, 73.

(56) Niemeyer, M.; Power, P. P. *Inorg. Chem.* **1997**, *36*, 4688.

(57) Battle, S. L.; Cowley, A. H.; Decken, A.; Jones, R. A.; Koschmieder, S. U. *J. Organomet. Chem.* **1999**, *582*, 66.

(58) (a) Herrmann, W. A.; Runte, O.; Artus, G. *J. Organomet. Chem.* **1995**, *501*, C1. (b) Gottfriedsen, J.; Blaurock, S. *Organometallics* **2006**, *25*, 3784.

(59) Lerner, H.-W.; Scholz, S.; Bolte, M.; Wiberg, N.; Noth, H.; Krossing, I. *Eur. J. Inorg. Chem.* **2003**, 666.

(60) Han, R.; Parkin, G. *Inorg. Chem.* **1993**, *32*, 4968.

(61) (a) Burkey, D. J.; Hanusa, T. P. *Comments Inorg. Chem.* **1995**, *17*, 41. (b) Jutzi, P. *Chem. Unserer Zeit* **1999**, *33*, 343. (c) Del Mar Conejo, M.; Fernandez, R.; Gutierrez-Puebla, E.; Monge, A.; Ruiz, C.; Carmona, E. *Angew. Chem., Int. Ed.* **2000**, *39*, 1949. (d) del Mar Conejo, M.; Fernandez, R.; Carmona, E.; Gutierrez-Puebla, E.; Monge, A. *Organometallics* **2001**, *20*, 2434. (e) Conejo, M. M.; Fernandez, R.; del Rio, D.; Carmona, E.; Monge, A.; Ruiz, C. *Chem. Commun.* **2002**, 2916. (f) del Mar Conejo, M.; Fernandez, R.; Carmona, E.; Andersen, R. A.; Gutierrez-Puebla, E.; Monge, M. A. *Chem.—Eur. J.* **2003**, *9*, 4462. (g) del Mar

Conejo, M.; Fernandez, R.; del Rio, D.; Carmona, E.; Monge, A.; Ruiz, C.; Marquez, A. M.; Sanz, F. J. *Chem.—Eur. J.* **2003**, *9*, 4452.

(62) (a) Almenningen, A.; Haaland, A.; Lusztyk, J. *J. Organomet. Chem.* **1979**, *170*, 271. (b) Nugent, K. W.; Beattie, J. K.; Hambley, T. W.; Snow, M. R. *Aust. J. Chem.* **1984**, *37*, 1601. (c) Wong, C. H.; Lee, T. Y.; Lee, T. J.; Chang, T. W.; Liu, C. S. *Acta Crystallogr., Sect. B* **1972**, *28*, 1662.

(63) Wiegand, G.; Thiele, K. H. *Z. Anorg. Allg. Chem.* **1974**, *405*, 101.

(64) (a) Chmely, S. C.; Hanusa, T. P. *Eur. J. Inorg. Chem.* **2010**, *2010*, 1321. (b) Solomon, S. A.; Layfield, R. A. *Dalton Transactions* **2010**, *39*, 2469.

(65) Sulway, S. A.; Girshfeld, R.; Solomon, S. A.; Muryn, C. A.; Poater, J.; Sola, M.; Bickelhaupt, F. M.; Layfield, R. A. *Eur. J. Inorg. Chem.* **2009**, 4157.

(66) Chmely, S. C.; Carlson, C. N.; Hanusa, T. P.; Rheingold, A. L. *J. Am. Chem. Soc.* **2009**, *131*, 6344.

(67) Gaussian 03: Frisch, M. J. T., G. W.; Schlegel, H. B.; Scuseria, G. E.; Robb, M. A.; Cheeseman, J. R.; Montgomery, Jr., J. A.; Vreven, T.; Kudin, K. N.; Burant, J. C.; Millam, J. M.; Iyengar, S. S.; Tomasi, J.; Barone, V.; Mennucci, B.; Cossi, M.; Scalmani, G.; Rega, N.; Petersson, G. A.; Nakatsuji, H.; Hada, M.; Ehara, M.; Toyota, K.; Fukuda, R.; Hasegawa, J.; Ishida, M.; Nakajima, T.; Honda, Y.; Kitao, O.; Nakai, H.; Klene, M.; Li, X.; Knox, J. E.; Hratchian, H. P.; Cross, J. B.; Bakken, V.; Adamo, C.; Jaramillo, J.; Gomperts, R.; Stratmann, R. E.; Yazyev, O.; Austin, A. J.; Cammi, R.; Pomelli, C.; Ochterski, J. W.; Ayala, P. Y.; Morokuma, K.; Voth, G. A.; Salvador, P.; Dannenberg, J. J.; Zakrzewski, V. G.; Dapprich, S.; Daniels, A. D.; Strain, M. C.; Farkas, O.; Malick, D. K.; Rabuck, A. D.; Raghavachari, K.; Foresman, J. B.; Ortiz, J. V.; Cui, Q.; Baboul, A. G.; Clifford, S.; Cioslowski, J.; Stefanov, B. B.; Liu, G.; Liashenko, A.; Piskorz, P.; Komaromi, I.; Martin, R. L.; Fox, D. J.; Keith, T.; Al-Laham, M. A.; Peng, C. Y.; Nanayakkara, A.; Challacombe, M.; Gill, P. M. W.; Johnson, B.; Chen, W.; Wong, M. W.; Gonzalez, C.; and Pople, J. A.; Gaussian, Inc., Wallingford CT, 2004. **Revision E.01**.

(68) Zhao, Y.; Lynch, B. J.; Truhlar, D. G. *J. Phys. Chem. A* **2004**, *108*, 2715.

(69) Feller, D.; Glendening, E. D.; Woon, D. E.; Feyereisen, M. W. *J. Chem. Phys.* **1995**, *103*, 3526.

(70) (a) Csaszar, P.; Pulay, P. *J. Mol. Struct.* **1984**, *114*, 31. (b) Farkas, O.; Schlegel, H. B. *J. Chem. Phys.* **1999**, *111*, 10806.

(71) Becke, A. D. *J. Chem. Phys.* **1993**, *98*, 5648.

(72) Perdew, J. P.; Wang, Y. *Phys. Rev. B* **1992**, *45*, 13244.

(73) (a) Smith, J. D.; Hanusa, T. P. *Organometallics* **2001**, *20*, 3056. (b) Ziegler, T. *Chem. Rev.* **1991**, *91*, 651.

(74) Sheldrick, G. M. *Acta Crystallogr A* **2008**, *64*, 112.

(75) Coates, G. E.; Green, S. I. E. *J. Chem. Soc.* **1962**, 3340.

(76) Plieger, P. G.; John, K. D.; Keizer, T. S.; McCleskey, T. M.; Burrell, A. K.; Martin, R. L. *J. Am. Chem. Soc.* **2004**, *126*, 14651.

(77) (a) Benn, R.; Lehmkuhl, H.; Mehler, K.; Rufinska, A. *Angew. Chem., Int. Ed.* **1984**, *23*, 534. (b) Heard, P. J. *Patai's Chemistry of Functional Groups*; John Wiley & Sons, 2008.

(78) (a) Kovar, R. A.; Morgan, G. L. *J. Am. Chem. Soc.* **1970**, *92*, 5067. (b) Gaines, D. F.; Coleson, K. M.; Hillenbrand, D. F. *J. Magn. Reson.* **1981**, *44*, 84.

(79) Sanders, J. R.; Ashby, E. C.; Carter, J. H. *J. Am. Chem. Soc.* **1968**, *90*, 6385.

(80) Marsch, M.; Harms, K.; Massa, W.; Boche, G. *Angew Chem Int Edit* **1987**, *26*, 696.

(81) Sanchez-Barba, L. F.; Hughes, D. L.; Humphrey, S. M.; Bochmann, M. *Organometallics* **2005**, *24*, 5329.

(82) (a) Hu, J. X.; Barbour, L. J.; Gokel, G. W. *Chem. Commun.* **2001**, 1858. (b) Kralik, M. S.; Stahl, L.; Arif, A. M.; Strouse, C. E.; Ernst, R. D. *Organometallics* **1992**, *11*, 3617.

(83) Vijay, D.; Sastry, G. N. *Phys. Chem. Chem. Phys.* **2008**, *10*, 582.

(84) (a) Reddy, A. S.; Sastry, G. N. *J. Phys. Chem. A.* **2005**, *109*, 8893. (b) Cheng, J.; Zhu, W.; Tang, Y.; Xu, Y.; Li, Z.; Chen, K.; Jiang, H. *Chemical Physics Letters* **2006**, *422*, 455. (c) Reddy, A. S.; Zipse, H.; Sastry, G. N. *J. Phys. Chem. B.* **2007**, *111*, 11546.

(85) Chung, L. W.; Chan, T. H.; Wu, Y.-D. *Organometallics* **2005**, *24*, 1598.

(86) Bunder, W.; Weiss, E. *J. Organomet. Chem.* **1975**, *92*, 1.

(87) Caro, C. F.; Hitchcock, P. B.; Lappert, M. F. *Chem. Commun.* **1999**, 1433.

(88) Jaenschke, A.; Paap, J.; Behrens, U. *Organometallics* **2003**, *22*, 1167.

(89) Quisenberry, K. T.; White, R. E.; Hanusa, T. P.; Brennessel, W. W. *New J. Chem.* **2010**.

(90) (a) Westerhausen, M. *Coordin Chem Rev* **1998**, *176*, 157. (b) Hanusa, T. P. *Comprehensive Coordination Chemistry, 2nd Ed.*; Elsevier: Oxford, 2004; Vol. 3. (c) Orzechowski, L.; Harder, S. *Organometallics* **2007**, *26*, 5501. (d) Hitzbleck, J.; Deacon, G. B.; Ruhlandt-Senge, K. *Eur. J. Inorg. Chem.* **2007**, 592.

(91) Hitchcock, P. B.; Lappert, M. F.; Lawless, G. A.; Royo, B. *J Chem Soc Chem Comm* **1990**, 1141.

(92) Bradley, D. C.; Chudzynska, H.; Backerdirks, J. D. J.; Hursthouse, M. B.; Ibrahim, A. A.; Motevalli, M.; Sullivan, A. C. *Polyhedron* **1990**, *9*, 1423.

(93) Westerhausen, M. *Inorg. Chem.* **1991**, *30*, 96.

(94) Drake, S. R.; Otway, D. J. *J Chem Soc Chem Comm* **1991**, 517.

(95) Gillett-Kunnath, M. M.; MacLellan, J. G.; Forsyth, C. M.; Andrews, P. C.; Deacon, G. B.; Ruhlandt-Senge, K. *Chem. Commun.* **2008**, 4490.

(96) (a) Tanner, P. S.; Burkey, D. J.; Hanusa, T. P. *Polyhedron* **1995**, *14*, 331. (b) He, X. Y.; Noll, B. C.; Beatty, A.; Mulvey, R. E.; Henderson, K. W. *J. Am. Chem. Soc.* **2004**, *126*, 7444.

(97) Hanusa, T. P.; Fitts, L. S.; Brady, E. D.; Jayaratne, K. C.; Overby, J. S.; Young, V. G. *Abstr Pap Am Chem S* **2000**, *219*, U789.

(98) Brady, E. D.; Chmely, S. C.; Jayaratne, K. C.; Hanusa, T. P.; Young, V. G. *Organometallics* **2008**, *27*, 1612.

(99) Hernandez-Sanchez, B. A.; Boyle, T. J.; Baros, C. M.; Brewer, L. N.; Headley, T. J.; Tallant, D. R.; Rodriguez, M. A.; Tuttle, B. A. *Chemistry of Materials* **2007**, *19*, 1459.

(100) Datta, S.; Roesky, P. W.; Blechert, S. *Organometallics* **2007**, *26*, 4392.

(101) Wendell, L. T.; Bender, J.; He, X. Y.; Noll, B. C.; Henderson, K. W. *Organometallics* **2006**, *25*, 4953.

(102) Barrett, A. G. M.; Crimmin, M. R.; Hill, M. S.; Hitchcock, P. B.; Lomas, S. L.; Mahon, M. F.; Procopiou, P. A.; Suntharalingam, K. *Organometallics* **2008**, *27*, 6300.

(103) (a) He, X. Y.; Allan, J. F.; Noll, B. C.; Kennedy, A. R.; Henderson, K. W. *J. Am. Chem. Soc.* **2005**, *127*, 6920. (b) He, X. Y.; Hurley, E.; Noll, B. C.; Henderson, K. W. *Organometallics* **2008**, *27*, 3094.

(104) Glock, C.; Gorls, H.; Westerhausen, M. *Inorg. Chem.* **2009**, *48*, 394.

(105) Boncella, J. M.; Coston, C. J.; Cammack, J. K. *Polyhedron* **1991**, *10*, 769.

(106) (a) Dunning, T. H. *J. Chem. Phys.* **1989**, *90*, 1007. (b) Woon, D. E.; Dunning, T. H. *J. Chem. Phys.* **1993**, *98*, 1358.

(107) Schafer, A.; Horn, H.; Ahlrichs, R. *J. Chem. Phys.* **1992**, *97*, 2571.

(108) Harder, S.; Muller, S.; Hubner, E. *Organometallics* **2004**, *23*, 178.

(109) Andersen, R. A.; Blom, R.; Boncella, J. M.; Burns, C. J.; Volden, H. V. *Acta Chem Scand A* **1987**, *41*, 24.

(110) Mccormick, M. J.; Sockwell, S. C.; Davies, C. E. H.; Hanusa, T. P.; Huffman, J. C. *Organometallics* **1989**, *8*, 2044.

(111) Tesh, K. F.; Hanusa, T. P.; Huffman, J. C. *Inorg. Chem.* **1990**, *29*, 1584.

(112) Cameron, T. M.; Xu, C. Y.; Dipasquale, A. G.; Rheingold, A. L. *Organometallics* **2008**, *27*, 1596.

(113) (a) Jutzi, P. *Adv Organomet Chem* **1986**, *26*, 217. (b) Jutzi, P. *Chem Rev* **1986**, *86*, 983.

(114) Fischer, E. O.; Schreiner, S. *Angew. Chem.* **1957**, *69*, 205.

(115) (a) Fischer, E. O.; Schreiner, S. *Chem. Ber.* **1960**, *93*, 1417. (b) Deubzer, B.; Elian, M.; Fischer, E. O.; Fritz, H. P. *Chem Ber-Recl* **1970**, *103*, 799. (c) Birkhahn, M.; Krommes, P.; Massa, W.; Lorberth, J. *J. Organomet. Chem.* **1981**, *208*, 161. (d) Lorberth, J.; Massa, W.; Wocadlo, S.; Sarraje, I.; Shin, S. H.; Li, X. W. *J. Organomet. Chem.* **1995**, *485*, 149.

(116) Berlitz, T. F.; Pebler, J.; Lorberth, J. *J. Organomet. Chem.* **1988**, *348*, 175.

(117) (a) Frank, W. *J. Organomet. Chem.* **1990**, *386*, 177. (b) Uffing, C.; Ecker, A.; Baum, E.; Schnockel, H. *Z Anorg Allg Chem* **1999**, *625*, 1354. (c) Sitzmann, H.; Wolmershauser, G. *Chem Ber* **1994**, *127*, 1335. (d) Sitzmann, H.; Wolmershauser, G.; Boese, R.; Blaser, D. *Z Anorg Allg Chem* **1999**, *625*, 2103. (e) Sitzmann, H.; Ehleiter, Y.; Wolmershauser, G.; Ecker, A.; Uffing, C.; Schnockel, H. *J. Organomet. Chem.* **1997**, *527*, 209.

(118) Ayala, P. Y.; Schlegel, H. B. *J. Chem. Phys.* **1997**, *107*, 375.

(119) (a) Jutzi, P.; Meyer, U.; Opiela, S.; Olmstead, M. M.; Power, P. P. *Organometallics* **1990**, *9*, 1459. (b) Ehleiter, Y.; Wolmershauser, G.; Sitzmann, H.; Boese, R. *Z Anorg Allg Chem* **1996**, *622*, 923.

(120) El Chaouch, S.; Guillemin, J. C.; Karpati, T.; Veszpremi, T. *Organometallics* **2001**, *20*, 5405.

(121) Sandström, J. *Dynamic NMR Spectroscopy*; Academic Press: London, 1982.

(122) Fisher, J. D.; Budzelaar, P. H. M.; Shapiro, P. J.; Staples, R. J.; Yap, G. P. A.; Rheingold, A. L. *Organometallics* **1997**, *16*, 871.

(123) (a) Avtomonov, E. V.; Li, X. W.; Lorberth, J. *J. Organomet. Chem.* **1997**, *530*, 71. (b) Avtomonov, E. V.; Megges, K.; Wocadlo, S.; Lorberth, J. *J. Organomet. Chem.* **1996**, *524*, 253. (c) Li, X. W.; Lorberth, J.; Harms, K. *J. Organomet. Chem.* **1994**, *483*, 229. (d) Wiacek, R. J.; Jones, J. N.; Macdonald, C. L. B.; Cowley, A. H. *Can J Chem* **2002**, *80*, 1518. (e) Jutzi, P.; Wippermann, T.; Kruger, C.; Kraus, H. J. *Angew Chem Int Edit* **1983**, *22*, 250.

(124) Power, P. P. *Nature* **2010**, *463*, 171.

(125) Frank, W. *J. Organomet. Chem.* **1991**, *406*, 331.

(126) Bartlett, R. A.; Cowley, A.; Jutzi, P.; Olmstead, M. M.; Stammler, H. G. *Organometallics* **1992**, *11*, 2837.

(127) Trotter, J.; Zobel, T. *Z Kristallogr Krist* **1966**, *123*, 67.

(128) Breunig, H. J.; Ebert, K. H.; Gulec, S.; Drager, M.; Sowerby, D. B.; Begley, M. J.; Behrens, U. *J. Organomet. Chem.* **1992**, *427*, 39.

(129) Mundt, O.; Becker, G.; Stadelmann, H.; Thurn, H. *Z Anorg Allg Chem* **1992**, *617*, 59.

(130) van Bolhuis, F.; Koster, P. B.; Migchels.T *Acta Crystallogr* **1967**, *23*, 90.

(131) Pauling, L. *The Nature of the Chemical Bond, 3rd ed.*; Cornell University Press: Ithaca, 1960.

(132) (a) Pye, C. C.; Xidos, J. D.; Burnell, D. J.; Poirier, R. A. *Can J Chem* **2003**, *81*, 14. (b) Pye, C. C.; Poirier, R. A. *Can J Chem* **2005**, *83*, 1299.

(133) Hurtado, M.; Mo, O.; Yanez, M.; Guillemin, J. C. *Croat Chem Acta* **2009**, *82*, 1.

(134) Kekia, O. M.; Jones, R. L.; Rheingold, A. L. *Organometallics* **1996**, *15*, 4104.

(135) (a) Shapiro, P. J. *Coordin Chem Rev* **2002**, *231*, 67. (b) Erker, G. *Polyhedron* **2005**, *24*, 1289. (c) Prashar, S.; Antinolo, A.; Otero, A. *Coordin Chem Rev* **2006**, *250*, 133. (d) Wang, B. *Coord. Chem. Rev.* **2006**, *250*, 242. (e) Voegele, J.; Dietrich, U.; Hackmann, M.; Rieger, M. *Metallocene-Based Polyolefins* **2000**, *1*, 485.

(136) (a) Alonso-Moreno, C.; Antinolo, A.; Carrillo-Hermosilla, F.; Otero, A.; Rodriguez, A. M.; Sancho, J.; Volkis, V.; Eisen, M. *Eur. J. Inorg. Chem.* **2006**, 972. (b) Bryliakov, K. P.; Babushkin, D. E.; Talsi, E. P.; Voskoboynikov, A. Z.; Gritzo, H.; Schroder, L.; Damrau, H. R. H.; Wieser, U.; Schaper, F.; Brintzinger, H. H. *Organometallics* **2005**, *24*, 894. (c) Antinolo, A.; Fajardo, M.; Gomez-Ruiz, S.; Lopez-Solera, I.; Otero, A.; Prashar, S. *Organometallics* **2004**, *23*, 4062. (d) Roesky, P. W.; Stern, C. L.; Marks, T. J. *Organometallics* **1997**, *16*, 4705.

(137) (a) Bourissou, D.; Freund, C.; Martin-Vaca, B.; Bouhadir, G. *Cr Chim* **2006**, *9*, 1120. (b) Shapiro, P. J. *Eur. J. Inorg. Chem.* **2001**, 321.

(138) Leyser, N.; Schmidt, K.; Brintzinger, H. H. *Organometallics* **1998**, *17*, 2155.

(139) Shin, J. H.; Bridgewater, B. M.; Parkin, G. *Organometallics* **2000**, *19*, 5155.

(140) Antinolo, A.; Fajardo, M.; Otero, A.; Royo, P. *J. Organomet. Chem.* **1984**, *265*, 35.

(141) Mosges, G.; Hampel, F.; Schleyer, P. V. *Organometallics* **1992**, *11*, 1769.

(142) Fichtel, K.; Hoxter, S.; Behrens, U. *Z Anorg Allg Chem* **2006**, *632*, 2003.

(143) Feil, F.; Harder, S. *Eur. J. Inorg. Chem.* **2003**, 3401.

(144) Johns, A. M.; Chmely, S. C.; Hanusa, T. P. *Inorg. Chem.* **2009**, *48*, 1380.

(145) (a) Reed, A. E.; Weinstock, R. B.; Weinhold, F. *J. Chem. Phys.* **1985**, *83*, 735. (b) Reed, A. E.; Curtiss, L. A.; Weinhold, F. *Chem Rev* **1988**, *88*, 899.

(146) ADF *Amsterdam Density Functional* **2008**, Vrije Universiteit Amsterdam The Netherlands.

(147) Becke, A. D. *Phys Rev A* **1988**, *38*, 3098.

(148) Perdew, J. P.; Yue, W. *Phys Rev B* **1986**, *33*, 8800.

(149) (a) Janak, K. E.; Shin, J. H.; Parkin, G. *J. Am. Chem. Soc.* **2004**, *126*, 13054. (b) Kirillov, E.; Toupet, L.; Lehmann, C. W.; Razavi, A.; Kahlal, S.; Saillard, J. Y.; Carpentier, J. F. *Organometallics* **2003**, *22*, 4038. (c) Dunn, A. R.; Sweet, L. E.; Wiser, D. C.; LoCoco, M. D.; Jordan, R. F. *Organometallics* **2004**, *23*, 5671. (d) Talarico, G.; Blok, A. N. J.; Wo, T. K.; Cavallo, L. *Organometallics* **2002**, *21*, 4939.

(150) Peckham, T. J.; Lough, A. J.; Manners, I. *Organometallics* **1999**, *18*, 1030.

(151) (a) Parr, R. G.; Yang, W. *Density Functional Theory of Atoms and Molecules*; Oxford University Press: Oxford, 1989. (b) Labanowski, J. K.; Andelm, J. W. *Density Functional Methods in Chemistry*; Springer: New York, 1991.

(152) Godfrey, S. M.; McAuliffe, C. A.; Mackie, A. G.; Pritchard, R. G. In Chemistry of Arsenic, Antimony, and Bismuth; Norman, N. C., Ed.; Springer: 1998.

(153) Reeske, G.; Cowley, A. H. *Chem. Commun.* **2006**, 1784.

(154) Atwood, J. L.; Cowley, A. H.; Hunter, W. E.; Mehrotra, S. K. *Inorg. Chem.* **1982**, *21*, 1354.

(155) Watson, B. T.; Lebel, H. *Sodium bis(trimethylsilyl)amide*; J. Wiley & Sons: New York, 2004.

(156) Michalik, D.; Schulz, A.; Villinger, A. *Inorg. Chem.* **2008**, *47*, 11798.

(157) Olmstead, M. M.; Power, P. P.; Sigel, G. A. *Inorg. Chem.* **1988**, *27*, 2045.